REMOTE SENSING EVAPOTRANSPIRATION USING GEONETCAST AND IN-SITU DATA STREAMS FOR DROUGHT MONITORING AND EARLY WARNING:
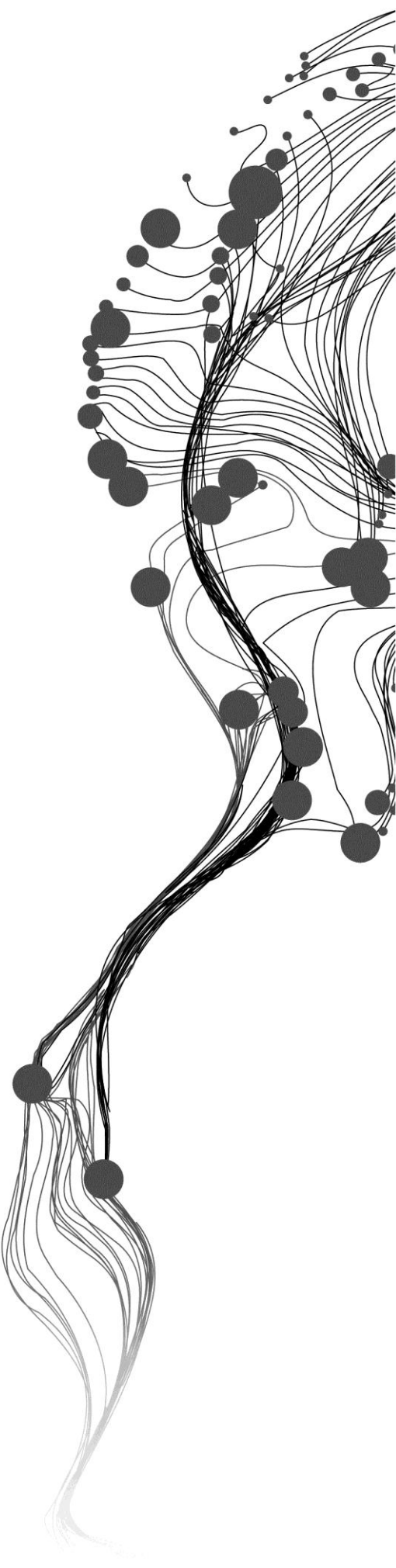# CASE STUDY FOR THE AMHARA REGION IN ETHIOPIA

TINEBEB YOHANNES GELASSIE

March, 2012

SUPERVISORS:
Dr. B.H.P. Ben Maathuis
Dr. Ir. C.M.M. Chris Mannaerts

REMOTE SENSING EVAPOTRANSPIRATION USING GEONETCAST AND *IN-SITU* DATA STREAMS FOR DROUGHT MONITORING AND EARLY WARNING:
CASE STUDY FOR THE AMHARA REGION IN ETHIOPIA

TINEBEB YOHANNES GELASSIE
Enschede, the Netherlands, March, 2012

ABSTRACT

Drought is one of the natural hazards that affect human life and usually occurs from a deficiency of precipitation and water availability from expected or normal amounts. This natural disaster is mainly pronounced in developing countries which rely on agriculture as the back bone of their economies. Thus, this study aims at using GEONETCast (GNC) data stream coupled with *In-situ* data for drought monitoring and early warning to ensure preparedness for the Amhara region in Ethiopia. To achieve this objective, spatial and temporal distribution of Actual Evapotranspiration (AET) was used. AET was estimated through Surface Energy Balance System (SEBS) model using GNC data stream together with *In-situ* data. On the other hand, the performance of the Land Surface Analysis Satellite Application Facility (LSA SAF) SAF AET was evaluated in relation to SEBS AET. Subsequently, the SEBS AET and the SAF AET have also been compared with reference ET_o calculated using the Penman-Monteith equation. Furthermore, temporal and spatial drought were analysed for the 2010 main growing season of the region and the historical drought situation was studied using time series SPOT VGT NDVI for 12 years (1999 to 2010). The temporal variations and the drought observed were possible by integrating hydro-meteorological variables (e.g. AET, rainfall and Potential Evapotranspiration (PET)), vegetation performance and drought indices. To examine the spatial distribution of drought three drought indices were used. These are the Water Requirement Satisfaction Index (WRSI), Vegetation Condition Index (VCI) and a deviation of current NDVI from the long term means (Drought Severity Index (DSI)).

Comparisons of SEBS AET and SAF AET results show strong relationship over rainfed croplands in the study area. Furthermore, the SEBS and the SAF AET compare well with reference ET_o calculated using FAO Penman Monteith during rainy season and dry period. Subsequently, the temporal drought analysis results indicated that drought can be detected using relationships obtained the hydro-metrological variables, vegetation responses and drought indices derived using GNC data stream and *In-situ* data. Consequently, the spatial drought examined by integrating the three drought indices (WRSI, VCI and DSI) showed that using the combined continuous method for drought classification (mainly derived from GNC data stream) indicated that drought can be distinguished and mapped in the study area. Finally time series NDVI were related with *In-situ* data of annual agricultural crop yield from 1999 to 2009. The correlation result demonstrates significant relationships between sum of maturity stage NDVI over the growing season and annual yield. Therefore, NDVI can be used to estimate the yield reduction during the growing period which is related to the occurrence of drought.

Keyword: Drought Monitoring, GEONETCast, Actual Evapotranspiration (AET), Surface Energy Balance (SEBS), Land Surface Analysis Satellite Application Facility (LSA SAF), Normalized Difference Vegetation Index (NDVI), Early Warning.

ACKNOWLEDGEMENTS

TABLE OF CONTENTS

LIST OF FIGURES

LIST OF TABLES

LIST OF ABBREVIATIONS

AET	Actual Evapotranspiration
ASCAT	Advanced Scatterometer
CSA	Central Statistics Agency
DEM	Digital Elevation Map
DIDSSF	Daily Downward Surfaces Shortwave Flux
DIV	Integer Division Operator
DRMFSS	Disaster Risk Management Unit of the Ministry of Agriculture
DSI	Drought Severity Index
ECMWF	European Center for Medium Range Weather Forecasts
ESA	European Space Agency
ET	Evapotranspiration
ET$_o$	Reference ET$_o$
EU	European Union
EUMETSAT	European Organization for Exploitation of Meteorological Satellite
EWS	Early Warning System
FAO	Food and Agricultural Organization
FAPAR	Fraction of Absorbed Photosynthetically Active Radiation
FEWS NET	Famine Early Warning System Network
FVC	Fraction Vegetation Cover
GEOSS	Global Earth Observation System of Systems
GIEWS	Global Information and Early Warning System
GIS	Geographic Information System
GNC	GEONETCast
ILWIS	Integrated Land and Water Information System
ITC	International Institute for Geo-information science and earth Observation
JRC	Joint Research Center
JRC/MARS	Joint Research Centre Monitoring Agricultural Resources
LAI	Leaf Area Index
LEAP	Livelihood Early Assessment and Protection
LSA SAF	Land surface Analysis Satellite Application Facilities
LTA	Long Time Average
LW	Long Wave
MoARD	Ministry of Agriculture and Rural Development
MOD	Modulus Operator Return
MPEF	Meteorological Products Extraction Facility
MSG	Meteosat Second Generation
NDVI	Normalized Difference Vegetation Index
NGO	Non-Governmental Organization
NMA	National Meteorology Agency
NWP	Numerical Weather Prediction
PET	Potential Evapotranspiration
RUM	Regional Unmixed Means
SAF	Satellite Application Facilities
SAF AET	Actual Evapotranspiration from Satellite Application Facility
SEBI	Surface Energy Balance Index
SEBS	Surface Energy Balance System

SEVIRI	Spinning Enhanced Visible and Infrared Imager
SPI	Standard Precipitation Index
SPIRITS	Software for the Processing and Interpretation of Remotely Sensed Image Time Series
SRTM	Shuttle Radar Topographic Mission
SVAT	Soil Vegetation Atmosphere Transfer
SW	Short Wave
TCI	Temperature Condition Index
UNWFP	United Nation World Food Program
UTM	Universal Transverse Mercator
VCI	Vegetation Condition Index
VITO	Flemish Institute for Technological Research
WFP	World Food Program
WHC	Water Holding Capacity
WMO	World Meteorological Organization
WRSI	Water Requirement Satisfaction Index

1. INTRODUCTION

1.1. Background

This section highlights drought, Livelihood Early Assessment and Protection (LEAP) model and the GEONETCast (GNC) data stream.

Drought

Drought is a natural hazard that results from a deficiency of precipitation and water availability from expected or normal amounts, usually extended over a season or longer period of time (Mishra and Singh, 2010). Its occurrence is associated with severe damage of agricultural production and causing an imbalance on food supply and demand (Boken, 2009). Though drought occurs in many parts of the world, developing countries are highly susceptible to drought. So far, Ethiopia is one of the most drought prone countries in Africa (Conway and Schipper, 2011). An estimated proportion of 80-85% of the population of depending on traditional rain fed agriculture (Temesgen *et al.*, 2009). Drought has severe impact on the livelihoods of farmers as their livelihood is dependent on rain fed agriculture. Farmers remain highly susceptible to extreme, uncontrollable drought events that can severely impact on both quality and quantity of the yield of their crops. To assess this problem the implementation of drought monitoring and Early Warning System (EWS) plays an important role.

Drought Monitoring and Early Warning System (EWS) means analyzing the drought situation on time and alerting public and drought management teams by announcing the possibility of any upcoming drought incidence (Boken, 2009). EWS is designed to identify climate and water supply trends and thus helping in the detection of drought onset. A comprehensive and integrated approach is required to monitor drought more effectively and provide early warning (Mishra and Singh, 2010). As a result, effective early warning system must integrate hydrological and climate variables (Ross *et al.*, 2009). Thus, numerous schemes have been developed with the aid of remote sensing and *In-situ* data for EWS. In 2006, a model called LEAP (Livelihood Early Assessment and Protection) was developed specifically for Ethiopia. It was initiated by the World Food Program (WFP) for drought indexing to support drought monitoring and early warning for the country.

Livelihood Early Assessment and Protection (LEAP) Model

The LEAP model was developed by combined efforts of the Ethiopian Government Disaster Risk Management Unit of the Ministry of Agriculture (DRMFSS), the National Meteorological Agency (NMA) with the support of United Nation World Food Program (UN-WFP). The model source is the water balance model developed by the Food and Agricultural Organization (FAO). The FAO model is used by other organizations such as the Famine Early Warning System Network (FEWS NET) and the Joint Research Center (JRC) of European Union (EU). The model is grid based with 0.1 x 0.1 degree spatial resolution and 10 day temporal resolution. It has a data archive consisting of rainfall, evapotranspiration and crop data of 13 major crops of Ethiopia, crop coefficients and FAO Water Holding Capacity (WHC) (Hoefsloot, 2010). The main outputs of the model are Water Requirement Satisfaction Indices (WRSI), yield reduction estimates, livelihood parameters, moisture indexes and other related issues to get timely

and accurate indicators for identification of drought assistance. Following the developments of the LEAP model, the Faculty of Geo-Information and Earth Observation (ITC) of the University of Twente is conducting a pilot project with the UN-WFP in collaboration with the Ethiopian government and Non-Governmental Organization (NGO) sectors to implement the use of near real time GEONETCast (GNC) data stream for drought monitoring and early warning to asses if the performance of LEAP can be improved.

GEONETCast (GNC)

GNC is a near real time, global network of satellite telecommunication based data dissemination systems designed to distribute space-based, air-borne and *In-situ* data, metadata and products to diverse communities. It is part of the emerging Global Earth Observation System of Systems (GEOSS), led by the Group on Earth Observation (GEO). The GNC data stream contains recoding from various satellites and environmental data necessary for the provision of wide area coverage (Figure 1-1) and frequent information required for spatial monitoring of (changing) environmental conditions. For reception of GNC data no internet connectivity is required, it can be received by constructing a low cost ground receiving station using off the-shelf components (Maathuis *et al.*, 2011a). The data stream contains various images/products to identify the onset of drought in near real time by satellite based hydro-meteorological retrieved remote sensing data and parameters. The products includes precipitation, Actual Evapotranspiration (AET), Normalized Difference Vegetation Index (NDVI), Fraction of Vegetation Cover (FVC), Fraction of Absorbed Photosynthetically Active Radiation (FAPAR) and more related products which help to analyze environmental risks in a timely manner. Therefore; for countries which are exposed to these serious environmental risks, GNC is supporting by delivering adequate information. Hence, to utilize the data disseminated through GNC the GEONETCast toolbox was developed as a plug-in using the Integrated Land and Water Information System (ILWIS) software (section 4.1.2).
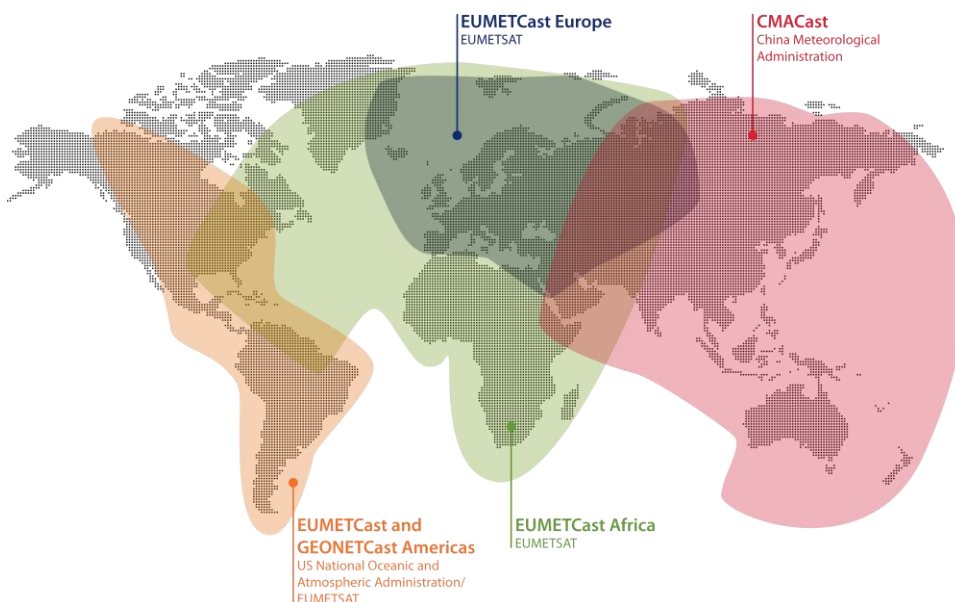
Figure 1-1: Global GEONETCast Coverage

In this study, temporal and spatial variability of Actual Evapotranspiration (AET) was assessed by two remote sensing applications using GNC Earth Observation (EO) data streams and *in-situ* data, that is using the Surface Energy Balance System (SEBS) model (SEBS AET) (Su, 2002) and a GNC delivered product called Land Surface Analysis Satellite Application Facility (LSA SAF) AET for the main growing season (14th of July to 30th of November 2010) of the study area. In addition, daily Potential Evapotranspiration

(PET) of FEWS NET from 2001 to 2010 and *In-situ* Reference Evapotranspiration (ET_o) from 1st of June 2010 to 30th of November 2010 was also examined. The SEBS AET and SAF AET methods were evaluated against reference ET_o. Furthermore, drought trend analysis using AET, PET, ETo, Long Time Average (LTA) Normalized Difference Vegetation Index (NDVI), recent year 2010 NDVI, remote sensing rainfall estimates, *in-situ* rainfall, together with derived drought indices were analyzed. Lastly, the time series NDVI was correlated with the locally obtained agricultural statistics (yield).

1.2. Research Problem

Major food production in Ethiopia, especially in the Amhara region, is almost fully dependent on rain fed agriculture and the area is often hit by periodic droughts. This drought causes serious economic, social and environmental problems (Gadisso, 2007). Conventional methods of drought monitoring and early warning using station point data is time consuming and tedious. Similarly, the data are often incomplete and inconsistent. These problems are even further compounded by limited number and distribution of observation stations which is rather a common concern for most African countries. On the other hand, station data are point measurements which lack spatial representation. In addition, the initiation for this study is the LEAP model mentioned in section 1.1. The model is currently supporting drought monitoring and early warning in Ethiopia. However, it has certain limitation such as it only incorporates low resolution near real time hydro-meteorological retrieved remotely sensed data. Therefore, this study attempted to apply higher temporal and spatial resolution GNC remote sensing data and products in conjunction with *in-situ* data to improve drought monitoring and early warning for Ethiopia.

1.3. Research Objectives

1.3.1. General Objective

The main objective of this study was identification of the occurrence of drought using remotely sensed estimate of Actual Evapotranspiration (AET) to improve drought monitoring and early warning.

1.3.2. Specific Objectives

The following are the specific objectives of the study:

- ➢ To estimate AET using the SEBS model applying GNC data stream in conjunction with *in-situ* data.
- ➢ To compare SEBS estimated AET with SAF AET and both AET's against *in-situ* reference ET_o.
- ➢ To assess the drought trend of the Amhara region of Ethiopia by applying GNC time series data stream and *In-situ* data together with derived drought indices for a selected period.
- ➢ To investigate the relationship between the NDVI and ground truth agricultural statistics (yield).

1.4. Research Questions

Following the above research objectives, the following research questions were formulated:

- • How does AET of SEBS and LSA SAF compare against each other and against *in-situ* reference ET_o in the study area?
- • Can GNC data stream and its derived drought indices sufficiently identify and distinguish drought?
- • How does time series NDVI correlate with agricultural statistics?

1.5.   Hypothesis

The following research hypotheses were formulated:

- Spatial and temporal variability of AET can be estimated and mapped using data from GNC in conjunction with *In-situ* data and the result can be evaluated again reference *in-situ* ET_o.
- Near real time GNC data stream in combination with *in-situ* data and derived remote sensing indices can be used to analyze the drought trend and it improves drought monitoring and early warning.
- Remote sensing derived drought indicators can be validated using agricultural (yield) statistics as ground truth.

1.6.   Outline of the Thesis

The thesis consists of seven chapters; chapter 1 is the introduction containing background, research problem, research objective, research questions, hypothesis and outline of the thesis. Chapter 2 provides a literate review on various drought concept, evapotranspiration and GEONETCast data stream. Chapter 3 describes the materials and methodology such as study area, dataset, field work and conceptual frame work of the study. Chapter 4 describes preprocessing steps taken for remote sensing and *in-situ* datasets. Chapters 5 elaborate on the data analysis and results obtained in order to answer the research objectives. Chapter 6 presents discussion of each result. Finally, chapter 7 provides conclusions and recommendations that can be drawn from the study and subsequently the list of references and appendixes are provided.

2. LITERATURE REVIEW

2.1. Drought Concept

Drought is a complex natural hazard caused by prolonged abnormally dry weather leading to hydrological imbalances (Wilhite and Svoboda, 2000). However its definition varies from place to place upon the normal precipitation type, behavior and the task for which is it defined. Moreover, it is obvious that when there is soil water deficiency, plant water stress and yield reduction will occur. In general, there are two main definitions of drought, a conceptual and operational one. The conceptual definition helps people to have an idea of drought and it is essential for development of drought policy. The methodology compares the current situation with a long term historical average. On the other hand, the operational definition helps people to identify drought frequency, severity and duration for a historical period and it is expressed by drought indices. It is often region specific and is established on a scientific basis through the analysis of certain hydro-meteorological variables.

2.1.1. Types of Drought

Drought is commonly classified by type as agricultural drought, meteorological drought, hydrological drought and socio-economic drought (Wilhite and Glantz, 1985).

    I.   **Agricultural drought** is defined more commonly by the availability of soil water to support crop and vegetation growth than by the departure of normal precipitation over some specified period of time.

    II.   **Hydrological drought** is defined as the departure of surface and subsurface water supplies from some average condition.

    III.   **Meteorological drought** is usually defined by a precipitation deficiency threshold over a predetermined period of time.

    IV.   **Socio-economic drought** differs markedly from the other types of drought because it reflects the relationship between the supply and demand for some commodity or economic good, such as water, livestock forage or hydroelectric power that is dependent on precipitation.

Agricultural drought occurs when there is not enough soil moisture to meet the needs of a particular crop at a particular time. It develops at some point after meteorological drought and is identified by linking the characteristics of a meteorological drought to agricultural impacts. This category of drought can develop quite suddenly and is usually the first economic sector to be affected by drought. Therefore, though there are four kinds of drought, the main notion of this study is to analyze the occurrence of agricultural drought which has a significant effect on the economy of the Amhara region in Ethiopia.

2.2. Drought in Ethiopia

There has been notable drought in Ethiopia throughout human history; previous drought conditions suggests that drought occur every 3-5 and 6-8 years in northern Ethiopia and every 8-10 years for the whole country (Temesgen*, et al.*, 2009). In recent years there were about 30 major drought episodes. Of these drought episodes 13 of them are known to have affected the entire nation and they have been reported as severe (Gebrehiwot *et al.*, 2011). Spatial distribution of Ethiopian drought further indicates

that most of the drought and food crises events are concentrated in the central and northern highlands extending from North Shewa through Wello and Tigray (Gebrehiwot, et al., 2011). Among them, the 1984/85 drought affected the lives of more than two hundred thousand people and millions of livestock in Ethiopia.

It is still ambiguous to conclude that the drought in Ethiopia is either caused by climate change or it is a trend (OXFAM, 2011). However the climate in Ethiopia is changing although not all relevant trends are clear. OXFAM (2011) reports that, according to the survey made questioning local people in Ethiopia, the climates is experiencing an increase in the rate of drought.

Meteorological data shows mean annual temperature increased 1.3oC from 1960 to 2006 and the frequency of hot days have increased in Ethiopia (OXFAM, 2011). Rainfall statistical trends are less clear according to the Inter-Governmental Panel on Climate Change Fourth Assessment Report (IPCC AR4) (2007). However, research suggests that rainfall decreased from 1980 to 2009 in the long rainy season (OXFAM, 2011). Generally, when temperature rises it causes more evapotranspiration from the surface; therefore assessment on temporal and spatial distribution of evapotranspiration from remote sensing could bring substantial information on the land surface characteristics.

2.3.   Remote Sensing Based Drought Indices

The development of earth observation satellites from the 1980s onward equipped with sensors mainly in the optical domain opened a new road for drought monitoring and detection (Niemeyer, 2008). Quantitative monitoring of drought or use of drought indices is the tool to identify the characteristics of drought such as the onset, severities and the spatial extent. Drought indices provide a basis for drought assessment and risk management which includes to identify the onset of drought and to be able to provide early warning. Thus, remote sensing based drought indices have a potential to improve drought monitoring and early warning because it allows the derivation of truly spatial information and at global or regional coverage with a consistent method and a high repetition rate. Drought indices do not have a universally accepted definition but with different types of droughts, several different drought indices have been introduced (Niemeyer, 2008). More than 80 types of drought indices are identified by the author and probably the total number is close to be double. This paper describes the used remote sensing methods for this study in the following section which includes Normalized Difference Vegetation Index (NDVI), drought indices derived using NDVI that is Drought Severity Index (DSI), Vegetation Condition Index (VCI) and index derived from evapotranspiration that is Water Requirement Satisfaction Index (WRSI).

2.3.1.   Normalized Difference Vegetation Index

The Normalized Difference Vegetation Index (NDVI) is related to the quantity of photosynthetically absorbed radiation. It is a measure of the amount and vigor of vegetation on the land surface. In general, NDVI values range from -1.0 to 1.0, with negative values indicating clouds and water, positive values near zero indicating bare soil, and higher positive values of NDVI ranging from sparse vegetation (0.1 - 0.5) to dense green vegetation (0.6 and above) (USDA, 2006). NDVI is also directly related to the:

- Leaf Area Index (LAI), which is often used in crop growth models
- Herbaceous or total green biomass (tons/ha) for given vegetation types,
- Photosynthetic activity of the vegetation
- Percent ground cover.

Green and healthy vegetation reflects much less solar radiation in the visible part of electromagnetic spectrum compared to those in near-infrared part. More importantly, when vegetation is under stress,

visible values may increase and near infrared values may decrease. The NDVI is calculated from two channels sensor, the near-infrared (NIR) and among the visible part the red portion of electromagnetic spectrum using the following algorithm:

$$NDVI = \frac{\lambda_{NIR} - \lambda_{RED}}{\lambda_{NIR} + \lambda_{RED}}$$

Equation 2-1

Where: λ_{RED} is red portion of electromagnetic spectrum (0.6-0.7 μm) and λ_{NIR} = near infrared portion of the electromagnetic spectrum (0.75-1.5 μm).

Two characteristics of the NDVI that make it good for vegetation monitoring are that no other surface exhibits higher NDVI values than vegetated surfaces and that, when vegetation vigour changes due to the nature of vegetation growth and development or environmental induced stress such as drought, the NDVI also changes (Tucker, 1987). Therefore, the NDVI does have potential in drought detection and climate impact assessment.

2.3.1.1. Drought Severity Index

NDVI itself does not reflect drought or non-drought conditions. But the severity of a drought (or the extent of wetness, on the other end of the spectrum) may be defined as NDVI deviation from its long-term mean (Thenkabail *et al.*, 2004).

$$DEV_{ndvi} = NDVI - NDVI_{mean}$$

Equation 2-2

Where: DEV_{NDVI}, $NDVI$ and $NDVI_{mean}$ the week, decadal or monthly deviation of NDVI from multiyear NDVI, the current NDVI and multiyear mean NDVI respectively.

2.3.1.2. Vegetation Condition Index

Vegetation Condition Index (VCI) is an indicator of the status of vegetation cover as a function of NDVI minima and maxima encountered for a given ecosystem over many years (Jain *et al.*, 2010). It quantifies the weather component of NDVI and it was first suggested by (Kogan, 1995). Although the NDVI has been extensively used in the past for vegetation monitoring, it is often very difficult to interpret in relation to vegetation condition, especially when comparing different ecosystems It shows, effectively, how close the current month's NDVI is to the minimum NDVI. VCI is an attempt to separate the short-term climate signal from the long-term ecological signal and in this sense it is a better indicator of water stress condition than NDVI calculated from the long-term record of remote sensing images (Kogan and Sullivan, 1993). It is defined as:

$$VCI = 100 \times \frac{(NDVI - NDVI_{min})}{(NDVI_{max} - NDVI_{min})}$$

Equation 2-3

Where: *NDVI*, *NDVI_{max}* and *NDVI_{min}* the week, decadal or monthly current NDVI, multiyear maximum NDVI and multiyear minimum NDVI respectively. The VCI values around 50% reflect fair vegetation conditions. The VCI values between 50 and 100% indicate optimal or above normal conditions. At the VCI value of 100%, the NDVI value for this month (week or decade) is equal to NDVImax. Different degrees of a drought severity are indicated by VCI values below 50% (Thenkabail, *et al.*, 2004). (Kogan, 1995) illustrated that the VCI threshold of 35% may be used to identify extreme drought conditions and suggested that further research is necessary to categorize the VCI by its severity in the range between 0 and 35%. The VCI value close to 0% reflects an extremely dry month, when the NDVI value is close to

its long term minimum. Low VCI values over several consecutive time intervals point to drought development Table 2-1 revises how the values of the VCI classes can be used to describe drought conditions.

Table 2-1 VCI based drought severity classes after Kogan and Thenkabail *et al*

No	VCI (%)	Drought Severity class
1	50-100	No drought
2	36-49	Slight drought
5	<35	Complete crop failure

The VCI captures rainfall dynamics better than the NDVI particularly in geographically non homogeneous areas (Kogan, 1995). The VCI not only permits the description of land cover and spatial and temporal vegetation change but also allows quantifying the impact of weather on vegetation. Also the VCI makes it possible for one to compare the weather impact in areas with different ecological and economical resources (Kogan, 1995). VCI values indicate easily how much the vegetation has advanced or deteriorated in response to weather and how far vegetation development is from the potential maximum and minimum defined by ecological limits.

2.3.2. Water Requirement Satisfaction Index

Water Requirement Satisfaction Index (WRSI) is an indicator of crop performance based on the availability of water to a crop during a growing season (Frère and Popov, 1979). As explained in section 1-1, the current drought model in Ethiopia, LEAP, defines drought by weather based indices using a water balance indicator WRSI (Hoefsloot, 2010). Originally, this drought index was designed by FAO. In addition, studies have shown that WRSI can be related to crop yield using a linear yield production function specific to a crop (Doorenbos and Pruitt, 1977). The FEWS NET model to calculate WRSI requires Start of Season (SOS) and End of Season (EOS) for each gird based calculation. SOS is calculated using a rainfall threshold amount and distribution of rainfall received in three consecutive decades. It is established when there is at least 25 mm of rainfall in one decade followed by a total of at least 20 mm of rainfall in the next two consecutive decades. The Length of Growing Period (LGP) for each grid is determined by the persistence, on average, above a threshold value of a climatological ratio between rainfall and potential evapotranspiration. Thus, EOS was obtained by adding LGP to the SOS decade for each grid (Verdin and Klaver, 2002) . WRSI defined as:

$$WRSI = (AET / WR) * 100$$
Equation 2-4

Where; *WRSI* is Water Requirement Satisfaction Index in (%), *AET* is the actual evapotranspiration (mm) and *WR* is crop water requirement (mm) calculated from the reference evapotranspiration of FAO-56 Penman-Monteith equation *(ET$_o$)* and crop coefficient *(K$_{cp}$)* of specific crop during the growing season. Table 2-2 shows values of the WRSI classes that can be used to describe drought conditions.

$$WR = K_{CP} * ET_o$$
Equation 2-5

Table 2-2: WRSI based drought severity classes after Hoefsloot.

No	WRSI (%)	Drought Severity class
1	80-100	No drought
2	70-79	Slight drought
3	60-69	Moderate drought
4	50-59	Severe drought
5	<50	Complete crop failure

2.4.   Concept of Evapotranspiration (ET)

Evapotranspiration (ET) is a term used to describe the loss of water from the Earth's surface to the atmosphere by the combined processes of evaporation from the open water bodies, bare soil and plant surfaces, etc. and transpiration from vegetation or any other moisture containing living surface (Li *et al.*, 2009). Both evaporation and transpiration occur at the same time and there is no easy way to distinguish. The energy needed to break water into gas is evaporation heat and latent heat is the energy needed for evaporation. The rate of ET is mainly depending upon by solar radiation, wind speed, vapor pressure deficit and air temperature.

I.   **Reference Evapotranspiration (ET_o)**: - The reference surface is a hypothetical grass reference crop with an assumed crop height of 0.12 m, a fixed surface resistance of 70 s m^{-1} and an albedo of 0.23. The reference surface closely resembles an extensive surface of green, well-watered grass of uniform height, actively growing and completely shading the ground. The fixed surface resistance of 70 s m^{-1} implies a moderately dry soil surface resulting from about a weekly irrigation frequency (Allen *et al.*, 1998).

II.   **Actual Evapotranspiration (AET)**: - The amount of water that evaporates from the surface and is transpired by plants if the total amount of water is limited.

III.   **Potential Evapotranspiration (PET)**:- is defined as the amount of evaporation that would occur if a sufficient water source were available. If the AET is considered the net result of atmospheric demand for moisture from a surface and the ability of the surface to supply moisture, then PET is a measure of the demand side. Surface and air temperatures, insolation, and wind all affect this.

In various practical applications, there are still no specific ways to directly measure the AET over a watershed (Li*, et al.*, 2009). Conventional ET estimations techniques (e.g. pan-measurement, Bowen ratio, eddy correlation system, and weighing lysimeter, scintillometer, sap flow) are mainly based on site (field)-measurements and many of these techniques are dependent on a variety of model complexities. Though they can provide relatively accurate estimates of ET over a homogeneous area, conventional techniques are of rather limited use because they need a variety of surface accessory measurements and land parameters such as air temperature, wind speed, vapor pressure at a reference height, surface roughness, etc., which are difficult to obtain over large-scale terrain areas and have to be extrapolated/interpolated to various temporal and spatial scales with limited accuracy in order to initialize/force those models (Li*, et al.*, 2009). Generally, as Rana and katerji (2000) discussed the ET measurement methods categorized as hydrological approaches (e.g. weighing lysimeters, soil water balance,), micrometeorological approaches (e.g. Energy balance and Bowen ratio, aerodynamic method, eddy covariance) or plant physiology approaches (e.g. sap flow method, chamber method). All these methods have some limitations and

strength. The best suited method should be selected based on the accessibility of the data, correctness or cost incurred or time and space scales.

2.4.1. Reference Evapotranspiration

The FAO- 56 Penman-Monteith method was developed by defining the reference crop as an imaginary crop with an assumed height of 0.12 m, a surface resistance of 70 s/m and an albedo of 0.23 which closely resembles the evaporation from surface of green grass of uniform height, actively growing and adequately watered (Allen*, et al.*, 1998). It uses meteorological data set the maximum and minimum temperatures (degree Celsius), relative humidity (%), wind speed (m/s) at 2m and sunshine hours to derive reference evapotranspiration (ET_o).

FAO-56 Penman-Monteith for grass reference ET_o use the original Penman-Monteith equation, aerodynamic equation and surface resistance equation as Allen, *et al* (1998).

$$ET_o = \frac{0.408\Delta(R_n - G) + \gamma \dfrac{900}{T + 273} u2(e_s - e_a)}{\Delta + \gamma(1 + 0.34u_2)}$$

Equation 2-6

ET_o - reference evapotranspiration [mm day^{-1}], R_n net radiation at the crop surface [MJ m^{-2} day^{-1}], G soil heat flux density [MJ m^{-2} day^{-1}], T mean daily air temperature at 2m height [°C], u_2 wind speed at 2 m height [m s^{-1}], e_s saturation vapour pressure [kPa], e_a actual vapour pressure [kPa], e_s - e_a saturation vapour pressure deficit [kPa], Δ slope vapour pressure curve [kPa °C^{-1}], γ psychrometric constant [kPa °C^{-1}]. The equation uses standard climatological records of solar radiation (sun shine), air temperature, humidity and wind speed. Hence the brief computation of each parameter is expressed in the in FAO-56 paper of Allen, *et al* (1998).

2.4.2. Evapotranspiration Estimation from Remote Sensing

The temporal and spatial characteristics of ET can only be measured from remote sensing. Remote sensing provides continuous spatial and temporal coverage and retrieve information from the areas where it is not accessible by human being. There are different ET estimation methods using remotely sensed land surface parameters. Generally as Li *et al* (2009) discussed the commonly applied ET from remote sensing data can be categorized into two types: empirical (semi) methods, which describes an empirical relationship of remote sensing data in conjunction with minimum set of ground based measurement. The analytical method is establishment of the physical processes from the remote sensing technology and ground based measurements.

2.4.2.1. Surface Energy Balance Systems Model

Surface Energy Balance (SEBS) developed to estimate atmospheric turbulent fluxes and evaporative fraction using remote sensing data in combination with meteorological data (Su, 2002). Its algorithm is an extension of SEBI concept with wide range account of roughness length for heat transfer, similarity theory and atmospheric boundary layer. It is a physically based energy balance algorithm that provides a good compromise between model complexity and input requirements. SEBS has been used to generate daily, monthly, and annual actual evaporation with acceptable accuracy (Su *et al.*, 2003). Furthermore, the model has been used for drought monitoring and prediction using data assimilation system with surface soil moisture over China (Su *et al.*, 2008).

SEBS requires three basic datasets:

I. Remote Sensing data of land surface parameters (albedo, Land Surface Temperature (LST), NDVI, emissivity, Leaf Area Index (LAI), Fraction Vegetation Cover (FVC).

II. Meteorological data (air temperature, air pressure, humidity, and wind speed at reference height) (meteorological stations).

III. Incoming Short Wave (SW) and Long Wave (LW) radiation from direct measurement, parameterization, remote sensing products or model outputs.

In addition, the model consists of three sets of tools: I) set to derive the land surface parameters from satellite data; II) a model to determine the roughness length of heat transfer, and III) a formulation to determine the evaporative fraction considering the limiting case for energy balance (Su, 2002). The general algorithm used for the SEBS model is given in appendix D.

2.4.2.2. Satellite Application Facility Evapotranspiration

Land Surface Analysis Satellite Application Facility (LSA SAF) is a specialized development and processing centre whose aim is to take full advantage of remotely sensed data, particularly those available from EUMETSAT sensors, to describe land surface properties. The LSA SAF products are currently available from the LSA SAF website (http://landsaf.meteo.pt) which contains real time examples of the products as well as updated information. One of these land surface properties product that LSA SAF provide is an ET product SAF AET. Although, direct measurement of ET from remote sensing is hardly possible, AET of SAF uses indirect measurement by forcing Soil-Vegetation-Atmosphere Transfer (SVAT) model (SAF, 2011). The SVAT scheme that uses as input combination of remote sensed data and atmospheric model outputs (Ghilain *et al.*, 2011). The remote sensed data are Daily Downward Surface Shortwave Flux and Long Wave Fluxes (DSSF, DSLF), albedo, FVC, and LAI. On the other hand, atmospheric model outputs are meteorological data such as air temperature, humidity, wind speed, atmospheric pressure obtained from European Center for Medium Range Weather Forecasts (ECMWF). ET maps covering the whole MSG field of view are produced from the model every 30 min, in near-real-time, for all weather conditions. The daily SAF AET obtained by temporal integration of instantaneous values (equation 2–7). The implemented procedure accounts for missing slots/values by allowing pixels evapotranspirate at a rate equivalent to the average between two existing slots (one previous the other after the missing slot/value). It is calculated as :

$$SAF\,AET = \int_{h1}^{h2} ET_i(t)dt$$ <div style="text-align: right">Equation 2-7</div>

Where: ET_i is the instantaneous evapotranspiration estimated, the integration limits (*h1*, *h2*) correspond to the first (theoretically at 00:30 UTC) and last (theoretically at 24:00 UTC) existing slots for a given day, *dt* is the integration step (30 minutes). In optimal situation (no missing slots) 48 images are integrated for a given day. The flowchart illustrating the general algorithm is given in appendix C.

2.5. Concept of GEONETCast

GEONETCast (GNC) as described in section 1-1 and 3-2-2, are part of the emerging Global Earth Observation System of Systems (GEOSS), led by Group on Earth Observation (GEO), a data dissemination system called GNC was put in place. The current partners within the GNC initiative include the China Meteorological Administration (CMA), the National Oceanic and Atmospheric Administration (NOAA), the World Meteorological Organization (WMO) and EUMETSAT, as well as many prospective data provider partners (EUMETSAT, 2011). GNC can be seen as the backbone to freely disseminate the

data acquired by ground, airborne and space based systems to the global user community and if possible in near real time .

The products and services are being made available to the GEONETCast user community contains Meteosat image data , GOES east and west image data , FungYun Cast image data (China), Land, ocean sea and ice Satellite Application Facility (SAF) products, EUMETSAT meteorological products, NOAA meteorological products, ocean color and sea surface temperature product, VEGETATION products from Flemish Institute for Technological Research (VITO), Moderate Resolution Imaging Spectroradiometer (MODIS) ocean color products, *In-situ* and observational data (EUMETSAT, 2011).

GNC data dissemination system is relatively new to various user groups in Africa, especially outside the meteorological community. Data disseminated is having various formats (HRIT-LRIT wavelet compressed, HDF4-5, TXT, BUFR, GRIB, NetCDF, etc The broadcasting system is particularly useful in Developing Countries, where it can help to avoid the high cost of maintaining a reliable internet connections that are sufficient in capacity to carry large volume of Earth Observation products (e.g. outside of major cities).Other advantages are (DevCoCast, 2011):

➢ The availability of low cost, off-the-shelf receiver equipment
➢ The high reliability and data transfer rate;
➢ The wide variety of freely available images and products;
➢ The long-term commitment to maintain the infrastructure, in particular by EUMETSAT towards Africa;
➢ The constantly growing receiver network, the growing number of products and (Third Party) data providers.

Using a single antenna both GNC and the European Space Agency Data Dissemination System (ESA DDS) can be received. Figure 2-1 illustrates single antenna for both GNC and the ESA DDS. The ESA DDS enables the user to receive (pre-processed) images and derived products from MEdium Resolution Imaging Spectrometer (MERIS), Advanced Along Track Scanning Radiometer (AATSR) and Advanced Synthetic Aperture Radar (ASAR) within 24 hours after sensing the Environmental Satellite (EnviSat) orbits acquired over Africa are transmitted (52north, 2012). Currently the GEONETCast data stream is a one way system, therefore only reception is possible. This is a continuous data stream. Data is broadcasted on a 24 hour – 7 days basis. Non operation of a ground receiving system results in a data gap, as data is broadcasted only once. The ESA DDS, however, can be configured as a two way data dissemination system, allowing one to receive broadcast data as well (52north, 2012).
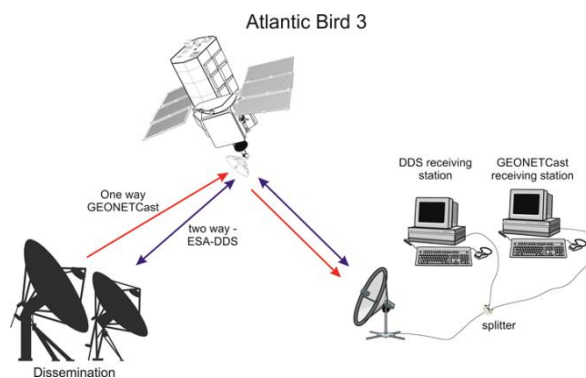
Figure 2-2: Single antenna for both GNC and the ESA DDS

3.   MATERIALS AND METHODOLOGY

3.1.   Study Area Description

3.1.1.   The Amhara Region

Amhara region is located in the north western and central parts of Ethiopia (Figure 3-1) between 8^0 42' N to 13^0 46' N latitude and 35^0 11' E to 40^0 13' E longitude. The region shares common borders with the state of Tigray in the north, Afar in the east, Oromiya in the south, Benishangul Gumuz in the south west, and the Sudan in the west. It has an estimated area of about 170, 000 square kilometer divided into 10 administrative zones (districts) and 105 woredas (provinces) and covers 11% of the total area of Ethiopia. Topographically, the region is divided into highlands in the north and high mountain ranges in the east and west, and lowlands in the northwest. The topographical features represent diverse elevation ranging from 700 meters above sea level (m.a.s.l) in the eastern edge to over 4600 m.a.s.l. in the northwest. Climatologically, the region is divided into three major zones, Kola (hot zones), Woyinadega (warm zones) and Dega (cold zones). The annual mean temperature of the area ranges from 15^0C to 21^0C, but in gorges and marginal areas it exceeds 27^oC. The two crop seasons in the area are the Belg and Meher seasons which receive rainfall from February to June and from June to October, respectively. The Meher crop season is the main season and produces 90-95 percent of the total cereal output. The Belg harvest provides the remaining 5-10 percent. To avoid confusion between this two crop seasons the Amhara Belg crop season is officially defined as any crop harvested between March and August, while the Meher crop season is defined as any crop harvested between September and February. Subsistence agriculture is the main economic activity in this area. Crops in most regions cultivated are cereals and pulses. Cereals accounts for 85 % of the total crop production. Teff, barley, wheat, maize, sorghum, and finger millet are considered dominant crop types in the area.

3.1.2.   Population

According to the 2007 population and housing census report conducted by the Ethiopian Central Statistics Agency (CSA), the population of the Amhara region is approximately 18 million people of whom 87% live in rural, agricultural households. The region has an estimated population density of 108 people per square kilometre. A population growth rate of 3 percent a year is leading to doubling of the population every 25 years. More than 90% of the population of the region are subsistence farmers. This rapid population growth rate has led to severe land shortages and rapid natural resource degradation. In the region, 94 percent of households have limited land to meet their food needs (DRMFSS, 2010). Rural households are compelled to clear and cultivate marginal lands on steep hillsides. Only one to three percent of the Amhara region remains forested. Overgrazing further denudes the land of vegetative cover.

3.1.3.   Drought History in Amhara Region

In general, during recent years, the Amhara region has suffered from frequent drought phenomena. It is the single most recurring climatic related natural hazard negatively impacting the region. Furthermore, as the Ethiopian Government Disaster Risk Management Unit of the Ministry of Agriculture (DRMFSS) (2010) reported, from 105 districts of the Amhara region 48 are drought prone and chronically food insecure.
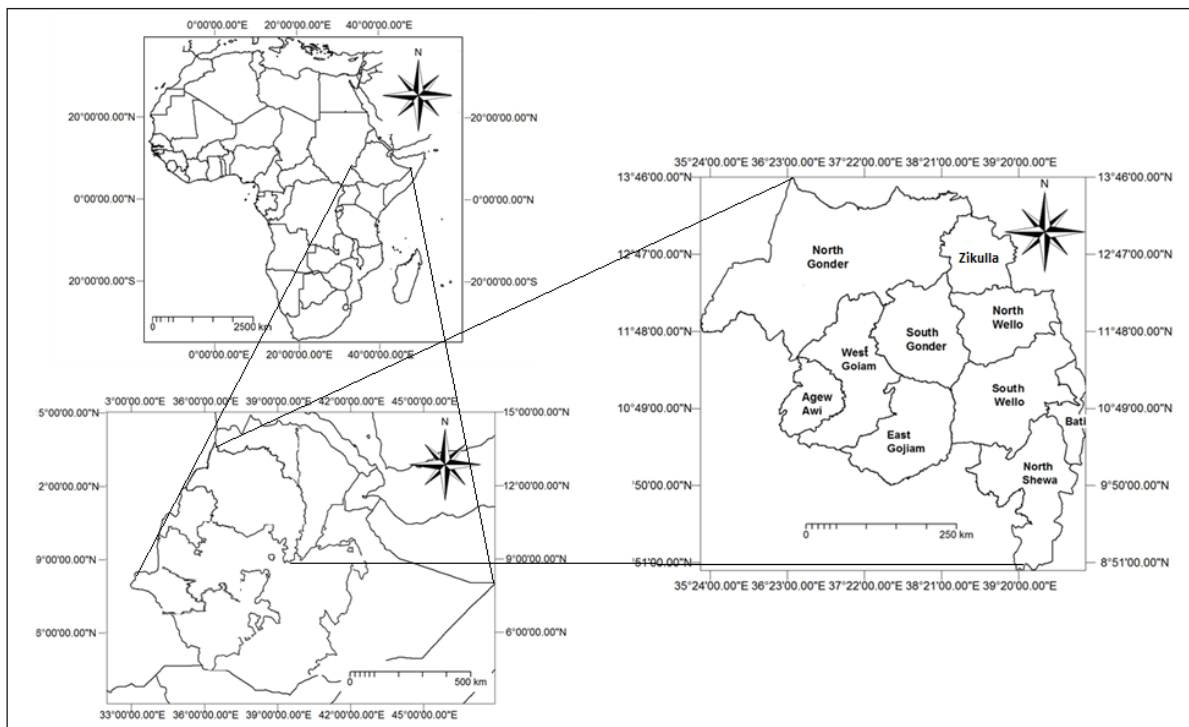
Figure 3-1: Location of the study area

3.2.   Acquired Data

3.2.1.   Ground Data from Amhara region

Field work was conducted from September 7th to 3rd October, 2011. The field work involved office secondary data collection in relevant institution and a field campaign. The offices where most of the data was obtained from are located in Addis Ababa and Kombolecha South Wello district of the Amhara region in Ethiopia. The Addis Ababa offices include the National Meteorological Agency (NMA), Ministry of Agriculture and Development (MOA), Central Statistics Agency (CSA), DRMFSS and UN-WFP. Regional offices visited are Kombolecha Regional and Rural Development, and the National Meteorological Agency Kombolecha branch office. A field campaign comprised of interviewing local farmers (section 3.2.1.3) and observations of land cover. Random land cover observation was made in Kombolecha provinces in places like Harbu, Kalu and Addis Mender. Table 3.1 shows the collected data with the equipment used.

Table 3-1 Field work land cover data collected and equipment used

No	Collected data	Equipment
1	Land cover class	Physical observation
2	Selected site picture	Digital camera
3	Geographic location ground control point	Global Positing System (GPS)

3.2.1.1.   Meteorological Data Acquisition

SEBS model algorithm and calculation of Penman-Monteith reference ET_o, requires meteorological data. This includes mean daily temperature, sunshine hours during the day, relative humidity and daily average

wind speed. The meteorological data were collected from the National Meteorology Agency (NMA) of Addis Ababa, and the National Meteorological Agency Kombolecha branch office in Ethiopia. Amhara synoptic or "Class A" categorized meteorological stations were selected which fulfills standard criteria and has fewer missing records. Figure 3.2 shows the spatial distribution of these stations. The data set taken from these stations are from 1st of January 2006 to 30th of November 2010 of the following variables: minimum and maximum temperature, wind speed measured at 2m height, sunshine hours and relative humidity on a daily basis. Even though the data was collected since 2006, the analysis was done only for 2010 main growing season from June 1st to 30th of November 2010. Nevertheless, other year's data were used to fill the gaps for the missing data for 2010. This was done be averaging each day value for the respective years and to calculate the average value for the missing day of 2010. Appendix A presents the list of meteorological stations with the location and elevation values of Amhara region.
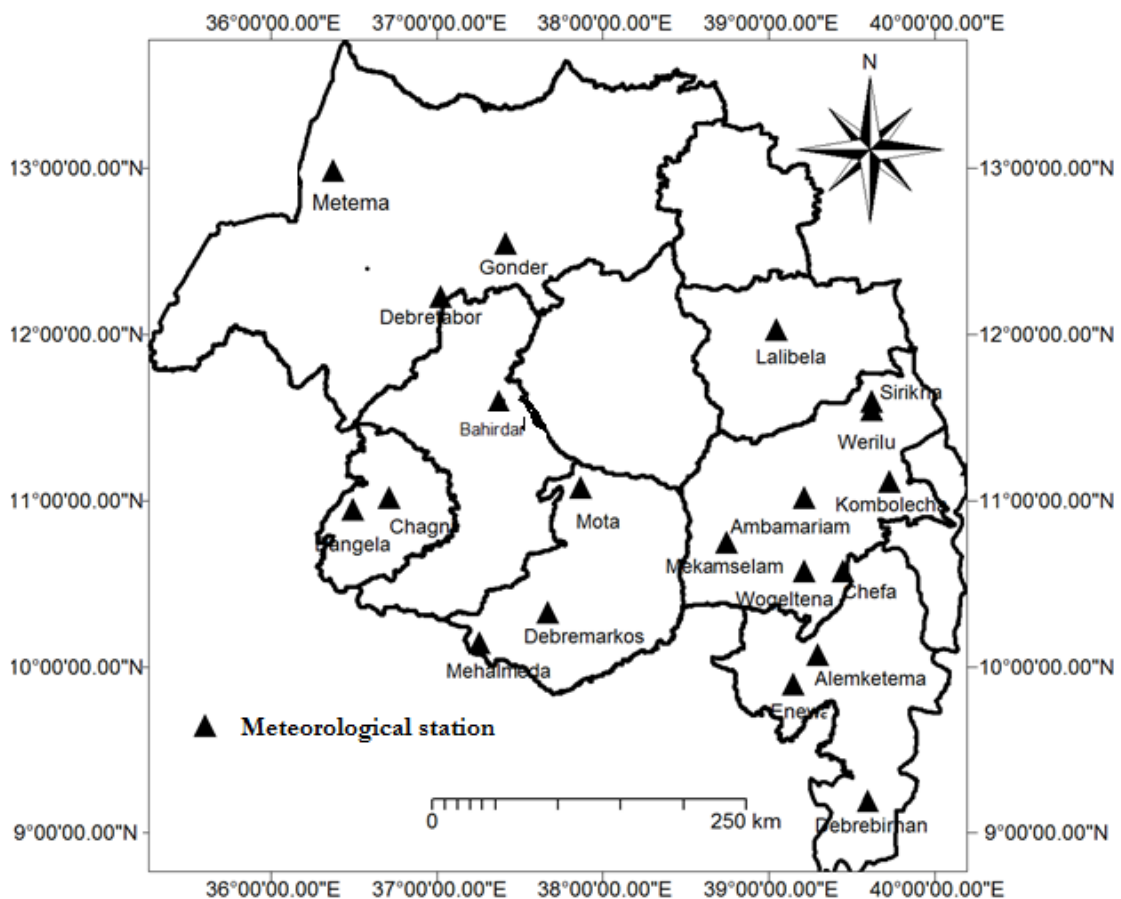
Figure 3-2: Distribution of meteorological stations in the Amhara region

In addition to the meteorological parameters mentioned above rainfall data was also collected. Similarly, the source of the data was NMA and it was collected for 20 synoptic station of the region. The temporal characteristics of the data was on daily basis from June 1st 2010 to 30th of November 2010 which is main rainy season of 2010 and on decadal basis from January 1st 19995 to December 21th 2010. The data were used to analyze the drought trend of the 2010 main growing season of the area and to determine if there is a relation between NDVI with variability of rainfall and through comparison of remote sensing evapotranspiration methods it can help to identify the behavior of the evapotranspiration during the wet and dry period. Figure 3-3 shows the spatial distribution of the sum of daily rainfall for the 2010 growing

period from 06/01/20010-30/11/2010 main rainy season interpolated using an inverse distance moving average method.
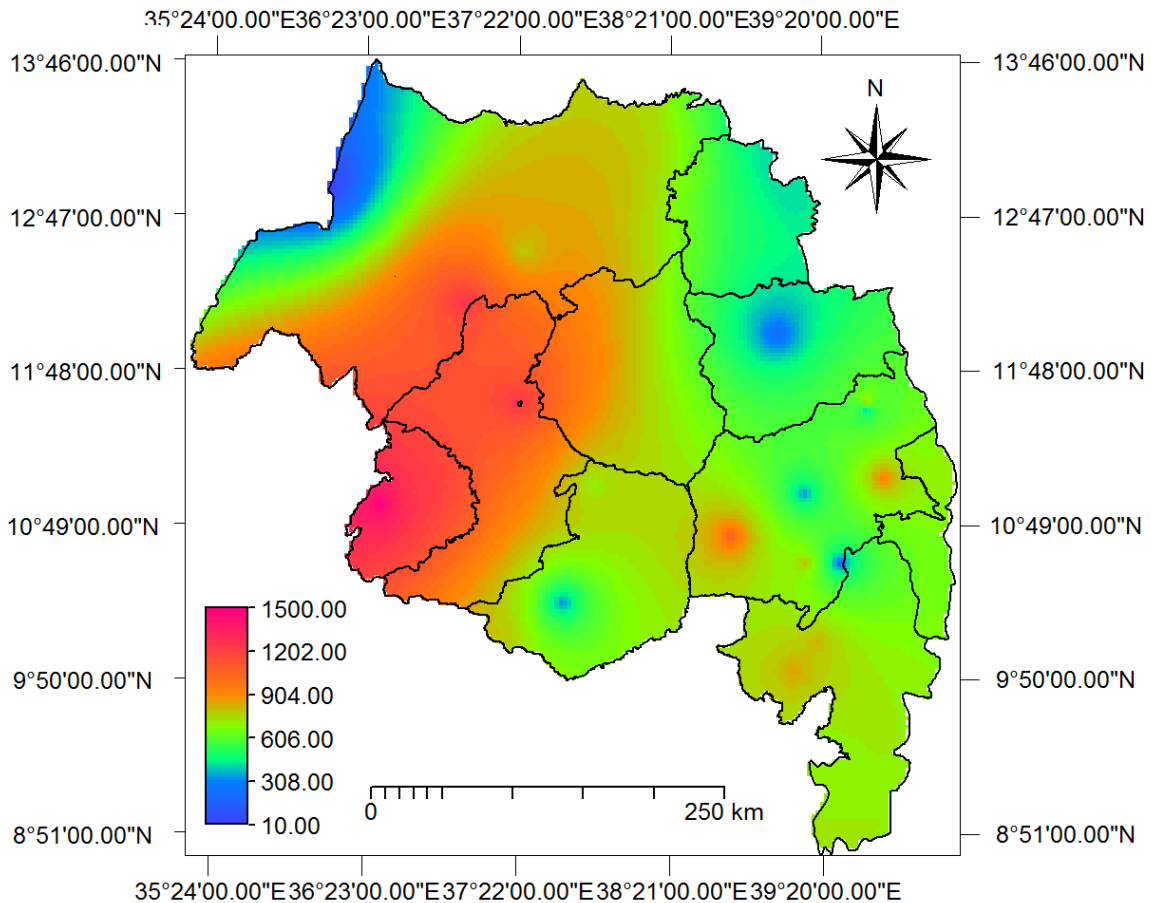
Figure 3-3: Total sum of *In-situ* rainfall, 2010 main rainy season in the Amhara region

3.2.1.2. Agricultural Production Yield Data

The characteristics of satellite derived hydro-meteorological parameters and the derived drought indexes must be validated by ground truth data. In this study the data used for validation purpose is mainly agricultural production yield. The agricultural yield production statistics were taken for 10 administrative zones of the Amhara region. The data was collected from the Central Statistics Agency (CSA) of Ethiopia (Addis Ababa) and the regional Agriculture and Rural Development office located in Kombolecha South Wello zone of Amhara region. CSA is responsible for the statistical result of different sectors and it administers, conducts and supervises surveys and census reports for Ethiopia. Agricultural production yield data is obtained for 11 years starting from 1999 to 2009 and the data are given in Appendix B.

3.2.1.3. Farmers Interview

During the field work, farmers were randomly interviewed. These helped in understanding the region historical crop production, the crop condition, pattern, drought years and total estimated annual end of season production per farmers cultivated land. The interviews were conducted in Amhara region South Wello district, the location is called Kombolecha. The district has 19 provinces; hence Harbu, Kalu and Addis Mender provinces were selected because they have a record of frequent drought occurrence.

According to the famers, the places were affected by severe drought condition every five years due to deficiency of rainfall during the main growing season. This caused reduction in their production/yield. Drought that happened during the year 2001 and 2006 resulted in a total devastation of their crops.

3.2.1.4. Crop Calendar

The crop calendar used for this study was obtained from the Global Information and Early Warning System (GIEWS). Table 3-3 shows the main crop calendar for the whole of Ethiopia which is considered similar to the Amhara region. This was further enhanced by field work to obtain the main crop calendar of the study area. Furthermore, the crop coefficients are taken from the LEAP model which contains the data for the 13 major crops grown in Ethiopia. For this study, the main crops of Amhara region namely teff, maize and barley crop coefficient (K_{cr}) values were taken. In table 3.2, LEAP model assigned K_{cr} values of the major crop are shown. According to the model, the K_{cr} values of the major crops are identical except for the ripening stage of maize.
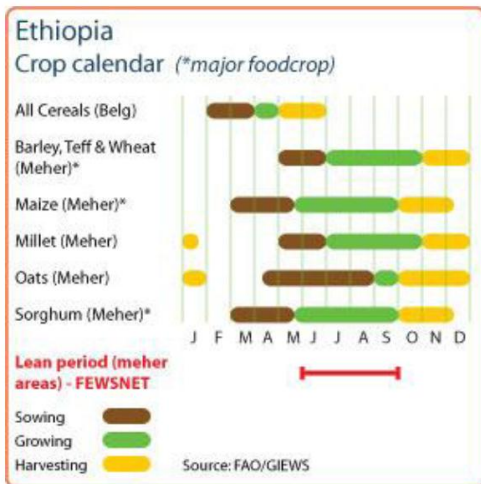
Crop	Initial	Vegetative	Flowering	Ripening
Teff	0.3	1.2	1.2	0.25
Barley	0.3	1.2	1.2	0.25
Maize	0.3	1.2	1.2	0.6

Table 3-2: Amhara region major crops and their K_{cr} values

Table 3-3: Crop calendar of Ethiopia (GIEWS, 2011)

3.2.2. Remotely Sensed Data

3.2.2.1. Meteosat Second Generation (MSG) Data

MSG transmits the raw data to the European Organization for Exploitation of Meteorological Satellites (EUMETSAT) control and processing centre in Germany (EUMETSAT, 2011). Figure 3-4 shows the near real time satellite reception. The raw data consists of images recorded by the Spinning Enhanced Visible and Infrared Imager (SEVIRI) and the Geostationary Earth Radiation Budget Experiment on board the satellite. After the SEVIRI data are received by EUMETSAT in Darmstadt (Germany), these are processed at the ground station and sent to a telecommunication satellite for broadcasting to the users (EUMETSAT, 2011). The images can be received using a low cost ground receiving station like the one installed at ITC .Nowadays receiving stations are also installed in many parts of the world; Ethiopia currently receives the data stream at 6 different places. At ITC, using a satellite dish pointed towards the Eurobird-9 satellite, the Digital Video Broadcasting (DVB) signal is received. The images are then archived in compressed format on external storage devices linked to the ITC network and are accessible by ordinary PCs.
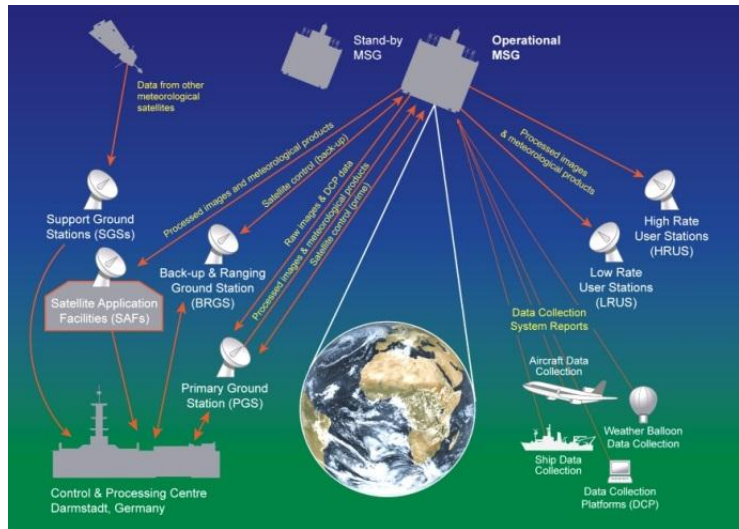
Figure 3-4: Near real-time satellite image reception, example MSG

The EUMETSAT Application Ground Segment (APS) includes a central processing facility and the distributed network of Satellite Application Facilities (SAF). The SAFs generate and disseminate operational EUMETSAT products and services and are an integral part of the distributed EUMETSAT APS. Of all networks, the Land Surface Application Satellite Application Facility (LSA SAF) archive data has been selected for this study. The archived products can be obtained free of charge from the LSA SAF website (https://landsaf.meteo.pt/products/prods.jsp). The products provided by the SAF on Land Surface Analysis are related to energy and water budget. Table 3.4 shows the data downloaded from LSA SAF. LSA SAF also started to deliver processed aggregated daily data from July 14 2010 onwards; therefore this study starts to use the daily AET from this day to November 30, 2010. The data has been imported using the GEONETCast toolbox SAF routines and a sub-image covering the study area (Amhara region) was selected from the LSA SAF original image covering the North Africa window.

Table 3-4: Remote sensing data set and their characteristics

Parameter	Temporal resolution	Spatial Resolution	Data Source	Unit
LST	15min → Daily	3km	MSG	(°C)
Albedo	daily	3km	MSG	-
FVC	daily	3km	MSG	-
LAI	daily	3km	MSG	-
DIDSSF	daily	3km	MSG	w/m²
SAF AET	daily	3km	MSG	mm/day

3.2.2.2. TAMSAT Rainfall Data

For this study, the Tropical Applications of Meteorology using SATellite (TAMSAT) rainfall, another rainfall data source from GEONETCast was used in conjunction with the other rainfall dataset. The TAMSAT archive has decadal rainfall for whole Africa since 1983 but during the time of this study the archive was inaccessible due to a new product calibration procedure. Hence, the 2010 dataset was used

from the ITC GNC archive and import was done using the GEONETCast toolbox version 1.3 plug-in. The data was used for computation of time series for the growing season of 2010 from 06/01/2010 to 11/21/2010. The whole data archive can be obtained from TAMSAT website (http://www.met.reading.ac.uk/~tamsat/data/rfe.html).

3.2.2.3. SPOT Vegetation Data

SPOT Vegetation historical 10 day syntheses (S10) archive is freely available through the website of the Vegetation Programme via the free S10 distribution server: http://free.vgt.vito.be/. As it is explained in the user manual, the product has full 1km x 1km spatial resolution with standard vegetation product format. The vegetation instrument is dedicated to the daily observation of terrestrial ecosystems and the environment, particularly for addressing change of vegetation and environmental risk related issues (Baret *et al.*, 2006). The vegetation tool sees the entire landscape every day because of its huge field of view and is an important tool for studies on world-wide vegetation (Baret*, et al.*, 2006). Ten-day composite data are processed by selecting pixels with the maximum NDVI during a 10 day period. Choosing pixels with the maximum NDVI is fundamental because it decreases cloud cover and water vapour contributions that negatively impact the NDVI value. Therefore, for this study decadal NDVI product were downloaded for Ethiopia from 01/01/1999 to 12/21/2010 and Amhara region NDVI values are extracted. The 10-day composite per month in this data set, is computed from the first of the month to the 10th, from the 11th to the 20th, and from the 21st to the end of the month. The last compositing period can differ from 8-11 days, depending upon the number of days in the month.

3.2.3. Ancillary Data

3.2.3.1. Digital Elevation Model Map

DEM was obtained from the Shuttle Radar Topography Mission (SRTM). SRTM is an international project lead by the National Geospatial Intelligence Agency (NGA) and the National Aeronautics and Space Administration (NASA) (NASA, 2009). A DEM was obtained on a near-global scale from 56° S to 60° N and is regarded as a homogenous complete high-resolution digital topographic database. DEM data features a 3 arc second (approximately 90m resolution) and 1 arc second (approximately 30m) resolution (NASA, 2009). The data is currently available free of charge to download but the 30 m resolution data is not available for all countries. Although, SRTM has a high resolution the 1km spatial resolution was selected because the DEM is used in combination with MSG data of 3km. Figure 3-5 shows the DEM of the Amhara region and the data can be downloaded freely from (http://www.cgiar-csi.org/data/elevation/item/45-srtm-90m-digital-elevation-database-v41). CGIAR is the international research centre that supplies GIS and RS data for sustainable agriculture (CGIAR-CSI, 2011) .
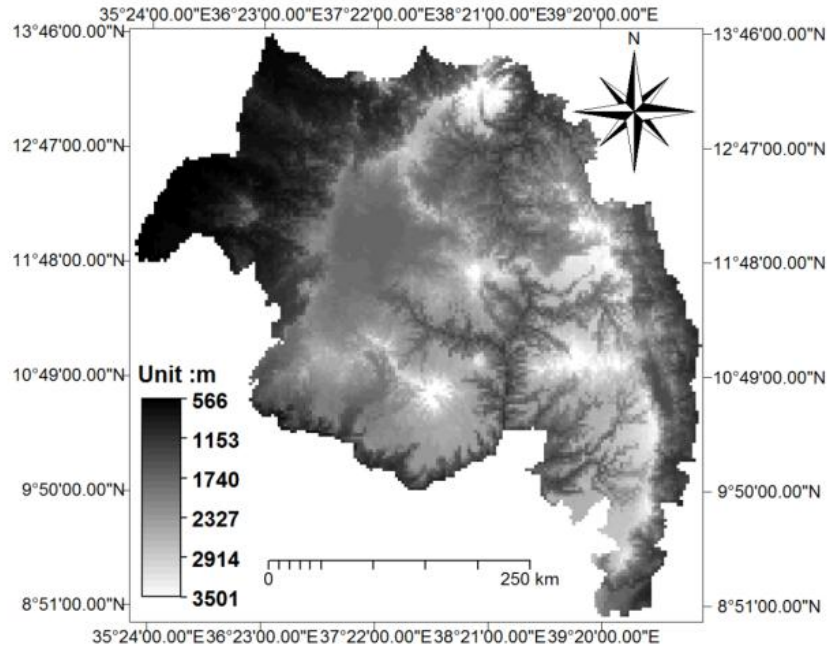
Figure 3-5: DEM of the Amhara region from SRTM 1km resolution

3.2.3.2. Vegetation and Land Cover Classes of Amhara Region

Over the past several years scientists have increasingly turned to remotely sensed land cover to define the geographic distribution of land cover at regional and global scale (Cihlar, 2000). For this study, by comparing different sources and products the LSA SAF land cover map has been selected due to its good correspondence with known rainfed croplands and good total area distribution of the rainfed crop classification of the study area. The data was downloaded freely from the LSA SAF product dissemination website (https://landsaf.meteo.pt/auxiliarDataFiles.jsp). This product classifies the land cover in 18 major classes but the Amhara region has been reclassified into 12 classes. The final land cover map is given in figure 3-6.
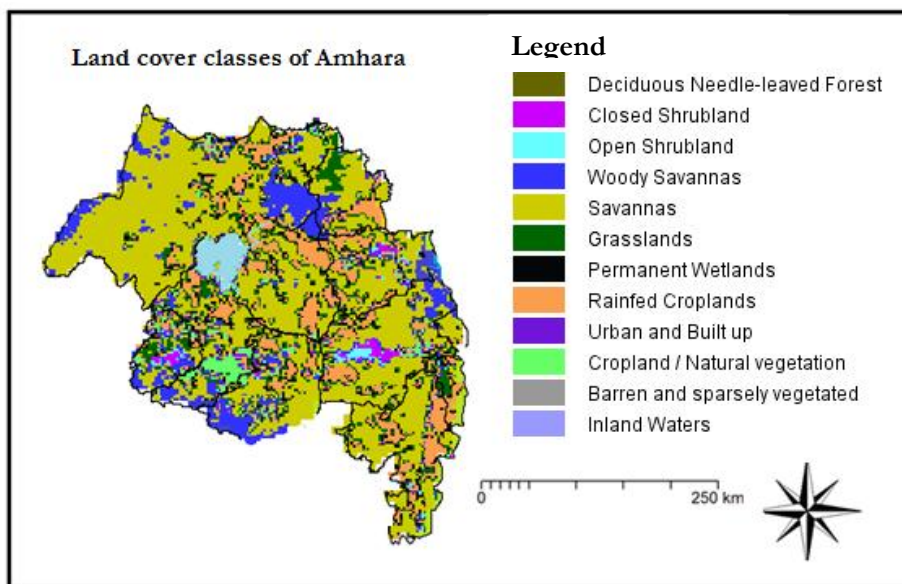
Figure 3-6: Vegetation and land cover classes of the Amhara region

3.2.3.3. Famine Early Warning System Network Data

The United States Geological Survey (USGS) FEWS NET data portal provides access to geo-spatial data, satellite image products and derived data products in support of FEWS NET monitoring needs throughout the world (FEWS NET, 2011). This portal is provided by the USGS FEWS NET Project, part of the Early Warning and Environmental Monitoring Program at the USGS Earth Resources Observation and Science (EROS) centre. Available products through FEWS NET Africa are Rainfall Estimates (RFE), called RFE1, RFE2 and daily global Potential Evapotranspiration (PET) that have been used for this study.

RFE1 ten day Africa rainfall estimates were produced from 1995-2000 by combining satellite temperature data, rain gauge measurements, and modelled wind and relative humidity to obtain decadal precipitation totals from 20W-55E, 40S-20N with 0.1 degree resolution (FEWS NET, 2011). The production of this type of RFE was discontinued from the year 2000 onwards; it is replaced by the RFE2.0 rainfall estimates produced by the same organization.

The daily global PET is produced from 2001 onwards and it is calculated from climate parameter data extracted from the Global Data Assimilation System (GDAS) analysis fields (FEWS NET, 2011) NET, 2011). The GDAS data are generated every 6 hours by the National Oceanic and Atmospheric Administration (NOAA). The GDAS fields used as input to the PET calculation include air temperature, atmospheric pressure, wind speed, relative humidity and solar radiation (long wave, short wave, outgoing and incoming). PET is computed for each 6 hour period and then summed to obtain daily totals. The product has a 1 degree ground resolution (FEWS NET, 2011).

For this study, decadal RFE1 from 1995 to 2000, RFE2 from 2001-2010 and daily PET from 2001-2010 were used. For importing the various products use has been made of newly integrated importing routines available in the GEONETCast toolbox version 1.3. The data can be obtained freely from the FEWS NET website (http://earlywarning.usgs.gov/fews/africa/web/datatheme.php).

3.3. Methodology

3.3.1. General

In this study, to investigate the drought trend analysis and derive the drought severity (drought classification) maps using GEONETCast and *In-situ* data sets a number of steps were taken. Hydro-meteorological parameters in conjunction with vegetation characteristics were analyzed for rainfed cropland of the Amhara region in Ethiopia. Among dataset provided or estimated using GNC, the actual evapotranspiration was selected as one of the principal constituent of the water cycle, apart from precipitation and runoff in semi-arid and humid areas (Mutiga, 2011). Evapotranspiration quantification from remote sensing is fundamentally important in giving rapid, regular, large area coverage to enable drought monitoring. It also gives early warning information for livelihood assessment and prediction by knowing the occurrence of drought. Therefore, to get a better AET estimation using remote sensing comparisons was made. The comparisons were processing results of remote sensing product with user formulated AET from remote sensing such as SAF AET against SEBS AET or remote sensing with ground variable such as the two AETs with reference ET_o. Subsequently, for trend analysis rainfall and climatology of rainfall were also computed. Finally computation of Long Time Average (LTA) vegetation characteristics from 1999 - 2010 was analyzed with 2010 NDVI.

Drought trends were studied by combining the hydro-meteorological variables with vegetation characteristics. Graphs were plotted per district to visual interpretation of the trends of each component

and integration of the trends using time series analysis. The temporal scale of the analysis was based on decadal time step. This scale was considered to provide sufficient detail for agriculture crops during the growing period for environmental risk analysis such as drought onset and early warning analysis. The spatial unit chosen was based on administrative district level because the acquired ground truth like agricultural statistics or crop production yield are based on administrative district level.

Finally, drought severity class (combined classified drought map) maps were produced, by integrating the three drought indices. These were Water Requirement Satisfaction Index (WRSI), Vegetation Condition Index (VCI) and Drought Severity Index (DSI). This method was selected because if the drought indices showed one places by all the three indices it increases the level of certainty compared to relaying only on a single drought index method. In addition, it helps to develop a new combined drought threshold. Lastly, the results were validated using ground truth data. The agricultural statistics on crop production yield were used as ground truth data. Annual yield was compared with NDVI. This helps to assess how the NDVI can be used as a proxy for yield. In addition, NDVI was correlated with actual evapotranspiration and rainfall. The idea of developing these relationships is to use one indicator as a proxy for the other. The conceptual framework of the study showing the general dataset and the used procedure is shown in Figure 3-8.

3.3.2. Estimation and Comparison of Evapotranspiration

AET was estimated using the SEBS model algorithm (Su, 2002). Simultaneously, the SAF AET was also retrieved for comparison with the SEBS AET. Subsequently, the two daily AET's were compared for each district rainfed croplands of the Amhara region. The comparison was needed because SEBS model requires numerous input parameters to get the AET but the SAF AET product is readily available in the GNC data stream at near real time at 30 minute intervals. Estimation of AET using remote sensing helps to determine firstly the spatial and temporal AET of the study area secondly to analyze the performance of readily available SAF AET compared to SEBS AET. Nevertheless, both AET estimations are based on remote sensing input, therefore their performance was evaluated against ground reference ET_0. In this study the time series computation starts from June 1St 1, 2010 till November 30, 2010 but for the AET estimation it starts from July 14th of 2010. This was because most of the LSA SAF products computed on a daily basis started to be produced from 14th July, 2010 onwards. Figure 3 -7 shows the comparison methods of SEBS against SAF AET as well as the two AET's against reference ET_0.
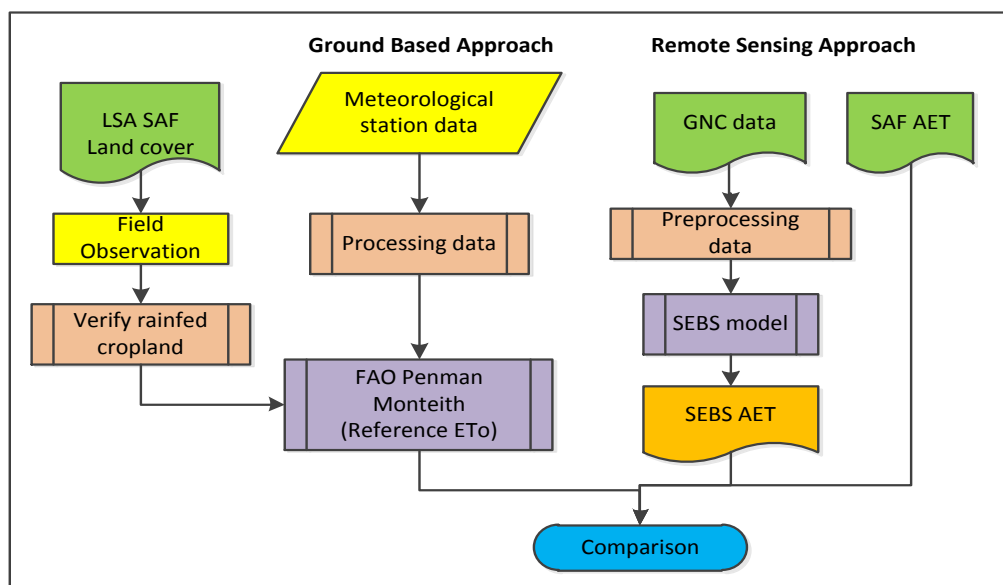

Figure 3-7: Comparison of two remote sensing AET; against each other and against *In-situ* reference ET_0.
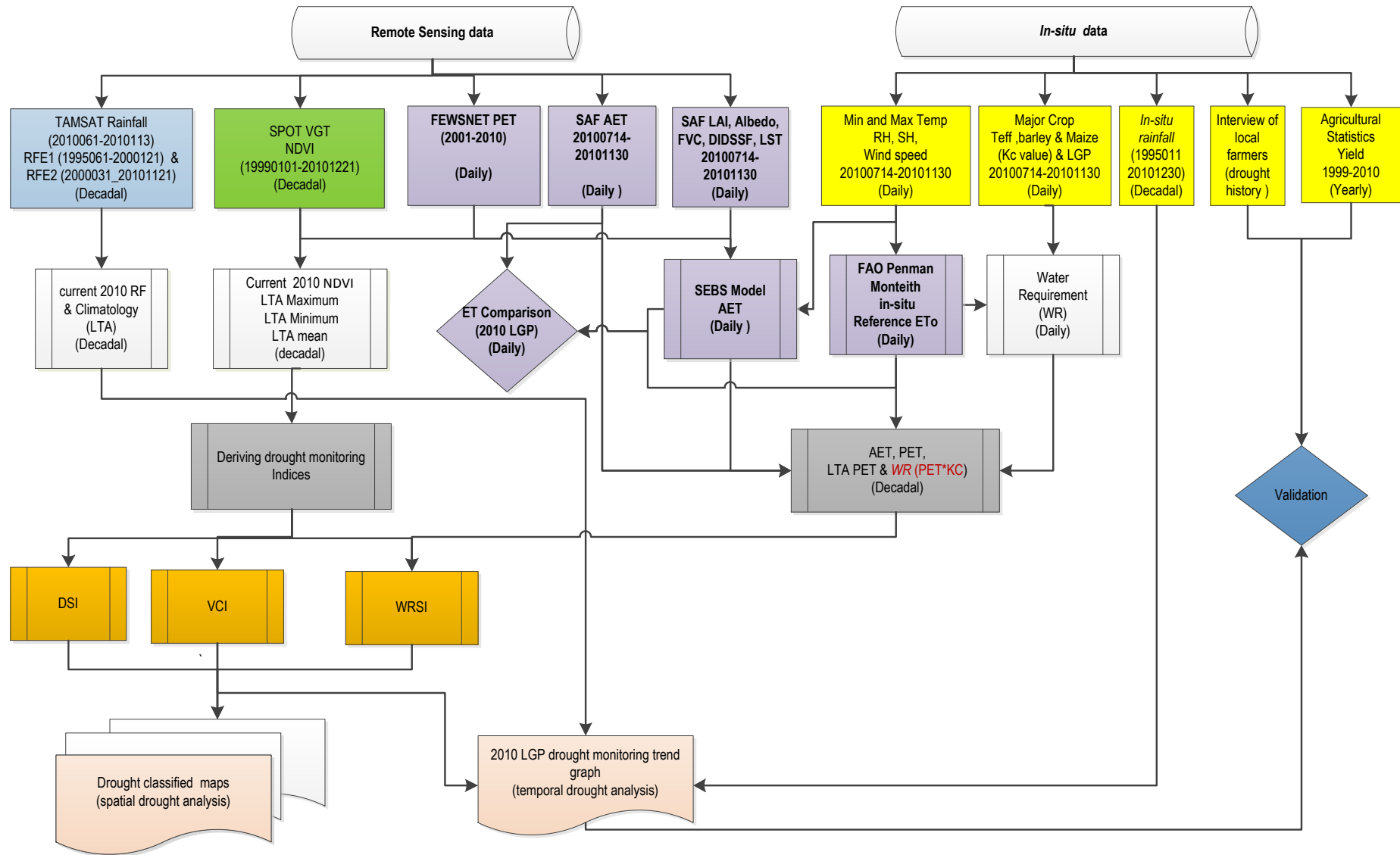
Figure 3-8: Conceptual frame work of the study

3.3.3.   Drought Classification Map

Drought classification maps were produced using two methods. The "Boolean method" and the "Continuous method". The Boolean method distinguishes drought according to the threshold distinction given by literature either as "drought" or "non-drought" condition. The continuous method could classify drought according to literature but can be adopted to reflect the regional / local conditions. The continuous method gives various options to classify the drought situation and new thresholds for classification can be implemented. A comparison was done to identify which drought classification method can be adopted. The drought indexes used for both classifications are Water Requirement Satisfaction Index (WRSI), Vegetation Condition Index (VCI) and Drought Severity Index (DSI). During the calculation the drought indexes, WRSI and VCI were not converted in percent values to enable summing and combining the three drought indices together.

WRSI is an indicator of the availability of water during a growing season. It is a ratio of actual evapotranspiration to water requirement (equation 2-5). In this study; it is calculated using two methods. The first is using the SEBS AET against water requirement using *In-situ* reference ET_o and the second one is using SAF AET against water requirement using FEWSNET PET. In order to get the water requirement, the crop coefficient (K_{cr}) was taken from LEAP model as mentioned in section (3.2.1.4). Distributed K_{cr} value per growing stage was used. Each growing stage K_{cr} value is calculated by giving a weighted mean of the major crops of the study area. The study area have major crop called teff as mentioned in (Section 3.1.1), therefore a 60% weight is given for teff, and 40% is given for the rest of the two major crops that is barley and maize. Accordingly 0.3, 1.2 and 0.32 for early (initial), vegetative (flowering) and late (ripening) stage were used respectively. That is according to the growing stage of a major crop in the study area which is showed in table 3.3. The WRSI index was originally developed by FAO for assessing crop yields in water limited crop growing regions (Doorenbos and Pruitt, 1977). This index is used in most African countries as a simple water balance model supplied by FEWS NET. Currently it is being applied in the LEAP model for Ethiopia (Hoefsloot, 2010). Afterwards, during calculation of the "Boolean method" a threshold of 0.5 or less was adopted as limit value after Silva (2010). However, for continuous method the WRSI as showed in table 2.1 was adopted after Hoefsloot (2010).

The second drought index used was VCI, which was originally developed by Kogan (1995), and accounts for the maximum amount of vegetation developed in years with optimal weather condition and minimum vegetation amount developed under extremely unfavorable weather (equation 2-3). Based on Kogan (1995) VCI value of 0.35 or less is considered to be an indicator of drought condition. Finally, the third index used was DSI which is an index showing the deviation of current NDVI from the long term mean (equation 2-2). DSI reveals drought or non-drought condition from a threshold value of zero (IWMI, 2006). The general procedure and the methods used for classification of drought are shown in figure 3-9.
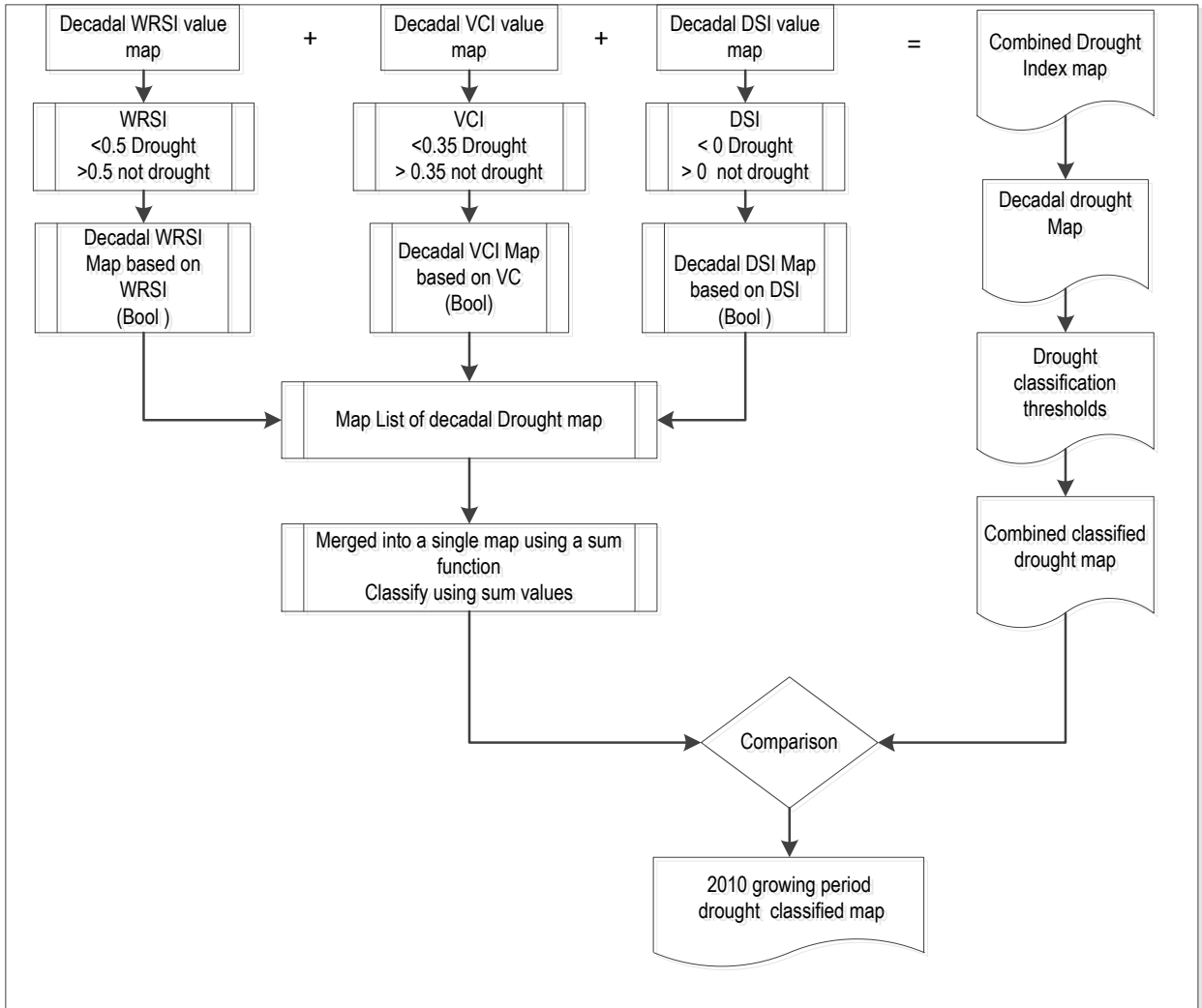
Figure 3-9: Procedure to derive drought classification maps using different methods

4. DATA PRE-PROCESSING

4.1. SEBS Model Data Pre-preprocessing

In this study, SEBS model proposed by Su (2002) was used for the estimation of actual evapotranspiration. Most surface energy balance model are based on the conservation of energy. Likewise the SEBS model is based on energy involved in the soil vegetation atmosphere interface which can be expressed as;

$$R_n = G_o + H + \lambda E$$

Equation 4-1

Where R_n is the net radiation [w m^{-2}], G_0 is the soil heat flux [w m^{-2}], H is the sensible Heat flux [w m^{-2}], and λE is the latent heat flux [w m^{-2}], where (λ) is the latent heat of vaporization and E is the actual evapotranspiration. In order to estimate these energy component SEBS uses meteorological data as well as remote sensing. The data used by SEBS model have been shown in figure 4-1; hence the core algorithm of the model is explained in detail in Appendix D.

In this study, the first preprocessing step was to transfer all images to have common spatial resolution, temporal resolution and same coordinate system. Projection system UTM, datum WGS 84 and zone 37 were selected as the main reprojecting units. Subsequently, SEBS model input parameters were prepared. Figure 4-1 shows the meteorological and remote sensing dataset used to get AET using SEBS model.
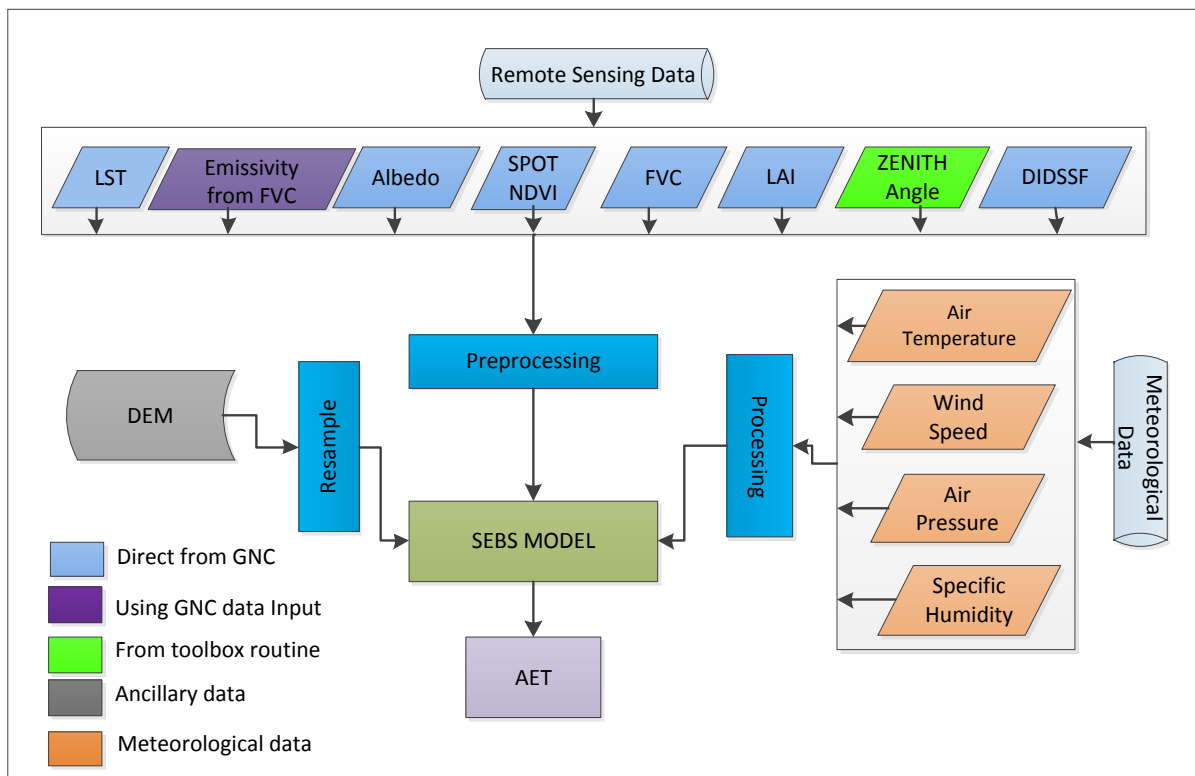
Figure 4-1: SEBS model input datasets

4.1.1. Meteorological Data Pre-processing

4.1.1.1. Mean Daily Air temperature

By using the daily maximum and minimum temperature collected from meteorological stations of the study area mean daily air temperature were obtained for 20 available stations.

$$T_{mean} = \frac{T_{max} + T_{min}}{2}$$ <div align="right">Equation 4-2</div>

Where T_{max} is the daily maximum temperature, T_{min} is daily the minimum temperature and T_{mean} is the daily mean temperature. Consequently, to acquire a spatially distributed mean air temperature, an interpolation using the DEM was applied. DEM and mean air temperature were crossed and days with high correlation values of -0.65 to -0.78 were selected; accordingly daily regression equations using the DEM were derived. This equation is used for interpolation of air temperature for the whole area. The equation for fitting as an example for one day is:

$$Temp = 25.159 + (-0.005 * DEM)$$ <div align="right">Equation 4-3</div>

Where *Temp*= Daily mean air temperature and *DEM*= Digital Elevation Model

4.1.1.2. Air pressure

Meteorological data for pressure was not available for the study area. Therefore, using the DEM the following equation is used to get reference pressure (Allen *et al.*, 2011).

$$P_{ref} = 101300 \times \left(\frac{293 - 0.0065 \times DEM}{293} \right)^{5.26}$$ <div align="right">Equation 4-4</div>

Where P_{ref} = reference pressure (pa), *DEM*= Digital Elevation Model (m)

Consequently, for surface pressure analysis, mean daily air temperature of 20 degree Celsius was used which accounts for pressure increase of 23 pa over a 2 meter difference, which is the reference height where other meteorological parameters have been measured (Maathuis and Mannaerts, 2012).

$$P_{sur} = P_{ref} + 23$$ <div align="right">Equation 4-5</div>

Where P_{sur} = Surface Pressure (pa) and P_{ref} =reference pressure (pa).

4.1.1.3. Specific Humidity

The ratio of water vapour pressure to the moist air pressure is called specific humidity. Usually, this parameter can be considered constant. For this study it is calculated using the following formula (Xin, 2007).

$$q = \frac{5}{8} \cdot \frac{e_a}{p}$$ <div align="right">Equation 4-6</div>

Where q= specific humidity, ea= actual water vapour pressure, and P is air pressure (pa). In addition e_a can be calculated using relative humidity and e_o and e_o can be calculated using the following formula (Allen*, et al.*, 1998):-

$$e_a = \frac{RH_{mean}}{100}\left[e^o \cdot T\right]$$
<div align="right">Equation 4-7</div>

Where:-RH is relative humidity, and e^0 is saturation vapour pressure at the air temperature T [kpa], T mean air temperature [ºc] (Allen*, et al.*, 1998).

$$e^o(T) = 0.6108\exp\left[\frac{17.27T}{T+237.3}\right]$$
<div align="right">Equation 4-8</div>

Finally a moving average inverse distance method was used for spatial representation.

4.1.1.4. Wind Speed

Daily wind speed measured at 2m was collected during the field work from meteorological stations. A moving average inverse distance method was used to interpolate it for spatial representation. Consequently, a correction factor of 0.75 is used to change to surface wind speed using the equation below (Maathuis and Mannaerts, 2012).

Wind Speed at surface= 0.75 * wind speed measured at 2m
<div align="right">Equation 4-9</div>

4.1.2. Remote Sensing Data Pre-processing

The remote sensing dataset was imported using the GEONETCast toolbox version 1.3 plugin in ILWIS. The main objective of GEONETCast toolbox is to allow the user, who operates a EUMETCast-GEONETCast ground receiving station to easily manage the incoming data stream and to import the data into a common freeware GIS-RS environment (Maathuis*, et al.*, 2011a).The toolbox allows import of various data sources relevant for environmental monitoring through a Graphical User Interface (GUI) using the ILWIS software. Figure 4-2 shows the toolbox in ILWIS. A description of functionality, installation and configuration of the toolbox is provided by the GEONETCast toolbox user guide (Maathuis*, et al.*, 2011a).
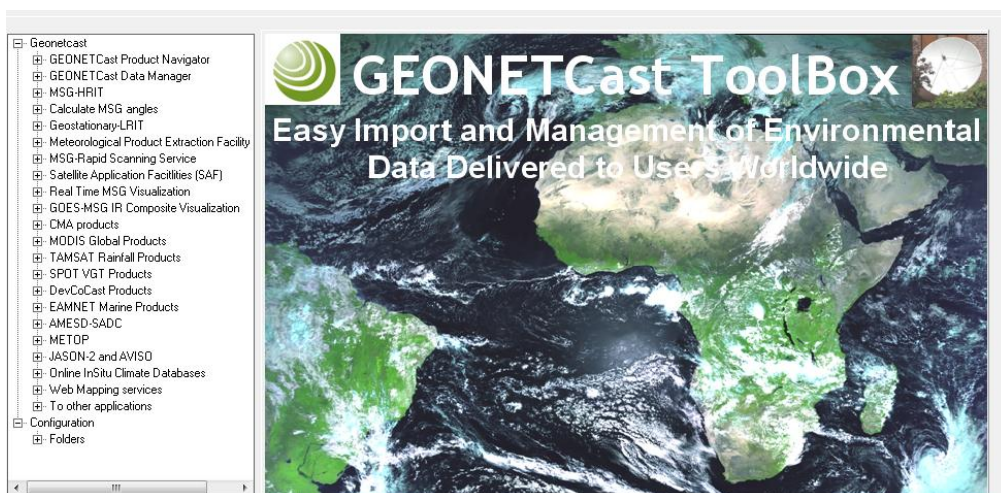

Figure 4-2: The GEONETCast toolbox version 1.3 menu structure as plug-in within ILWIS.

All input parameters for the SEBS model were found or derived on a daily basis. The products found from LSA SAF on a daily basis are Albedo, Leaf Area Index (LAI), Fraction Vegetation Cover (FVC), and Daily Downward Surfaces Shortwave Flux (DIDSSF). These products were imported using the

GEONETCast toolbox plugin version 1.3, from July 14/ 2010 - November 30/2010. Other input parameters such as sun angle was computed using GEONETCast toolbox calculation routine " calculate MSG angle" providing the year, month, day and time to calculate solar and zenith angle maps. In addition, NDVI is another input for SEBS model; here a constant value for a consecutive 10 days period is used because the data used were obtained from the decadal SPOT VGT product. Another input is the DEM map. For this purpose the 1km DEM was resampled into 3km to use it in combination with the MSG data of 3km resolution. Other input required, such as LST (available at 15 min interval) and emissivity (not available) are further explained in the next section.

4.1.2.1. Land Surface Temperature

LST produced by LSA SAF has a temporal resolution of 15 min. For this study daily LST is required in order to be used in the SEBS model. To get a representative LST per day the following steps were taken. First, all the images at 15 min time interval were obtained for each day of the months, then the 1st, 11th and 2lst day of each month (from August 14th to November 30th of 2010) are selected to plot LST against time. This is used to obtain maximum, minimum and mean representative LST per day. It shows the change of LST along the day as well as the change over the months selected. Finally, mean LST was found at 7 A.M UTC time (local time 10.00 A.M.). Therefore, the 0.7:00 A.M. LST is taken as a representative LST for the whole period of the study. Figure 4-3 shows an example of the variation in LST observed on 21st September 2010 over 24 hours of the day. As can been seen from the graph the maximum LST was recorded around 10 A.M UTC and the minimum was recorded around 4 A.M. UTC. The mean LST of 37°C observed at 7 A.M UTC.
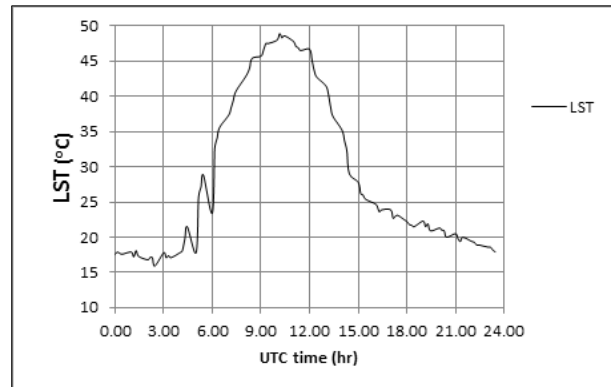
Figure 4-3: One day LST observation 21st September, 2010 daily distribution

Apparently, LST cannot be observed or calculated if there is cloud cover. For the pixels which had undefined values because of the clouds a relationship was developed between LST and the DEM. A high correlation value of -0.768 was found. Therefore, the DEM was used to interpolate for the undefined pixels using a linear least square fitting method to obtain continues spatial distributed value of LST for each pixel. The equation for fitting is as follows:

$$LST = 27.926 + (-0.01 * DEM)$$

<div align="right">Equation 4-10</div>

Where *LST*= Land Surface Temperature and *DEM*= Digital Elevation Model and finally the unit was changed into degree Kelvin.

4.1.2.2. Emissivity

Emissivity is the ratio of energy radiated by a surface in relation to a black body and can be derived from the FVC using the formula after Wittich (1997).

$$Emis = 0.985FVC + 0.96(1 - FVC) + 0.015 \hspace{3cm} \text{Equation 4-11}$$

Where: *Emis* = Emissivity and *FVC* is Fraction of Vegetation Cover.

4.2. SPOT Vegetation NDVI Pre-processing

SPOT Vegetation NDVI (SPOT VGT NDVI) as explained in section 3.2.2.3 are a ten-day composite data as processed by selecting pixels with the maximum NDVI during a 10 day period with full 1km x 1km spatial resolution Thus, in addition to the SPOT VGT NDVI map a status map was provided which is used to filter the NDVI values on their quality. This map was used to extract only pixels that meet the following criteria: cloud free, land pixel and having a good radiometry in the red and near infrared channels. Therefore, to extract only NDVI values meeting the selection criteria, a procedure using Integer Division Operator (DIV) and Modulus Operator Return (MOD) was used in ILWIS. Further explanation on the procedure adopted is given by (Maathuis *et al.*, 2011b). Subsequently, the NDVI map was imported into the **S**oftware for the **P**rocessing and **I**nterpretation of **R**emotely **S**ensed **I**mage **T**ime **S**eries **(SPIRITS)** (section 4.3).

Time series analysis of Long Time Average (LTA) NDVI statistics extraction was performed using SPIRIT following the methodology proposed by Genovese *et al* (2001). According to Genovese *et al* (2001) integration of NDVI with administrative region and the land cover data allows a better exploitation of the NDVI time series by partly reducing the problem of mixed values. The use of an independent land cover can increase the information content of the extracted time series of NDVI. Hereafter, extractions of NDVI for Amhara districts for rainfed cropland were performed. The computation starts from 1st of January 1999 to December 21th 2010 on decadal basis using maximum, minimum and mean NDVI. This was then compared to the recent 2010 growing season NDVI.

4.3. Data Pre-processing for SPIRITS

Software for the **P**rocessing and **I**nterpretation of **R**emotely **S**ensed **I**mage **T**ime **S**eries **(SPIRITS)** is newly available software used to analyze time series remote sensing data. It was developed by the Joint Research Centre's Monitoring Agricultural Resources (JRC/MARS) Unit in collaboration with Flemish Institute for Technological Research (VITO). The general overview of its function illustrated in Figure 4-4. The software allows extracting input dataset statistics per administrative region and land cover class. Therefore, for this study to extract the time series of all dataset in SPIRITS, a district level and masked rainfed crop land mask as classified by the LSA SAF land cover product was used. The main consideration of land cover and administrative region was to create Regional Unmixed Means (RUM) to facilitate the statistics extraction for each administrative level / unit (country, province or districts) based on land cover/land use types (Tote *et al.*, 2011). RUM was used to consider only pixels which are covered by 100% of the land cover for each administrative level. The data was imported using batch routine scripts from ILWIS in order to process the data in SPIRITS. Data requirements for LTA extraction, for example NDVI, RFE1, RFE2 and FEWS NET PET their mean, maximum and the minimum values were conducted using SPIRITS. The general method followed for the import of datasets to SPIRITS is shown in figure 4-5.
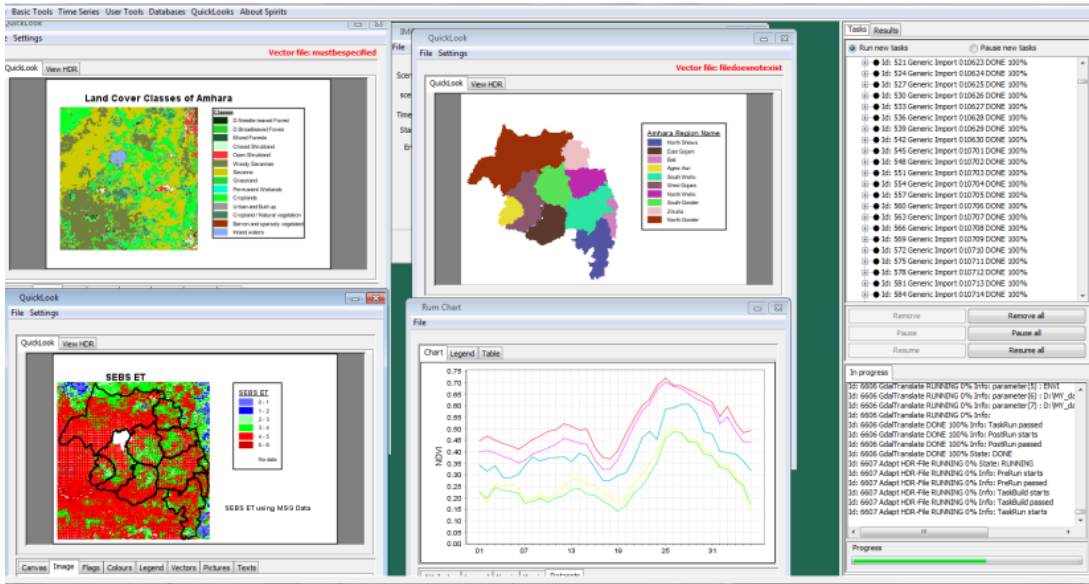
Figure 4-4: General overview of SPIRITS functionality.
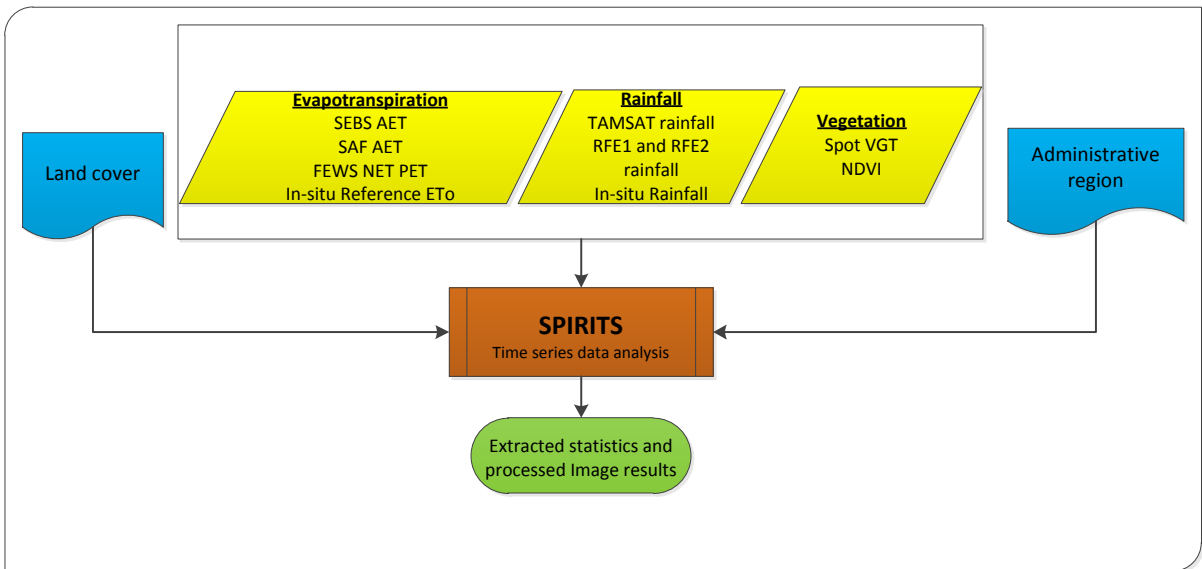
Figure 4-5: SPIRITS time series statistics extraction of variables using land cover and administrative regions.

5.   DATA ANALYSIS AND RESULTS

5.1.   Land Cover Data Analysis

5.1.1.   Amhara Region Rainfed Cropland

Figure 5-1 illustrates the classification procedure to mask the rainfed agriculture in the study area. Verification was done by the visual observation during the field work. Observed points (84) on rainfed croplands successfully overlaid on four different pixels of LSA SAF land cover product; a success rate of 100%. Figure 5-1 shows LSA SAF land cover and mask made for rainfed croplands overlaid by the point map showing field observations together with rainfed agricultural crops pictures taken at the same time.
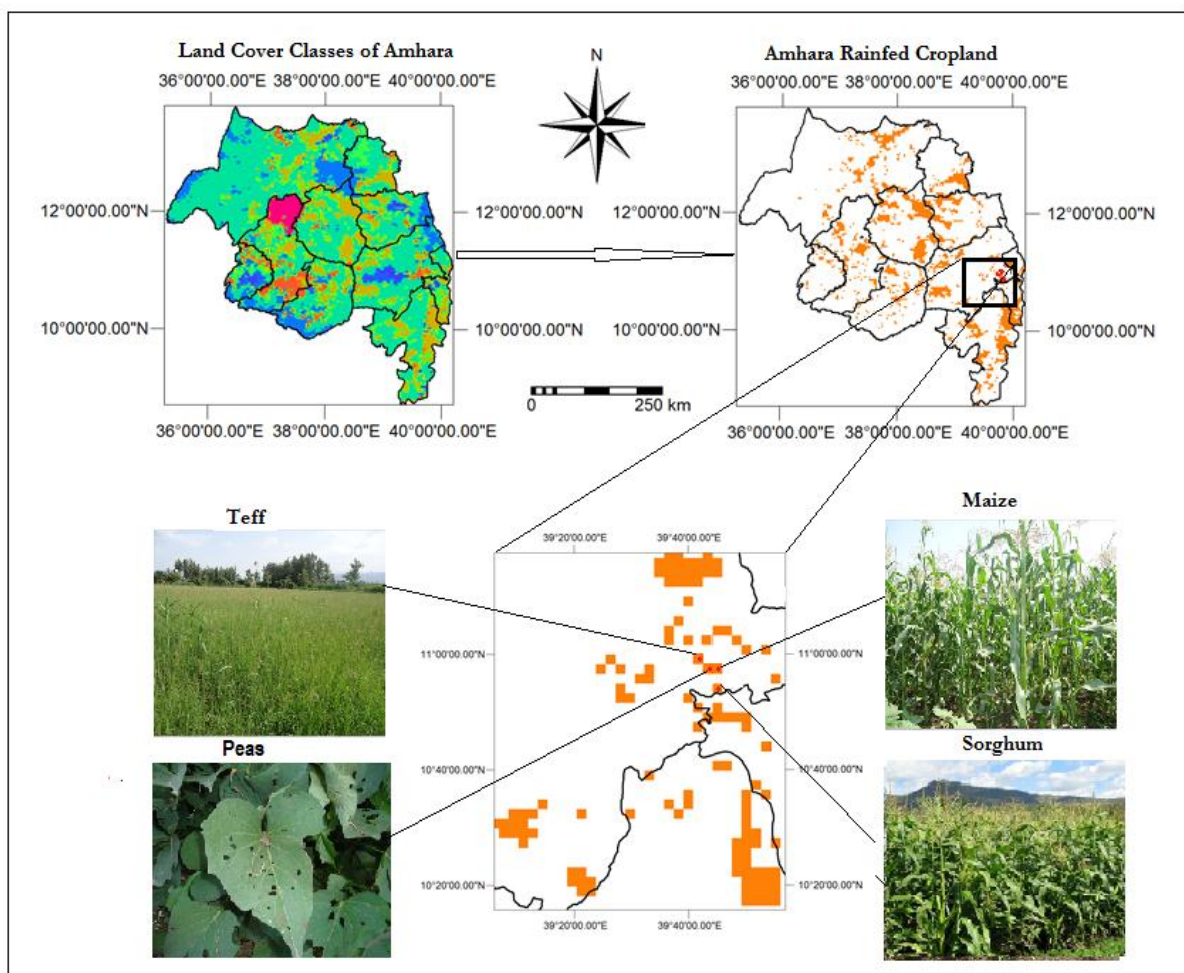
Figure 5-1: LSA SAF land cover classification and masked rainfed croplands with overlaid point map of observed cropland location in the study area.

5.2.   Evapotranspiration Data Analysis

5.2.1.   Temporal and Spatial Distribution of Remote Sensing Actual Evapotranspiration

The temporal and spatial distribution of AET is shown in figures 5.2 and 5.3 below. The figures illustrate estimation of both SEBS and SAF AET during the 2010 growing season. The result shows both remote

sensing methods estimate AET in a comparable manner. The AET varied between 1 to 3 mm/day during July and August which is the main rainy season of the area which coincides with the initial stage of the crop. The AET observed from 1.5 to 3.5 mm/day in September that is during end of rainy season or maturity stage and 0.5-1.5 mm/day in October and November which is during harvest time of the crops. The highest values of AET in both estimations can be observed in September. This might be associated with high vegetation growth directly after the rainy season. On the other hand, although the estimation of AET is similar, a discrepancy of SEBS AET on daily values estimation was observed during the harvest period compared to SAF AET which showed a solid more or less straight line from the 2nd of October to 30th of November.
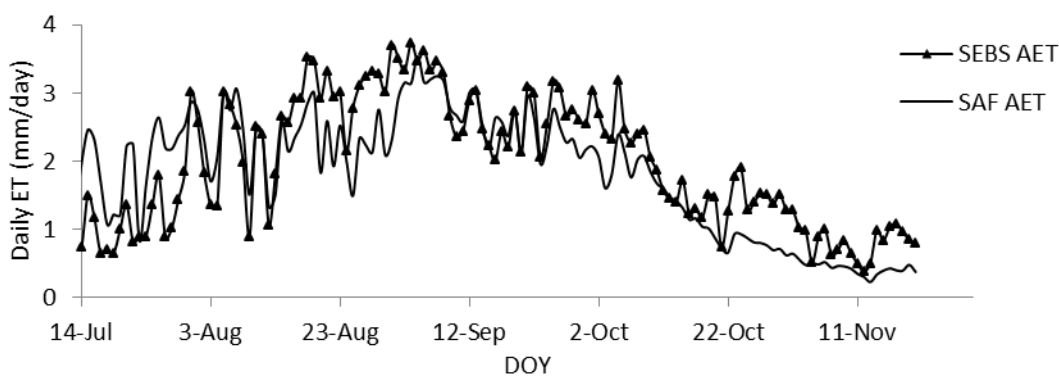
Figure 5-2: Daily estimation of SEBS AET and SAF AET over the rainfed croplands of East Gojiam (upper figure) and North Shewa (lower figure).

Figure 5-3 shows the result of the two AET spatial distributions for the whole Amhara region over the growing season of 2010. The result shows that the amount of AET follows the trend of the growing season. Decadal sum values of AET ranged from 10-30mm in the initial stage or sowing period of the crop, 30-45mm during the maturity stage or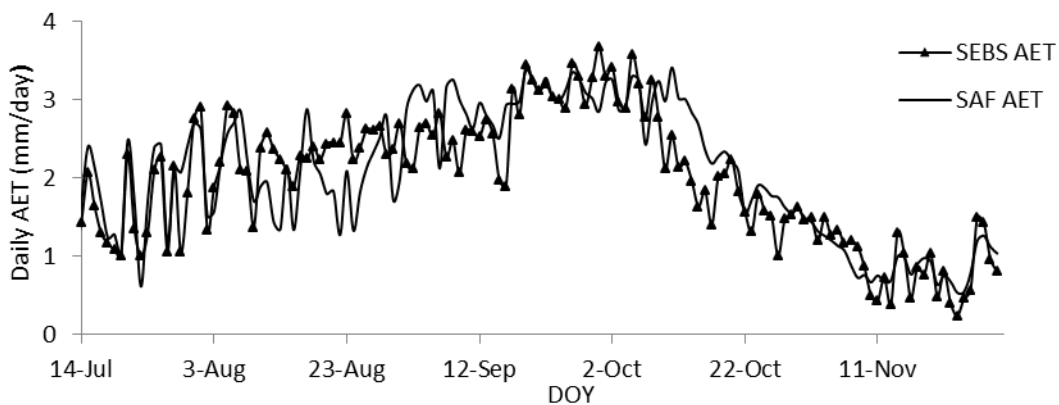 peak period and 5-20 mm during the late stage or harvest time for most of the districts in the Amhara region. Furthermore it can be observed that there was an underestimation of the SAF AET during the initial stage in the south west and during maturity stage in south east part (figure 5-3 lower figure).
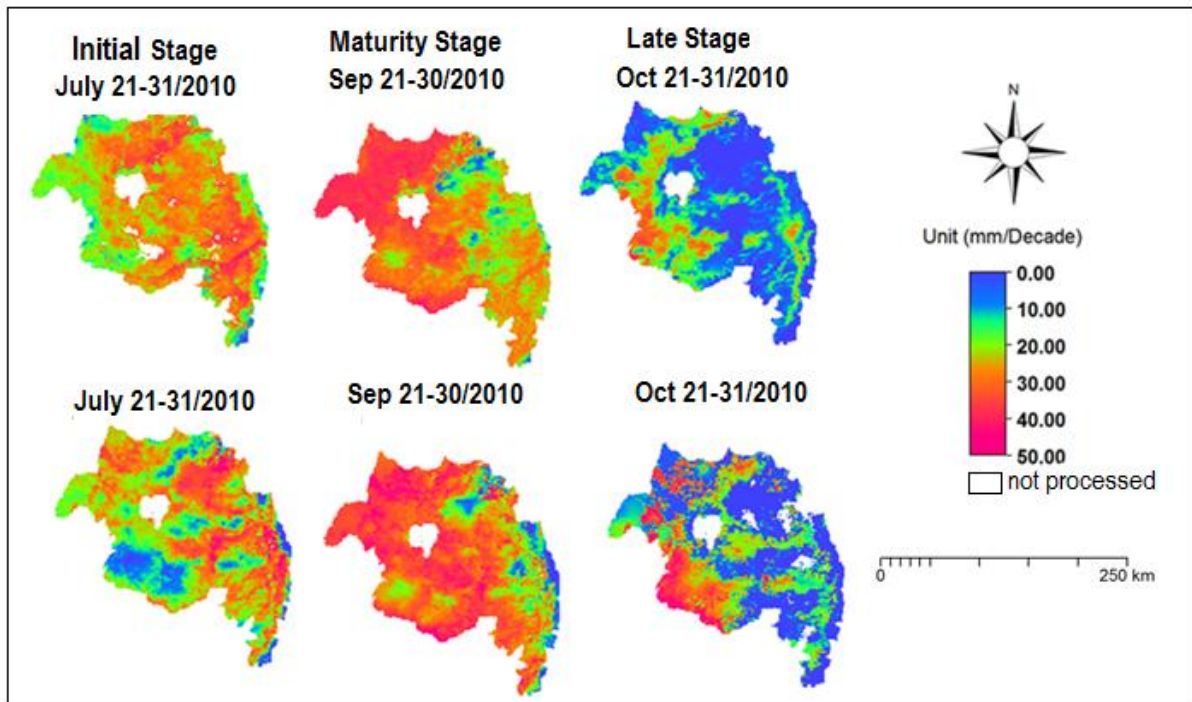
Figure 5-3: Decadal SEBS AET (upper maps) and SAF AET (lower maps) for the initial or sowing season, maturity or peak season and late or harvest season of the Amhara region.

5.2.2. Comparison of SAF with SEBS Estimated

Comparisons of SAF AET against SEBS AET are shown in figure 5-4. The figure shows the scatter plots of SEBS AET against SAF AET for six districts, the other four district figures are indicated in Appendix E. The result indicates that the two estimation of AET have a strong relation for rainfed crop lands with R^2 =0.88, 0.85, 0.84, 0.79, 0.79, 0.76, 0.76, 0.74, 0.72, 0.50 for South Gonder, North Wello, West Gojiam, South Wello, Zikulla, North Shewa, North Gonder, East Gojiam, Agew/Awi and Bati respectively.
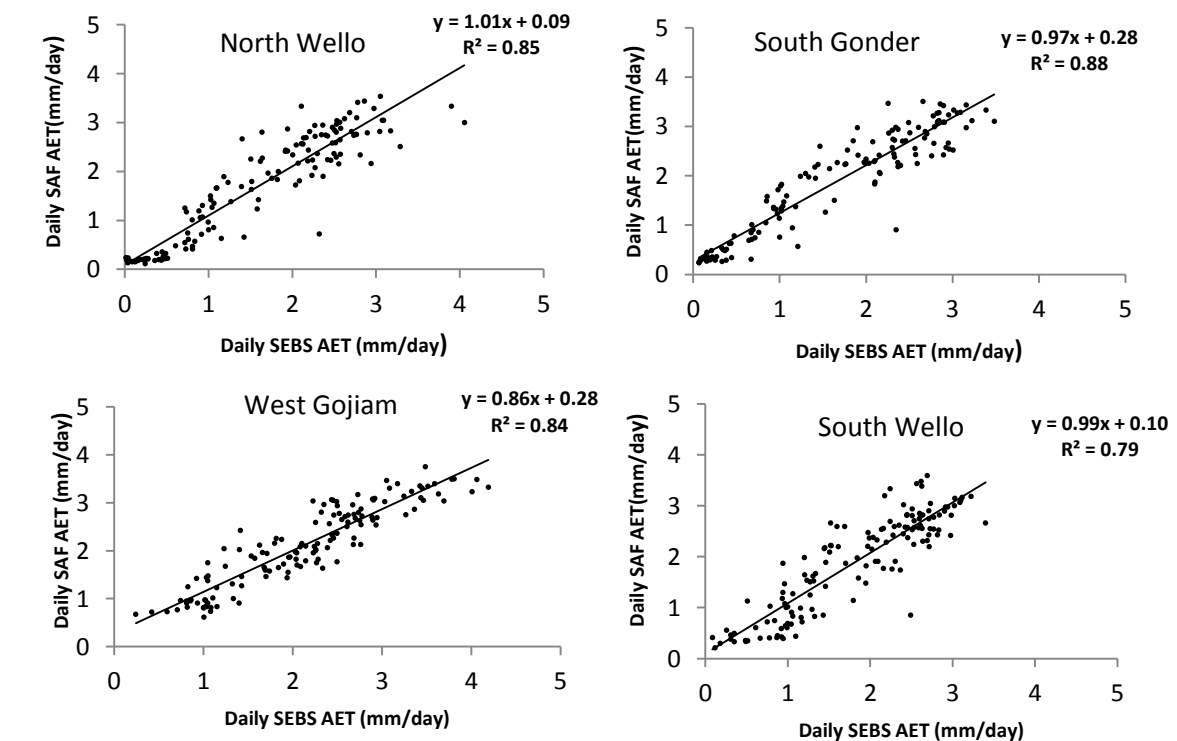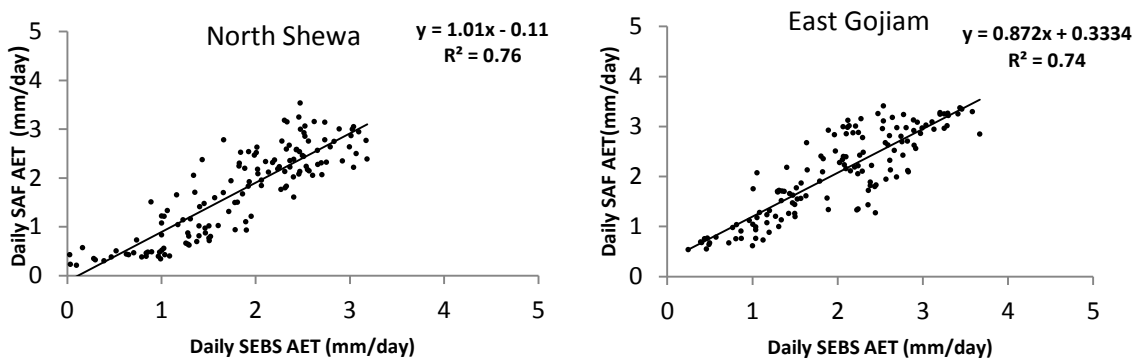
Figure 5-4: Scatter plot of daily SAF AET and daily SEBS AET on rainfed cropland of Amhara districts.

5.2.3. Comparison of SEBS AET and SAF AET with Reference ETo

Figure 5-5 illustrates the two remote sensing AET compared with reference ET_o. It can be observed that during the rainy season the relative evaporation (ratio of AET to the reference ET_o) was approximately one. In addition, during the dry season the AET shows smaller values ranging between 0.5-1.5mm/day but the ET_o shows high values (3.5 - 4 mm/day). The result also shows that for the two days which receive rainfall during the dry period (15th October 2010 and 26th October 2010) of 4.5mm/ day and 3.0 mm/day respectively), the two AET's show an increase of 0.5mm/day and the reference ETo exhibits a tendency to decrease.
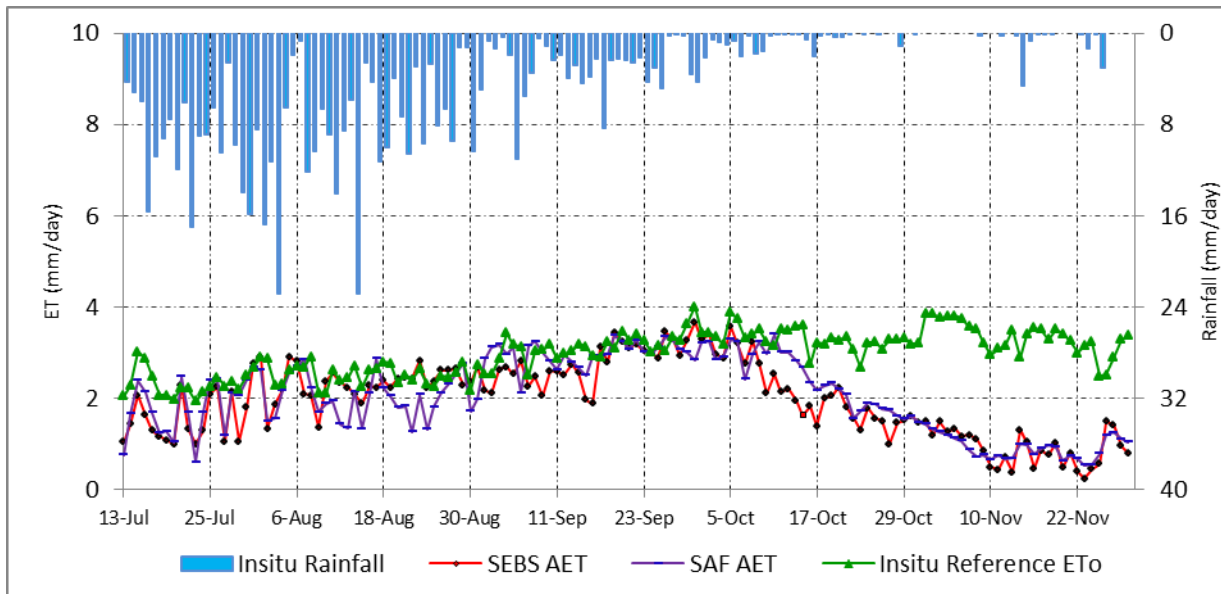
Figure 5-5: SEBS and SAF AET against reference ETo in North Gonder district.

5.3.   SPOT VGT NDVI Data Analysis

5.3.1.   Temporal and Spatial Distribution of SPOT VGT NDVI

Figure 5-6 and figure 5-7 shows LTA and current 2010 temporal NDVI characteristics together with LTA and current 2010 rainfall for North Gonder and East Gojiam districts respectively. The time series trend shows a slightly below average NDVI during the growing period. The NDVI might be associated with a lower amount of rainfall compared to the average during the start and end of the rainy season. On the other hand, the rainfall received during the 21st July 2010 up to 10th of August 2010 was above average, subsequently the NDVI showed an improvement and reached up to the average. In East Gojiam NDVI was even slightly higher than the average.
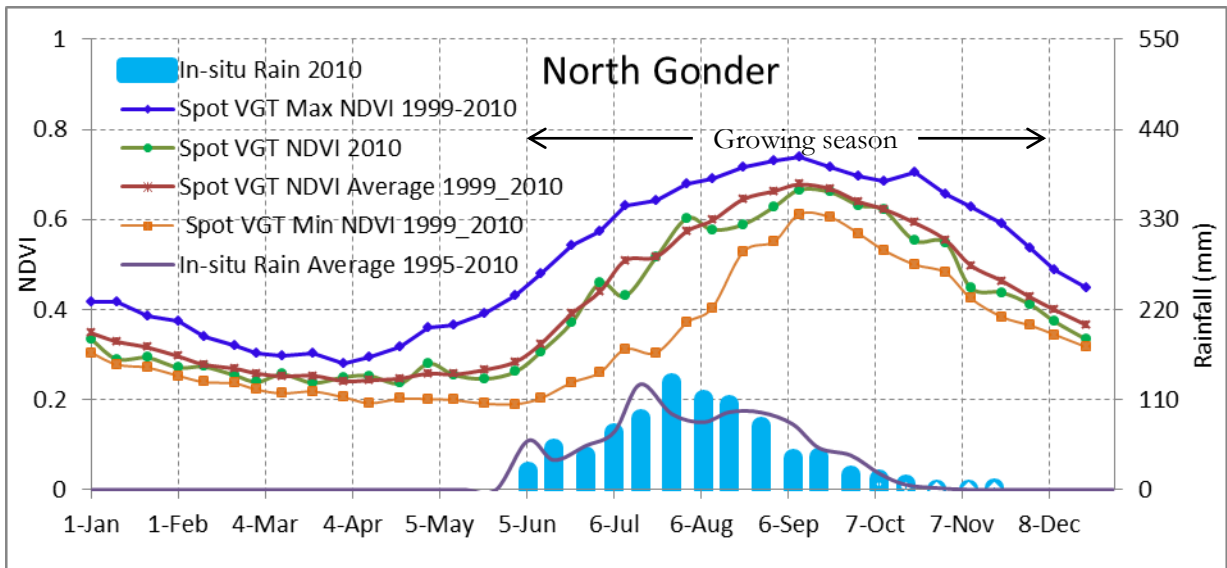
Figure 5-6: Long time average and 2010 NDVI with long time average and current 2010 rainfall for North Gonder district.
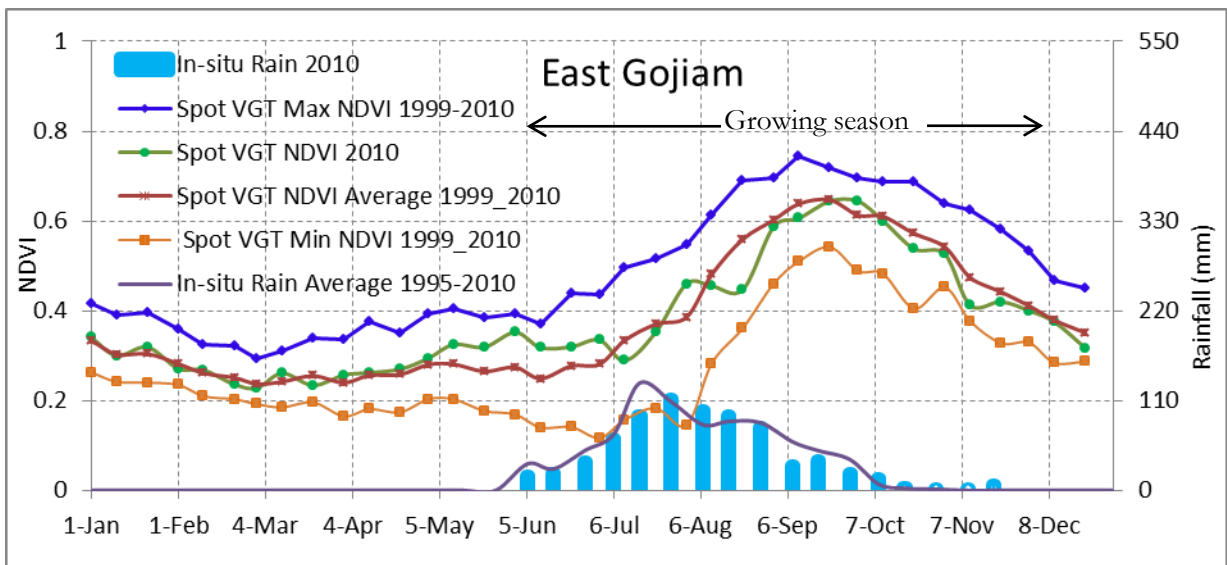
Figure 5-7: Long time average and 2010 NDVI with long time average and current 2010 rainfall for North Gonder district.

NDVI was further analysed based on the patterns showing the phenology of NDVI from 1999 to 2010 for each district of Amhara as presented in Figure 5-8. It had been used to classify the drought situation for each year using the mean and standard deviation (SD) of the maximum NDVI. Table 5-1 shows the analysis of drought situation for each district. It was clearly evident that for all of the districts 1999 and 2009 were the wettest years. Most districts showed 2001 as the driest year except Bati district. This could be explained by the fact that cultivation is usually done during the second rainy season (February to June). 2006 was also observed to be a dry year for most of the districts except North Shewa and East Gojiam districts. The graphs showing the same trends for the other districts are given in appendix F.
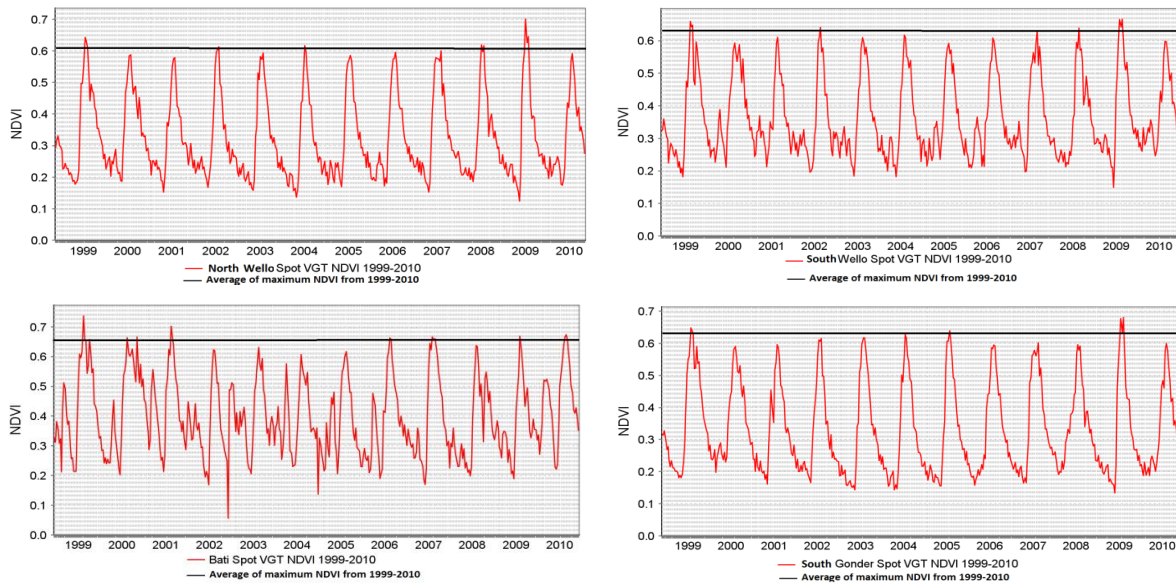
Figure 5-8: Pattern of decadal NDVI during the 11 years (1999-2010)

Table 5-1: Analysis of drought using maximum NDVI

| Districts	Mean	SD	Drought affected years	Slight drought affected years	No drought affected years
North Shewa	0.632	0.024	2001, 2004, 2005, 2007, 2010	2002, 2003, 2006, 2008	1999, 2000, 2009
East Gojiam	0.669	0.031	2001, 2003, 2004, 2010	2000, 2002, 2005, 2006, 2007, 2008	1999, 2009
Bati	0.657	0.037	2002, 2003, 2004, 2005, 2008	-	1999, 2000, 2001, 2006, 2007, 2009, 2010
Agew/ Awi	0.709	0.018	2000, 2001, 2006	2002, 2005, 2008	1999, 2003, 2004, 2007, 2009, 2010
South Wello	0.622	0.025	2000, 2001, 2005, 2006, 2010	2003, 2004	1999, 2002, 2007, 2008, 2009
West Gojiam	0.698	0.024	2001, 2006	2000, 2002, 2007, 2008, 2010	1999, 2003, 2004, 2005, 2009
North Wello	0.610	0.034	2000, 2001, 2005	2003, 2006, 2007, 2010	1999, 2002, 2004, 2008, 2009
South Gonder	0.617	0.027	2000, 2001, 2006, 2007, 2008, 2010	2002, 2003, 2004	1999, 2005, 2009
Zikulla	0.615	0.029	2000, 2001, 2006	2003, 2004, 2005, 2007, 2010	1999, 2002, 2008, 2009
North Gonder	0.686	0.023	2000, 2001, 2006, 2007, 2008, 2010	2004, 2005	1999, 2002, 2003, 2009
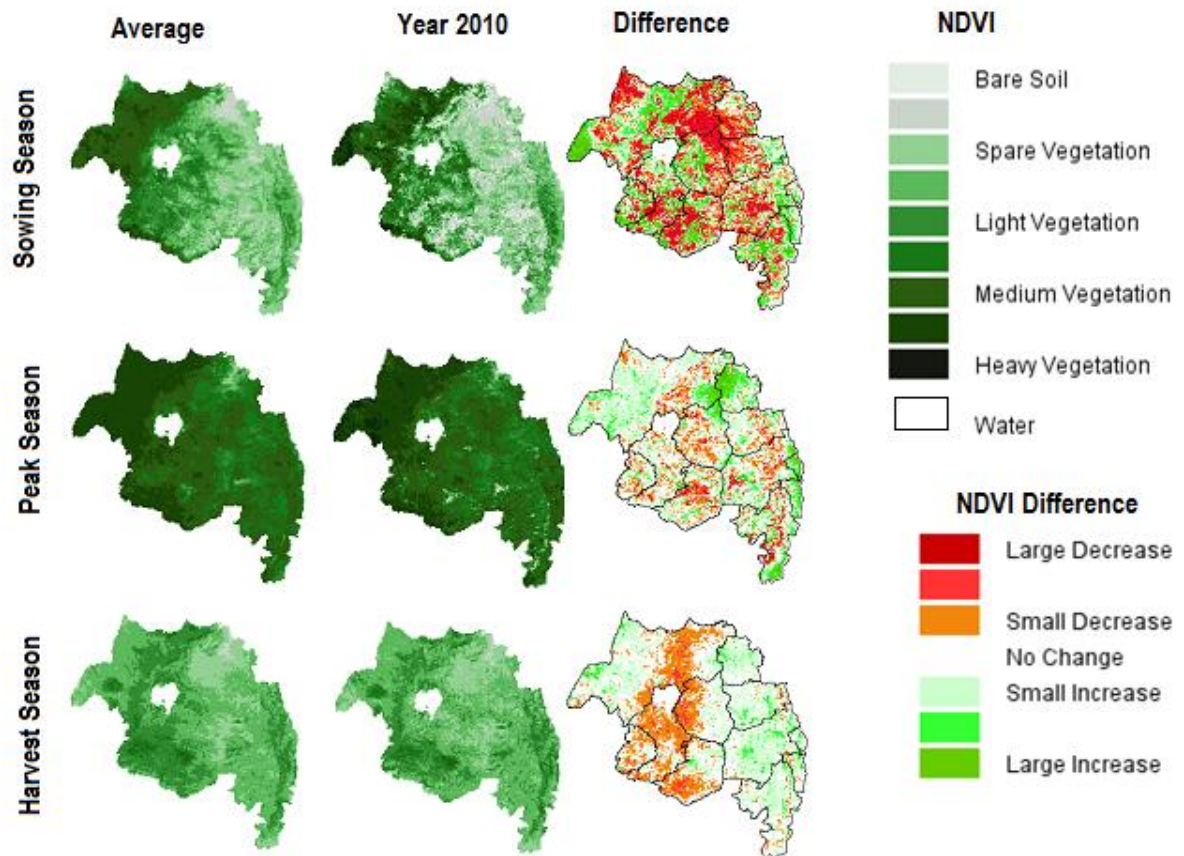
Figure 5-9: NDVI difference images for Amhara region assessing the growing season in 2010.

The 2010 spatial distribution of NDVI was analysed together with the LTA NDVI and the difference from the LTA average during the sowing, maturity and harvest stage. In 2010 the growing season started with a distinct unfavourable condition showing lower than normal amount of vegetation for North Gonder, North Wello, Zikulla, North Wello and South Wello (figure 5-9 sowing season). The situation changes drastically during the peak season. Previously affected vegetation showed a change and it now only shows a slight deviation of vegetation condition compared to the average (figure 5-9 peak season). However, the situation did not continue until the harvest period. North Gonder, South Gonder, West Gojiam and East Gojiam regions shows below average NDVI but the eastern part of Amhara shows a higher than normal amount of biomass throughout the region (figure 5-9 harvest season).

5.4.   Drought Analysis

5.4.1.   Temporal Drought Analysis

Temporal drought was analyzed by merging remote sensing and *In-situ* data. The datasets utilized includes: LTA and 2010 main growing season hydro-meteorological variables, LTA and 2010 NDVI together with derived drought indexes. Figure 5 -10 and figure 5 -11 presents the temporal drought analysis made for North Gonder and East Gojiam districts respectively. In both figures part "A" presents the relationship of rainfall and evapotranspiration (both AET and PET), part "B" shows trends of NDVI and part "C" illustrates the derived drought indexes. The following sections firstly describe the relationships that can be observed (A, B, C) individually and later the overall relationship among parts A, B and C are given.

Rainfall and ET (AET and PET) (see figure 5-10 and 5-11 "A") analysis results showed

- The three used rainfall estimates (RFE, TAMSAT and *In-situ*) shows comparable trend in estimating the rainfall for the study area.
- The LTA mean found from RFE underestimate the rainfall compared to the LTA mean *In-situ* rainfall.
- Similar estimation of decadal AET was observed for the SAF and SEBS except a slight underestimation of SAF.
- FEWS NET PET underestimates PET during the rainy season but in overall estimation it overestimates PET compared to reference ET_o.
- Maximum AET is observed during September.
- The 2010 main growing season receives below normal rainfall in all decades of the growing season except last decade of August for North Gonder districts. However for east Gojiam it is on below average at the start and end of the growing season.

NDVI trend analysis (See figure 5 -10 and figure 5- 11 "B") indicated that

- The NDVI profile shows below average NDVI during the 2010 main growing season in both North Gonder and East Gojiam districts. This was with the exception over the last decade of September for East Gojiam district.
- The 2010 vegetation development for East Gojiam and North Shewa districts are far from the potential maximum NDVI.

Analysis of the drought indices (See figure 5-10 and figure 5-11 "C") suggested that

- According to the threshold from literature, drought is indicated for all decades during 2010 main growing season for North Shewa and East Gojiam districts, except the first decade of August for North Gonder district and first decade of August and last decade of September for East Gojiam districts.

Interrelation of the Part A, B, C

- There was a strong relation between NDVI and rainfall. The response of NDVI can be observed two decades after the rainfall changes.
- There was also a relation of NDVI with AET, maximum AET was observed when there is maximum NDVI during September.
- Generally the trend of AET along the growing season follows the trend of NDVI. When NDVI increases AET also increases and the reverse is true.
- At North Gonder during the last decade of July, giving lag period of the two decades with respect to the rainfall, the NDVI was above average for North Gonder and the drought indices do not classify this time period as drought condition
- At East Gojiam, last decade of July and during the middle of September, giving lag period of the two decades with respect to the rainfall, the NDVI was above average for East Gojiam and the drought indices do not classify this time period as drought condition
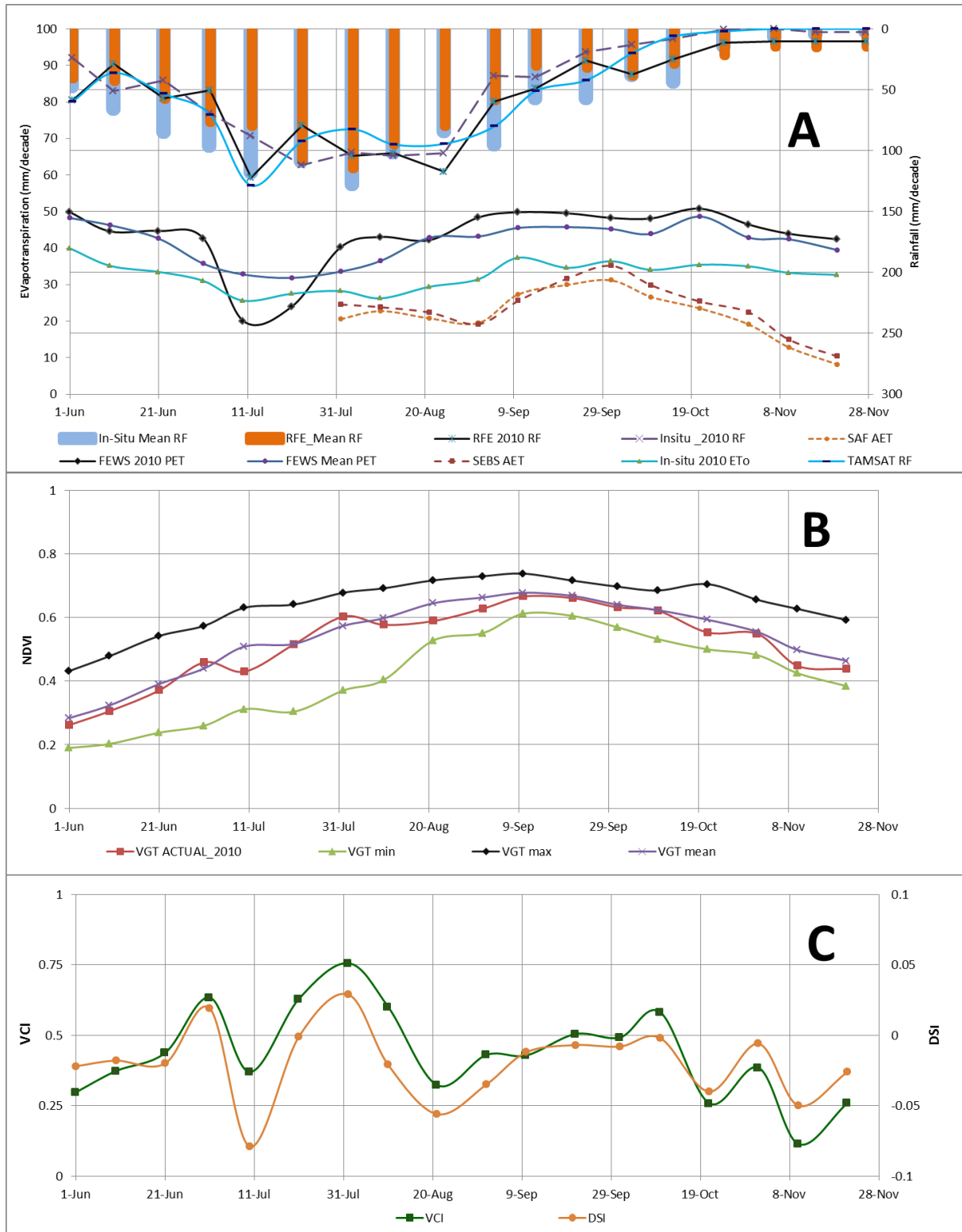
Figure 5-10: Time series LTA rainfall (RF) (*In-situ* Mean RF and RFE_mean RF), current 2010 remote sensing and *In-situ* dataset of rainfall (RFE RF, TAMSAT RF and *In-situ* -2010 RF) together with current 2010 PET and AET (SEBS AET, SAF AET, FEWS PET) with LTA PET from FEWSNET (FEWS mean PET) (**A**), 2010 NDVI and LTA NDVI (VGT ACTUAL_2010, min , max and mean) (**B**) and drought indexes VCI and DSI (**C**) for North Gonder district.
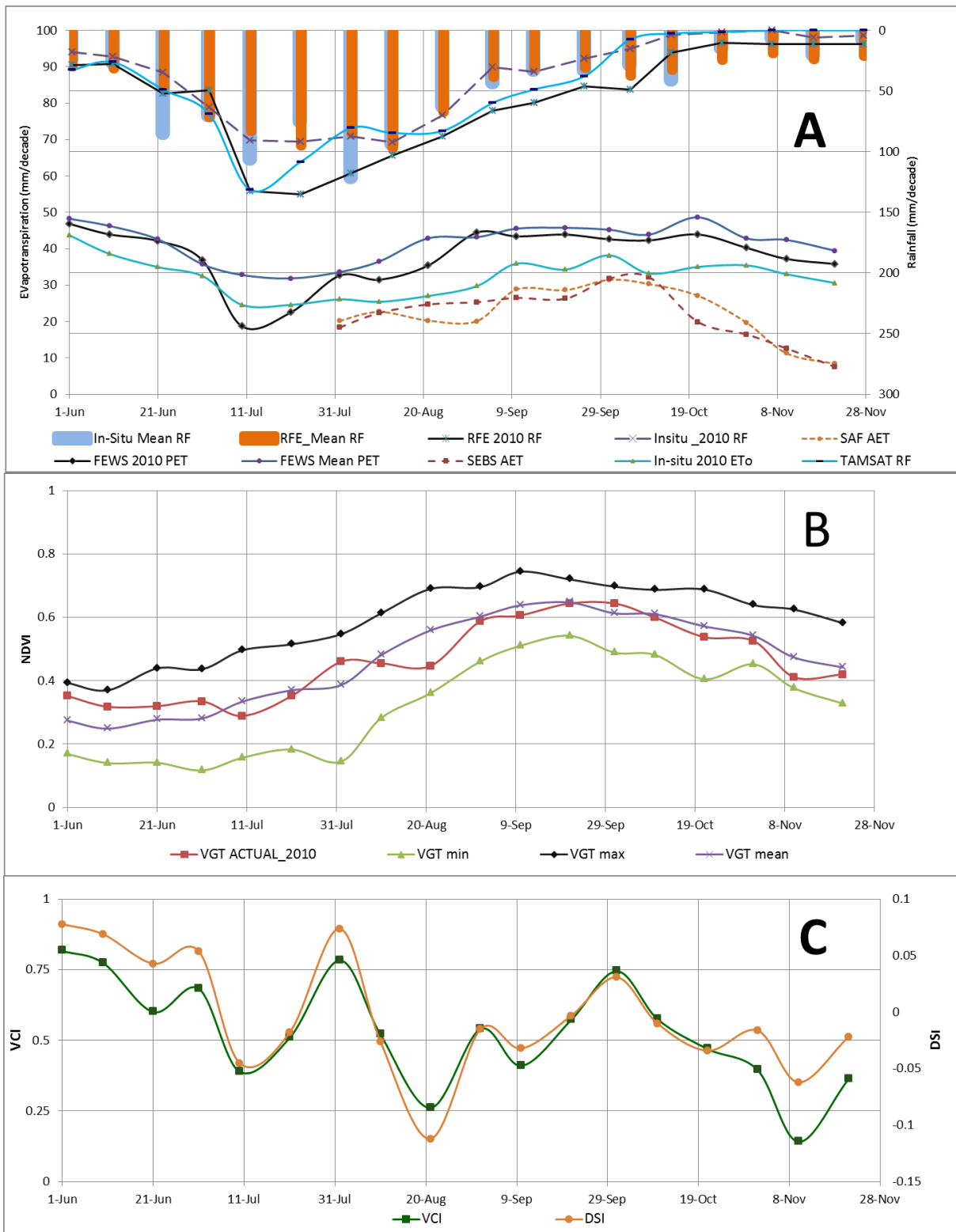
Figure 5-11: Time series LTA rainfall (RF) (*In-situ* Mean RF and RFE_mean RF), 2010 remote sensing and *In-situ* dataset of rainfall (RFE RF, TAMSAT RF and *In-situ* -2010 RF) together with current 2010 PET and AET (SEBS AET, SAF AET, FEWS PET) with LTA PET from FEWSNET (FEWS mean PET) (**A**), 2010 NDVI and LTA NDVI (VGT actual, VGT Min , VGT max and VGT mean) (**B**) and drought indexes VCI and DSI (**C**) for East Gojiam district.

5.4.2. Spatial Drought Classification Maps

The spatial drought classification maps for Amhara region are produced by integrating the three drought indexing methods (section 3.3.3). The drought indexing methods are WRSI, VCI and DSI. The results are presented in figure 5-12 and figure 5-13. Figure 5-12 are decadal drought maps made using "Continuous Method" starting from the first decade of August to the last decade of November. The thresholds used for classification for decadal drought maps are:

- -0.4 - -0.1:extreme drought
- -0.1-0.2: severe drought
- 0.2- 0.5: moderate drought
- 0.5-0.8: average
- 0.8-1.1: moderately moist
- 1.1-1.4: very moist and
- 1.4-1.7: extremely moist

The white areas in both figures 5-12 and 5-13 are the inland water body (Lake Tana) and cloud contaminated pixels for the SAF AET which is used for computing the WRSI_1.

The final map displayed in figure 5-13 are classified into severe drought, sporadic drought, normal, and no drought, based on the sum of each of the decadal drought indexes maps, whether a pixel has an accumulated drought situation or not. The thresholds used for the final classification are <7: severe drought, 7-11: sporadic droughts, 11-15: normal and >15: no drought.
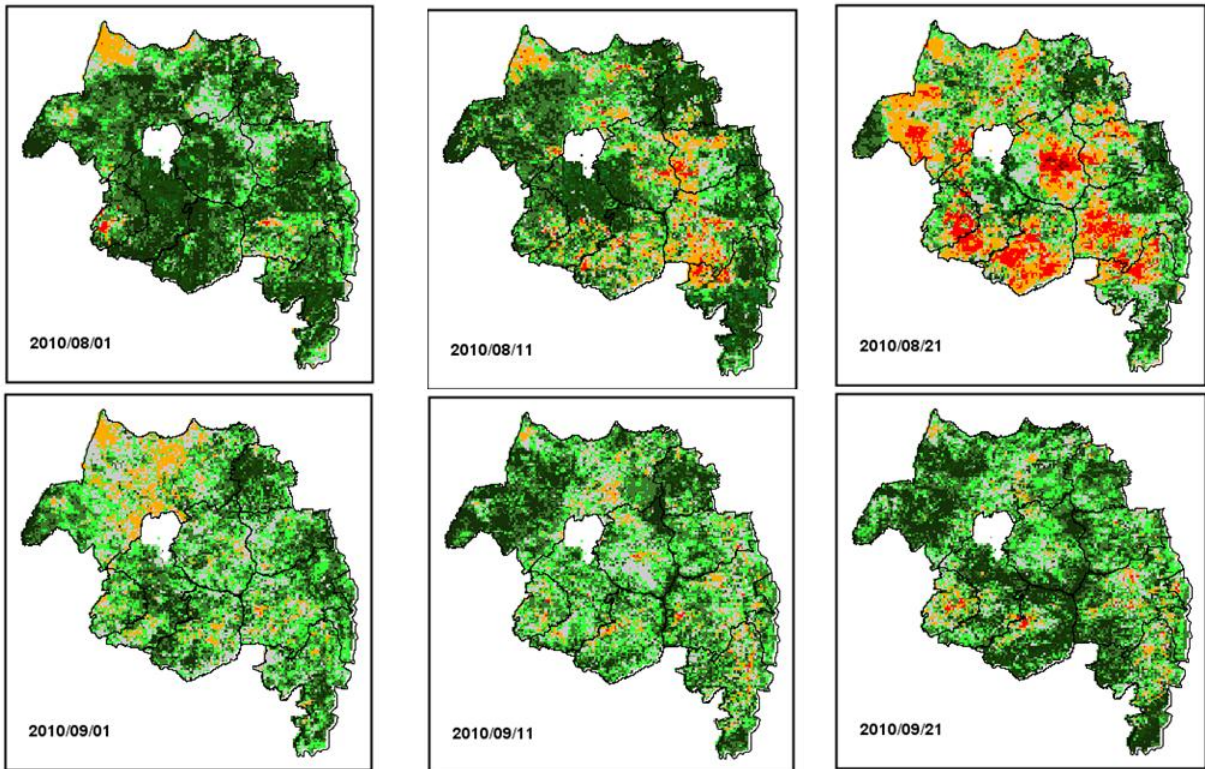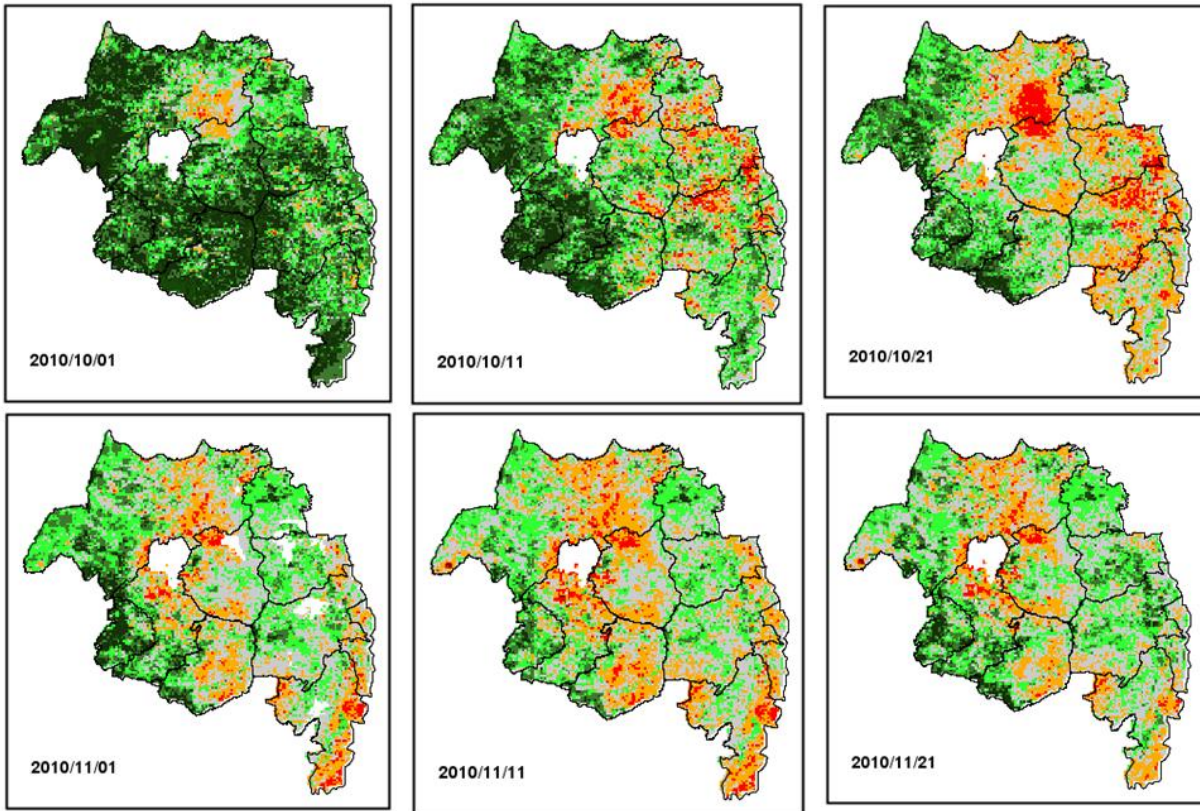
Figure 5-12: Decadal drought classification map integrating three drought indexes VCI, DSI and WRSI
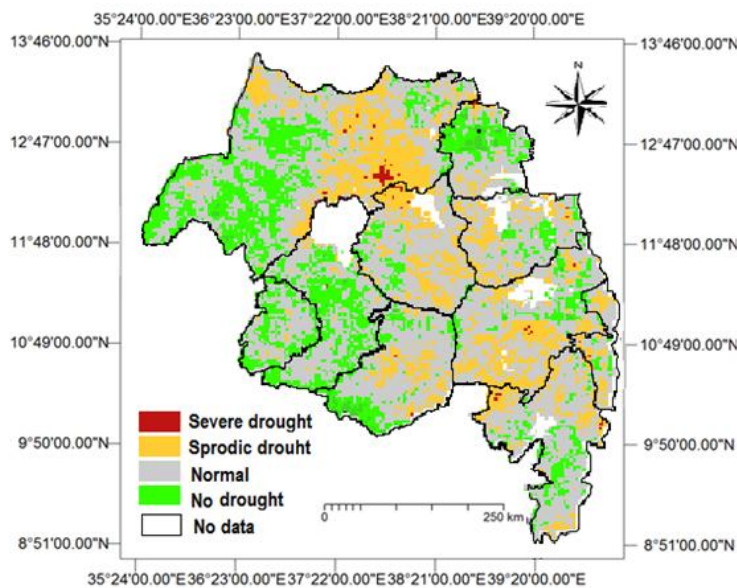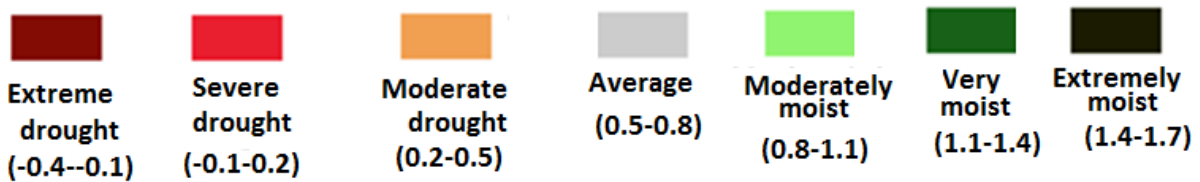
Figure 5-13: "Continouse method" drought classfied map of the Amhara region for the 2010 main growing season.

5.4.3. Comparison of Boolean With Continuous Drought Classification Map

Comparison of "Boolean classification" map with "Continuous classification" approach has been conducted according to the procedure explained in section 3.3.3. Figure 5 -14 presents the two maps. The comparison shown here is for the drought map which is made for the last decade of August. The map could not be classified using the same scale because the "Boolean method" classification does not have more than four thresholds (0-3), since the sum of the three drought indictors will not be greater than 3 (on a pixel basis). The result shows the "Boolean Classification" only provides a rough indication, on the other hand the "Continuous classification" allows more classes to be defined and the classification thresholds can be easily adapted once more appropriate local thresholds are known.
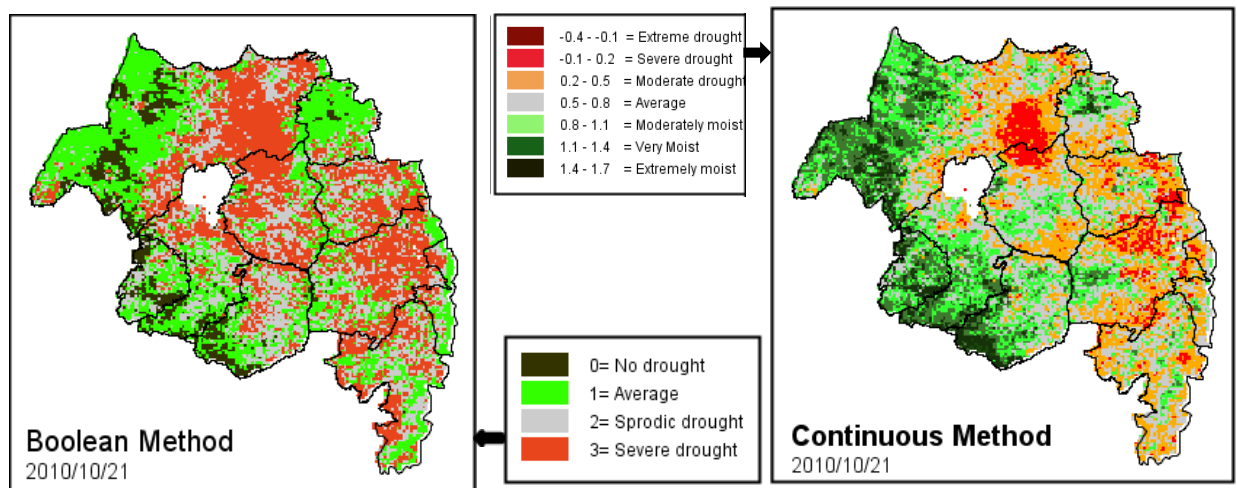
Figure 5-14: Comparison of Boolean drought with continuous drought classification method.

5.5. In-situ Data Analysis

5.5.1. Agricultural Statistics -Yield

To check the reliability of the agricultural statistical data, correlation between cultivated land (in hectare) and production yield (in tons) was made for each district. The result showed that there are better degrees of correlation for only five of the districts of the region. Figure 5 -15 shows the scatter plot between the agricultural yield and cultivated land for West Gojiam district and East Gojiam districts. The scatters plots for the other districts are given in Appendix (G). For districts which showed low correlation a double mass curve data analysis method was used to investigate the behaviour of the records.
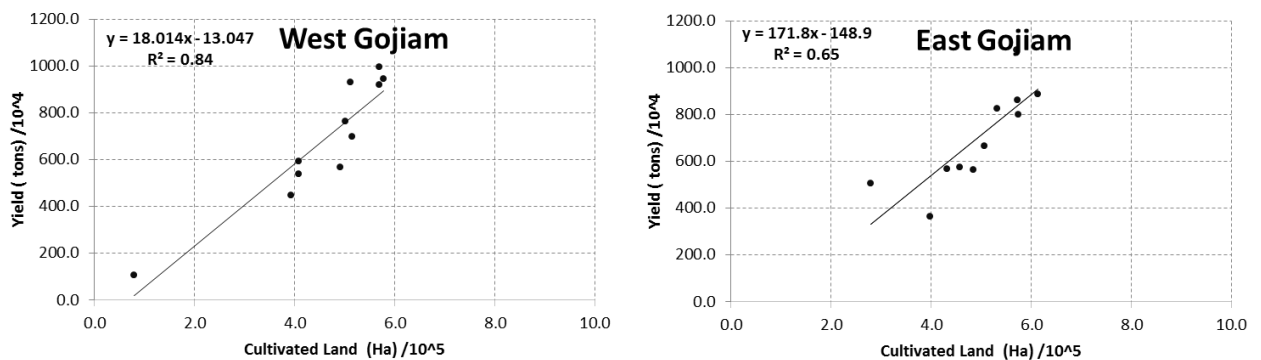
Figure 5 -15: Graph showing the correlation between agricultural production yield and cultivated land for West Gojam and East Gojiam district.

The double mass curve examines cumulative yield (kg/ha) of a district which has a good correlation (West Gojiam) against each districts cumulative yield (kg/ha) which has a low correlation. Figure 5-16 shows a double mass curve of cumulative yield of West Gojiam against cumulative yield of Zikulla and South Wello districts. A break in slope in figure 5-16 shows there is a change of recording from that year onwards. Therefore, outlier values have been discarded for the low correlated districts. Table 5-2 shows the correlation between cultivated land and production yield for all districts in the Amhara region. Table 5-2 also shows the improved correlation found after the outlier values have been omitted together with the omitted years. However, there is no improved correlation found for South Wello and Bati districts, therefore for these two districts no correlation could be formulated with NDVI as well. The reason for Bati is as explained in section 5-3-1 might be due to a different cropping pattern, and for South Wello because the data collected from CSA shows a large change of yield (ton) for a similar area of cultivated land (ha) (see Appendix B South Wello yield data). Therefore, no matter what the growing years are omitted, the correlation could not be improved. Figure 5-17 shows the improved correlation for Agew Awi and North Shewa after the outlier years have been discarded.
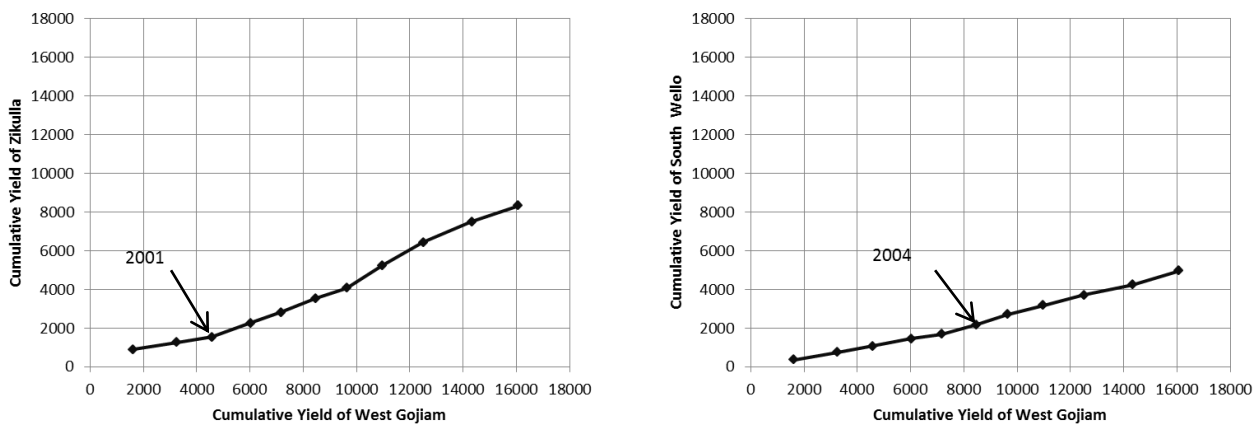
Figure 5-16: Double mass curve of cumulative yield of West Gojiam against cumulative yield of Zikulla (left figure) and South Wello district (right figure).

Table 5-2: Correlation coefficient between agricultural production yield and cultivated land for Amhara districts.

Districts	Correlation Coefficients(R^2)	Improved Correlation (R^2)	Omitted Years
West Gojiam	0.84		
East Gojiam	0.65		
North Gonder	0.63		
North Wello	0.66		
South Gonder	0.41	0.58	1999 and 2009
North Shewa	0.25	0.42	1999 and 2006
Agew/Awi	0.13	0.92	1999 and 2009
South Wello	0.08	-	
Zikulla	0.01	0.46	1999 and 2001
Bati	0.10	-	
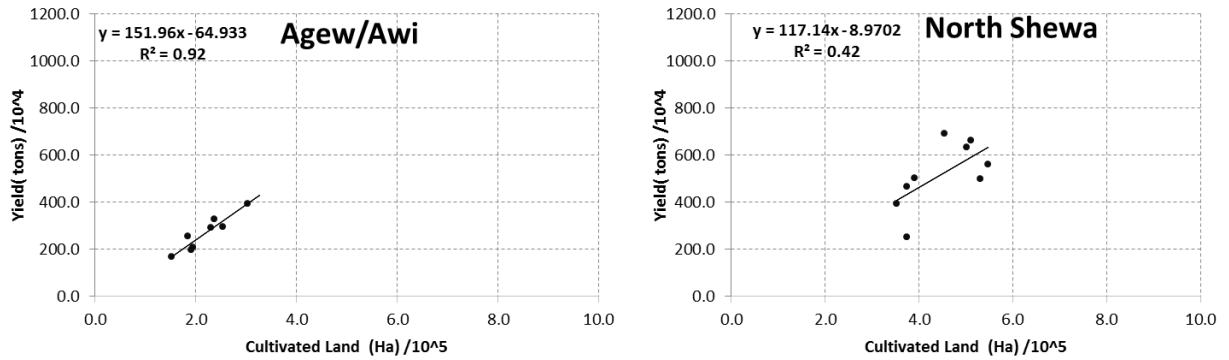
Figure 5-17: Graph showing the improved correlation for Agew/Awi and North Shewa districts after omitted outlier years.

5.5.2.   Correlations

5.5.2.1.   Relationship between NDVI and Production Yield

Correlation between NDVI and annual crop production yield for all the districts of the Amhara region was analyzed based on the mask for rainfed crops only. The relation was examined using the sum of the decadal NDVI during the maturity stage of the main growing season, from the first decade of August up to the third decade of September. There was a significant correlation between sum of maturity stage of the main growing season NDVI and total production yield. Tables 5-3 shows the correlation coefficients obtained for all districts and figure 5 -18 the scatter plot of South Goner and North Wello districts. Scatter plots for the other districts showing the same trend are illustrated in Appendix H.

Table 5-3: Correlation coefficient between sum of maturity stage main growing season NDVI and total production annual yield.

Districts	Correlation coefficient (R^2)
West Gojiam	0.50
North Wello	0.75
North Shewa	0.69
North Gonder	0.53
South Gonder	0.68
Zikulla	0.44
Agew Awi	0.39
East Gojiam	0.51

As discussed in section 5-1-1 some outlier values presented in the agriculture statistics have been discarded. In addition, the NDVI obtained in 1999 and 2009 was the maximum for all districts therefore these were omitted. The rainfed agriculture mask from the land cover classification of LSA SAF was prepared in 2005, thus for this study the land cover was assumed not to have changed significantly from 1999-2009. However, Amhara region has experienced intensified agriculture within these years because the population increased from 15 million in 2005 to 18 million in 2010. Hence, it was likely to obtain a less reliable relationship between sum of maturity stage main growing season NDVI and total yearly agricultural yield.
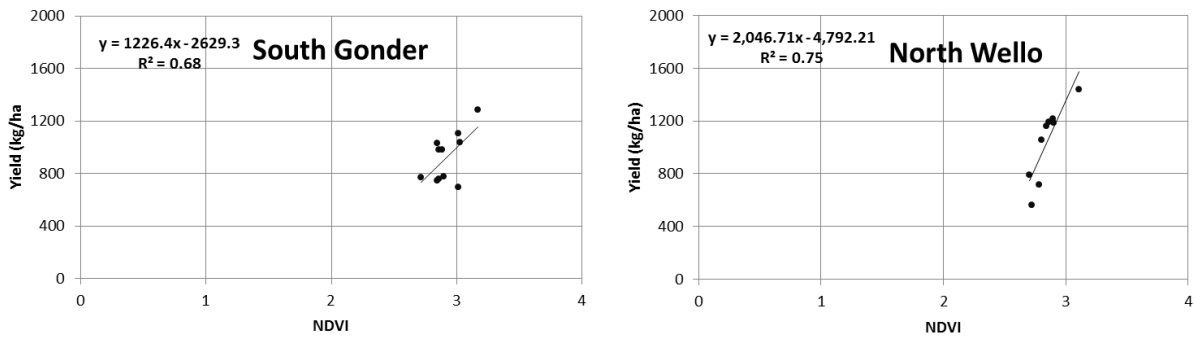
Figure 5-18: Graph showing the scatter plot and correlation coefficient between NDVI and agricultural yield in West Gojiam (left figure) and South Gonder (right figure).

5.5.2.2. Relationship between NDVI and Actual Evapotranspiration

The relationship between NDVI and actual evapotranspiration using the SAF AET was computed for all the districts in the study area. Since NDVI was one of the input parameter for the SEBS model, the SAF AET was used, which can be considered as a more or less independent variable compared to SEBS AET. The result showed there was a strong relationship between NDVI and SAF AET. The relationship was computed from the second decade of August to the last decade of November. Figure 5-19 shows the scatter plot of decadal SAF AET with decadal NDVI with $R^2 = 0.89$ and $R^2 = 0.72$ for West Gojiam and East Gojiam districts respectively. Appendix I shows the other districts scatter plots. Table 5-4 shows the correlation coefficient obtained for each district.

Table 5-4: Correlation coefficient between decadal SAF AET and NDVI

Districts	Correlation coefficient (R^2)
West Gojiam	0.96
North Wello	0.84
North Shewa	0.62
North Gonder	0.94
South Gonder	0.91
Zikulla	0.95
South Wello	0.50
East Gojiam	0.72
Agew/ Awi	0.83
Bati	0.58
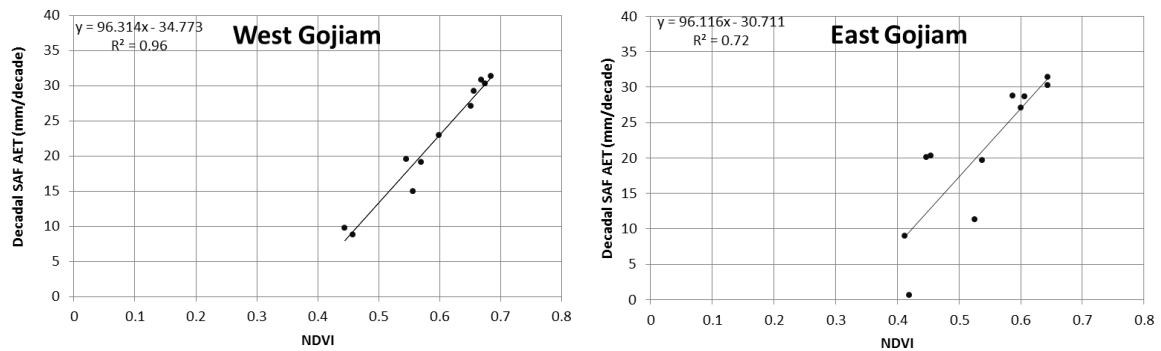
Figure 5-19: Graph showing the scatter plot and correlation coefficient between decadal SAF AET and NDVI for West Gojiam and East Gojiam district.

5.5.2.3. Relationship between NDVI and Rainfall

The correlation between NDVI and rainfall was computed for all the districts and a significant correlation was obtained for a lag time of two decades. The relation was based only on the masked rainfed cropland classified from the LSA SAF land cover. Table 5 -5 shows the correlation coefficient of all districts. Figure 5-20 shows the correlation of decadal NDVI and rainfall for North and South Gonder district. Figures showing the same trend for the other districts are presented in Appendix J.

Table 5-5: Correlation coefficient between decadal rainfall and NDVI

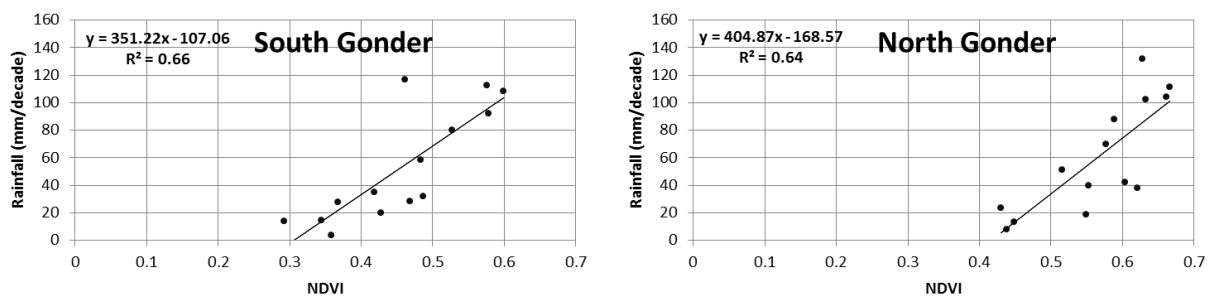| Districts	Correlation coefficient (R^2)
West Gojiam	0.56
North Wello	0.54
North Shewa	0.62
North Gonder	0.64
South Gonder	0.66
Zikulla	0.52
South Wello	0.48
East Gojiam	0.71
Agew/ Awi	0.63
Bati	0.68

Figure 5-20: Graph showing the scatter plot and correlation coefficient between *In-situ* rainfall and NDVI.

6.   DISCUSSION

The main objective of this study was identification of the occurrence of drought using remotely sensed estimate of Actual Evapotranspiration (AET) to improve drought monitoring and early warning. To achieve this objective, AET was estimated and analyzed for the main growing season in 2010 in the Amhara region in Ethiopia. The next step was to investigate the relationship of AET with other variables obtained from GNC data stream and *In-situ* data. To be able to relate AET to the occurrence of drought, a quantitative the crop performance indictor the so called Water Requirement Satisfaction Index (WRSI) was calculated using AET and Potential Evapotranspiration (PET). This was done to evaluate the availability of water to the crop during the growing season. The advantage of this approach was the direct quantification of water availability to the vegetation. In order to achieve the main objective and facilitate the subsequent discussion, the following sections discuss the output of the work with emphasis on the specific objectives and the subsequent research questions formulated during this research.

6.1.   Estimation and Comparison of Actual Evapotranspiration

The SEBS model and LSA SAF AET was used to estimate AET for the 2010 main growing season of the Amhara region. The results showed that both remote sensing methods were feasible to estimate AET over rainfed croplands of the study area. Considering that the SEBS model uses numerous local climatological - meteorological *In-situ* data a discrepancy was observed on the daily values of AET in SEBS compared to the SAF product during harvest period. The cause of such differences might be due to the fact that the SAF AET uses the SVAT model to estimate evapotranspiration from soil and vegetation independently using soil moisture, soil temperature, vegetation and weather information. On the other hand, SEBS is an energy balance model that uses surface temperature, surface bio physical parameters and weather information to estimate turbulent heat fluxes. Therefore the absence of soil moisture during harvest time might influence the SAF AET estimation. Furthermore, a comparison was conducted between daily estimation of SEBS AET and the LSA SAF AET. The results showed that for rainfed cropland they were significantly correlated. However, it is important to note that a number of input layers used in the SEBS model were actually derived from LSA SAF products, which are also used to compute the SAF AET product. Furthermore, the slight underestimation of the SAF AET probably linked to the used instantaneous SAF albedo (one of the key input parameter for the SAF AET) which had been found to underestimate 75% in compare to the measured albedo according to the investigation of Mutiga *et al* (2010) in Sub Saharan Africa.

Ground measurement used to compare the AET's was reference ET_o, calculated using the FAO Penman Monteith equation. The AET's were equal to the ET_o during the wet season indicating that, during this period AET was equal with reference ET_o. During the rainy season there was moist air with sufficient moisture from the surface and no water stress of the soil, therefore the AET increased and was similar to atmosphere demands as evapotranspiration which was represented by reference ET_o. However, during dry season the AET reduces, but the reference ET_o remains high because ET_o is highly influenced by meteorological variables such as incoming solar radiation and wind speed. The characteristics found between AET with reference ET_o were similar compared to the result of Nigussie et al (2011).

6.2. Potential of GEONETCast and *In-situ* Data Stream for Drought Monitoring and Early warning

In this study, the SPOT VGT NDVI was analysed to monitor the development of biomass in the Amhara region for the year 1999 to 2010. However, special attention was given to the 2010 main growing season which was also considered to study the relation of NDVI with AET and interrelationship of hydro-meteorological variables. The 2010 growing period of Amhara was compared with long time average, maximum and minimum NDVI. Establishment of base line climatology, here the Long Time Average (LTA), helps to distinguish deviations with respect to the normal vegetation productivity over the region. The study showed the 2010 growing season was normal for most of the Amhara districts except for two districts which showed a drought situation (North Shewa and East Gojiam districts). Therefore, the vegetation condition scenario was constructed from the deviation compared to the LTA NDVI for these two districts in conjunction with rainfall. Results of time series NDVI presented in figure 5 - 6 and 5 -7 signify the dependency of NDVI with variability of rainfall. When rainfall increases the NDVI also increases after two decades. This result is more or less in agreement with Wang et al (2003), who also found that i the response time of NDVI to a major precipitation events occurred typical 2-4 weeks- later.

Moreover, the historic drought situation was analysed using time series trend analysis of NDVI for each year from 1999-2010.The trend analysis of NDVI was studied using the mean and Standard Deviation (SD) of the maximum NDVI. The result depicted in table 5 -1 was compared to the interviews which were made during the fieldwork; the farmers' reports confirmed the result. According to the analysis made from the deviation of the maximum NDVI, 1999 and 2009 were the wettest years for most of the districts and drought situation was observed in most districts in 2001 and 2006, except North Shewa and East Gojiam districts. This was also confirmed by the farmers' interview (section 3-2-1-3). Finally, for the 2010 main growing season a temporal and spatial drought analysis was made for two districts.

Data from GNC, *In-situ* and ancillary data (PET and rainfall estimates from FEWSNET) together with drought indices were used for analysis of drought trend. It was used to observe possible occurrences of drought for the Amhara region during the main growing season of 2010. The results presented in figure 5 -10 and 5 - 11 show the inter dependency of hydro-meteorological variables, NDVI and drought indices. According to the temporal analysis made for two districts it can be concluded that the AET was highly dependent on the vegetation growth, maximum AET of both SAF and SEBS estimates were observed when NDVI was high because there was high vegetation growth during that time. In addition, NDVI was highly dependent on the rainfall. The response of NDVI to rainfall can be observed two decades later.

Furthermore, drought classifications by combined continuous method of drought indices were produced for each decade during the growing season of the area. These spatially distributed drought maps enhances the result found in the temporal drought trend analysis. The final map illustrated in figure 5 -15 showed severe and sporadic drought could be observed in North Gonder as well as sporadic drought in East Gojiam districts during the 2010 main growing season. This was observed in the temporal drought analysis which showed lower values of NDVI and rainfall compared to the average during most of the growing decades. In addition, the drought indices indicate that drought conditions were observed in almost all decades during the growing period in these two districts.

6.3. Relationship of Remote Sensing data with In-situ data

As mentioned in section 5 -5, correlation was made between cultivated land and yield of a crop to check the reliability of *In-situ* agricultural statistical data. In doing so, an outlier value of yield of some districts was observed. For these districts, a double mass curve analysis was done. A break in slope in the analyses

of the double mass curve showed a problem of recording of the annual yield of a crop. Therefore outlier values of the agricultural yield were discarded in order to develop a relationship between NDVI and annual yield. Overall improvement in the correlation was noted except for two districts (Bati and South Wello). For Bati, the reason could be cultivation of crops during the second growing season. The South Wello total cultivated land presented for the annual yield was most likely not computed correctly, it was noted that a small change of cultivated area showed a large change of yield.

A relation between sums of NDVI during maturity stage of the main growing season correlated with *In-situ* data of agricultural yield. A significant positive correlation was observed for the districts in the region. This shows that near real time NDVI products provided from GNC can be used to provide information about yield during the growing season. Furthermore, the SAF AET product was correlated with NDVI to see how vegetation conditions consequently result in the amount of evapotranspiration retrieved from remote sensing. Results showed that there is a strong correlation between the SAF AET with decadal NDVI. Therefore real time SAF AET can be used to analyse the occurrence of drought in conjunction with other hydro-meteorological variables or can be used to calculate the WRSI. In addition the relationship of NDVI and rainfall was analysed and a positive correlation could be established. Therefore, NDVI, AET and crop yield are dependent on rainfall in the study area. The correlation defined rainfall as a basic and major factor. However, the AET presented best agreement with NDVI rather than with rainfall. This could be due to the fact that this variable (AET) integrates information on rainfall, temperature and soil water holding capacity.

7.   CONCLUSIONS AND RECOMMENDATIONS

7.1.   Conclusions

This study aimed to identify of the occurrence of drought using remotely sensed estimate of Actual Evapotranspiration (AET) to improve drought monitoring and early warning in the study area. For this, the AET was estimated using two remote sensing methods and was used to analyse the spatial and temporal drought situation in combination with other hydro-meteorological variables and drought indices for the 2010 main growing season of the study area. From the result and discussion the following conclusions can be drawn.

It was found that AET from SEBS model and SAF had high agreement in terms of spatial and temporal distribution. Also a high correlation was found between SEBS and SAF AET for most of Amhara districts on rainfed croplands. Furthermore, results revealed that the two remote sensing methods compare well with reference ET_0 calculated using FAO Penman Monteith. Therefore, SEBS and SAF provide an appropriate estimate of AET which is an important component to calculate drought indices such as the WRSI as well as to analyse the occurrence of drought using time series drought trend analysis together with other hydro-meteorological variables.

The temporal and spatial characteristics of drought was analysed and mapped using satellite data obtained from GEONETCast in conjunction with *in-situ* data at district level. Drought trend analyses were done by integrating hydro-meteorological variables in combination with NDVI and drought indices. Temporal drought trend analysis given in figure 5 -10 and 5 -11 provided sufficient information on actual evapotranspiration, rainfall and NDVI together with drought indexing methods. It was observed that satellite derived drought indices can sufficiently identify and characterize the occurrence and severity of drought during the growing period. Subsequently, the drought maps derived from GNC data presented in figure 5 -11 and 5-12 provides a powerful tool for early warning and agricultural monitoring to quickly identify drought sensitive areas at districts level. Therefore, GNC data is useful to the near real time monitoring of the agricultural drought.

This study utilized the relationship between NDVI and agricultural yield for early warning and mitigation measures during the growing season which can be applied for forecasting the yield reduction in case of a drought situation. Therefore, the study established that there was a significant positive relationship between NDVI and annual yield as well as rainfall and NDVI. A relation was observed between sum of maturity stage main growing season NDVI and annual agricultural production yield. This shows that NDVI can be used to estimate crop yield which is vital to inform the relevant governmental and non-governmental authorities on areas which need drought relief. Furthermore, rainfall has a significant effect on the NDVI within two decades during the growing stage of the crop. Therefore effective drought mitigation measures could be executed prior to the onset of drought as part of preparedness and strategic planning within this time period. The relationship results are vital for successful near real time drought assessment and detection of vegetation stress resulting in yield reductions.

7.2. Recommendations

The following are recommendations related to the estimation of remote sensing AET and drought index calculated using AET such as the WRSI:

- Actual methods of comparison to validate the AET are required such as ground based flux measurement or comparison of AET with the measured value at location of stations.
- Daily parameters of NDVI could be used to improve the daily output of AET using SEBS model such as the NDVI from MSG (a new Meteorological Products Extraction Facility (MPEF) product).
- For seasonal applicability of WRSI a full water balance calculation is essential. Therefore, integration of satellite remote sensing soil moisture data (e.g. from Advanced Scatterometer (ASCAT)) and detailed information on the crop calendar are required.
- Start of season, end of season and crop coefficient values are the most determinant factor for WRSI therefore detailed crop calendar and ground truth is essential.

The following are recommendation in relation to the GNC data stream application:

- This study classifies drought thresholds in a general way. Some values might fall in drought or non- drought conditions, therefore integration of ground data to validate the result and the thresholds applied is necessary.

- GEONETCast has ample of choices to identify the occurrence of drought using hydro-meteorological variables interrelationships as well as using drought indexes methods such as Palmer Drought Severity (PDS) index, Temperature Condition Indexes (TCI), Evaporative Deficit Index (ETDI) Evaporative Stress Indexes (ESI). These could be applied to analyse agricultural, meteorological, hydrological and socio-economic droughts.

- Integration of satellite near real time dataset with the exact location where the crops are grown will provide a better understanding on the extent and severity of drought. Therefore a detailed ground validated land use map together with satellite driven high resolution land cover map would provide sufficient detail on land use and cover

The following are recommendations in relation to the ground truth data:

- Ground truth is important to crosscheck the remote sensing derived dataset(s); therefore extensive field observations with comprehensive local farmers' interviews enhance the knowledge of the historic drought situation, yield reduction and the trend of hydro-meteorological variables such as rainfall.

- Validation of remote sensing with the ground truth (agricultural statistics) at a lower spatial extent for example rather than at district level to go into a lower level and analyse the situation at province (Woreda) level.

In general the results demonstrate that there are good relationships between vegetative response and hydro-meteorological variables as well as between cumulative vegetative responses and yield. The methodology presented here can also be replicated in other districts. The thresholds used for the combined continuous drought classification method can then be adjusted to reflect the regional drought conditions for Ethiopia.

LIST OF REFERENCES

52north, (2012). About ESA-DDS. Available at:
http://52north.org/communities/earth-observation/about-esa-dds, (accessed 2012-Feb-27)

Allen, R. G., Pereira, L. S., Howell, T. A. and Jensen, M. E. (2011). Evapotranspiration Information
Reporting: I. Factors governing measurement accuracy. *Agricultural Water Management, 98*(6), 899-
920.

Allen, R. G., Pereira, L. S., Raes, D. and Smith, M. (1998). Crop Evapotranspiration - Guidelines for
Computing crop water requirements - FAO. *Irrigation and Drainage Paper 56, FAO Rome.*

Baret, F., Bartholome, E., Bicheron, P., Borstlap, G., Bydekereke, L.and Combal, B. (2006).
VGT4AFRICA user manual. Available at:
http://www.vgt4africa.org/PublicDocuments/VGT4AFRICA user manual, last retrieved 2010-
Aug-20).

Boken, V. K. (2009). Improving a Drought Early Warning Model for an Arid Region Using a Soil-
Moisture Index. *Applied Geography, 29*(3), 402-408.

Brutsaert, W. (2005). *Hydrology: An introduction* Cambridge: Cambridge University Press.

CGIAR-CSI. (2011). SRTM 90m Digital Elevation Database v4.1. Available at:
http://srtm.csi.cgiar.org/(accessed 2011-Oct-12).

Cihlar, J. (2000). Land cover mapping of large areas from satellites: status and research priorities.
International Journal of Remote Sensing, 21(6-7), 1093-1114.

Christensen, J.H., B. Hewitson, A. Busuioc, A. Chen, X. Gao, I. Held, R. Jones, R.K. Kolli, W.-T. Kwon,
R. Laprise, V. Magaña Rueda, L. Mearns, C.G. Menéndez, J. Räisänen, A. Rinke, A. Sarr and P.
Whetton, 2007: Regional Climate Projections. In: Climate Change 2007: The Physical Science
Basis. Contribution of Working Group I to the Fourth Assessment Report of the
Intergovernmental Panel on Climate Change [Solomon, S., D. Qin, M. Manning, Z. Chen, M.
Marquis, K.B. Averyt, M. Tignor and H.L. Miller (eds.)]. Cambridge University Press, Cambridge,
United Kingdom and New York, NY, USA. Avialable at: http://www.ipcc.ch/pdf/assessment-
report/ar4/wg1/ar4-wg1-chapter1, last retrieved 2012-Feb-15.

Conway, D.and Schipper, E. L. F. (2011). Adaptation to climate change in Africa: Challenges and
opportunities identified from Ethiopia. *Global Environmental Change, 21*(1), 227-237.

DevCoCast. (2011, March 31,2011). GEONECast for and by Developing Countries. Available at:
http://www.devcocast.eu/ViewContent.do?pageId=110 (accessed 2011-Nov-15)

Doorenbos, J.and Pruitt, W. O. (1977). Crop Water Requirements - FAO. *Irrigation and Drainage Paper 24,
FAO Rome.*

Enku Nigussie, T., van der Tol, C., Gieske, A. S. M.and Rientjes, T. H. M. (2011). Evapotranspiration
modeling using remote sensing and empirical models in the Fogera floodplain, Ethiopia. *In: Nile
River Basin : Hydrology, Climate and Water Use : e-book / editor A.M. Melesse. - Dordrecht : Springer, 2011.
- 419 p. ISBN 978-94-007-0689-7. pp. 163-178.*

EUMETSAT. (2011). Monitoring Weather and Climate from Space. Available at:
http://www.eumetsat.int/Home/Main/Satellites/MeteosatSecondGeneration/index.htm?l=en
last retrieved 09,10, 2011(accessed 2011-Sep-03)

FEWS NET. (2011). Famine Early Warning System Network. Available at: http://earlywarning.usgs.gov/fews/global/web/readme.php?symbol=pt, (accessed 2011- Nov - 19)

Frère, M.and Popov, G. F. (1979). Agro-meteorological Crop Monitoring and Forecasting. *FAO Plant Production and Protection paper No. 17,FAO ,Rome, Italy* .

Gadisso, B. E. (2007). Drought assessment for the Nile basin using meteosat second generation data with special emphasis on the upper Blue Nile region, *Water Resources and Environmental Management* (pp. 91). ITC, Enschede: MSc Thesis.

Gebrehiwot, T., van der Veen, A.and Maathuis, B. (2011). Spatial and temporal assessment of drought in the Northern highlands of Ethiopia. *International Journal of Applied Earth Observation and Geoinformation, 13*(3), 309-321.

Genovese, G., Vignolles, C., Negre, T.and Passera, G. (2001). A methodology for a combined use of normalised difference vegetation index and CORINE land cover data for crop yield monitoring and forecasting. A case study on Spain. *Agronomie, 21*(1), 91-111.

Ghilain, N., Arboleda, A.and Gellens-Meulenberghs, F. (2011). Evapotranspiration modeling at large scale using near-real time MSG SEVIRI derived data. [Article]. *Hydrology and Earth System Sciences, 15*(3), 771-786.

GIEWS. (2011). Global Information and Early Warning System on Food and Agriculture.   Available at: http://www.fao.org/giews/countrybrief/country/ETH/pdf/ETH.pdf (access date 2012- Jan-10)

Hoefsloot, P. (2010). LEAP version 2.4 for Ethiopia User manual. Available at: http://www.hoefsloot.com/en/leap-for-Ethiopia (accessed 2010-May-20).

IWMI. (2006). Drought Assessment and Mitigation in Southwest Asia. Available at: http://www.iwmi.cgiar.org/droughtassessment/files/pdf/workshop%20docs/Background.pdf, last retrieved 2010-Sep-02).

Jain, S. K., Keshri, R., Goswami, A.and Sarkar, A. (2010). Application of meteorological and vegetation indices for evaluation of drought impact: A case study for Rajasthan, India. *Natural Hazards, 54*(3), 643-656.

Kogan, F. N. (1995). Droughts of the late 1980s in the United States as derived from NOAA polar-orbiting satellite data. *Bulletin - American Meteorological Society, 76*(5), 655-668.

Kogan, F. N.and Sullivan, J. (1993). Development of global drought-watch system using NOAA/AVHRR data. *Advances in Space Research, 13*(5), 219-222.

Kustas, W. P.and Daughtry, C. S. T. (1990). Estimation of the soil heat flux/net radiation ratio from spectral data. *Agricultural and Forest Meteorology, 49*(3), 205-223.

Li, Z. L., Tang, R. L., Wan, Z. M., Bi, Y. Y., Zhou, C. H., Tang, B. H., Yan, G. J.and Zhang, X. Y. (2009). A Review of Current Methodologies for Regional Evapotranspiration Estimation from Remotely Sensed Data. *Sensors, 9*(5), 3801-3853.

Maathuis, B. H. P.and Mannaerts, C. M. (editors) (2012). GEONETCast-DevCoCast Application Manual. Chapter 4: Elizabeth ,F. Antonio, A. Aguilar, D. Alfredo, G, G: Estimation of Evapotranspiration in Minas Gerais State, Brazil. Available at: http://www.itc.nl/Pub/WRS/WRS-GEONETCast/Application-manual.html, last retrieved 2012-Feb-10.

Maathuis, B. H. P., Mannaerts, C. M., Schouwenburg, M., Retsios, V.and Lemmens, R. L. G. (2011a). Capacity Building In Earth Observation: Data Dissemination Systems for Food and Water Security Analysis and Monitoring In Africa. *Available at* http://52north.org/communities/earth-observation/documents, last retrieved 15,10, 2011.

Maathuis, B. H. P., Mannaerts, C. M., Schouwenburg, M., Retsios, V.and Lemmens, R. L. G. (2011b). GEONETCast TOOLBOX: Installation, Configuration and User Guide of the GEONETCast TOOLBOX Plug-in for ILWIS 3.7: ITC, Enschede, the Netherlands. 2011. Available at: http://52north.org/downloads/earth-observation/geonetcast/toolbox, last retrieved 2011-Aug-20

Mutiga, J. K. (2011). Planning of System Innovations in Watersheds Using Satellite Remote Sensing to Assess Evapotranspiration: Chapter 5: A case study of Upper Ewaso Ng' North Basin , Kenya Supplement 1), S77-S95: Phd thesis

Mutiga, J. K., Su, Z., Woldai, T.and Maathuis, B. (2010). Validation of Satellite Derived Surface Albedo and Temperature for Regional Estimation of Evapotranspiration in Data Scare Area of Sub - Saharan Africa. *Remote Sensing of Environment*. Phd thesis

NASA. (2009). Shuttle Radar Topogrpahy Mission The mission to Map the World.   Available at: 01/09, 2011, from http://www2.jpl.nasa.gov/srtm/(accessed 2011-Sep-01).

Niemeyer, S. (2008). New Drought Indices. *European Commission, DG Joint Research Center , Insitution for Enviromental sustainability, T.P.261, JRC-IES, I-21020 Ispra (VA) Italy.*

OXFAM. (2011). Briefing on the Horn of Africa Drought: Climate change and future impacts on food security.   Available at http://www.oxfam.org/sites/www.oxfam.org/files/briefing-hornofafrica-drought-climatechange-foodsecurity-020811.pdf, last retrieved 2012-Feb-26.

Rana, G.and Katerji, N. (2000). Measurement and estimation of actual evapotranspiration in the field under Mediterranean climate:

Ross, K. W., Brown, M. E., Verdin, J. P.and Underwood, L. W. (2009). Review of FEWS NET biophysical monitoring requirements. *Environmental Research Letters, 4*(2).

SAF, L. (2011). The EUMETSAT Satellite Application Facility on Land Surface Analysis (LSA SAF) Product User Manual Evapotranspiration (ET). Available at: http://landsaf.meteo.pt/algorithms.jsp?seltab=7&starttab=7, last retrieved 2011-Oct-01.

Silva, V. d. P. R., Campos, J. H. B. C., Silva, M. T.and Azevedo, P. V. (2010). Impact of global warming on cowpea bean cultivation in northeastern Brazil. *Agricultural Water Management, 97*(11), 1760-1768.

Su, Z. (2002). surface energy balance system SEBS for estimation of turbulent heat fluxes. *JournalHydrology and earth system sciences (HESS), 6*(1), 85-99.

Su, Z., Chen, Y., Menenti, M., Sobrino, J. A., Li, Z. L., Verhoef, W., Wang, L., Ma, Y., Wan, L., He, Y., Liu, Q. H., Li, C., Wen, J., van der Velde, R., van Helvoirt, M. D., Lin, W.and Xin, S. (2008). Drought monitoring and prediction over China. *In: Proceedings of the 2008 Dragon symposium, Dragon programme, final results, 2004-2007, Beijing, China 21-25 April 2008. / ed. by H. Lacoste and L. Ouwehand. Paris : ESA, 2008. ISBN 978-92-9221-219-3 (ESA SP ; 655) 8 p.*

Su, Z., Li, X., Zhou, Y., Wan, L., Wen, J.and Sintonen, K. (2003, 21-25 July 2003). *Estimating areal evaporation from remote sensing.* Paper presented at the Geoscience and Remote Sensing Symposium, 2003. IGARSS '03. Proceedings. 2003 IEEE International.

Temesgen, M., Hoogmoed, W. B., Rockstrom, J.and Savenije, H. H. G. (2009). Conservation tillage implements and systems for smallholder farmers in semi-arid Ethiopia. *Soil and Tillage Research, 104*(1), 185-191.

Thenkabail, P. S., Gamage, M. S. D. N.and Smakhtin, V. U. (2004). The Use of Remote Sensing Data for Drought Assessment and Monitoring in Southwest Asia.

Tote, C., Felix, R., Herman, E.and Dominique, H. (2011). SPIRITS Tutorial.

Tucker, C. J., compton J, Choudhury, Bhaskar J. . (1987). Satellite remote sensing of drought conditions. *Remote Sensing of Environment (ISSN 0034-4257), vol 23, p. 243-251., 23.*

USDA. (2006). United States Department of Agriculture Foreign Agricultural Service. Available at: http://www.pecad.fas.usda.gov/cropexplorer/description.cfm?legendid=6&regionid=rs (aceessed 2011- Nov-20)

Verdin, J.and Klaver, R. (2002). Grid-cell-based crop water accounting for the famine early warning system. *Hydrological Processes, 16*(8), 1617-1630.

Wang, J., Rich, P. M.and Price, K. P. (2003). Temporal responses of NDVI to precipitation and temperature in the central Great Plains, USA. *International Journal of Remote Sensing, 24*(11), 2345-2364.

Wilhite, D. A.and Glantz, M. H. (1985). Understanding the drought phenomenon: the role of definitions. *Water International, 10*(3), 111-120.

Wilhite, D. A.and Svoboda, M. D. (2000). *Drought early warning systems in the context of drought preparedness and mitigation.* Geneva: World Meteorological Org.

Wittich, K. P. (1997). Some simple relationships between land-surface emissivity, greenness and the plant cover fraction for use in satellite remote sensing. *International Journal of Biometeorology, 41*(2), 58-64.

Xin, S. (2007). Regional Evapotranspiration over the Arid Inland Heihe River basin in Norhtwest China (pp. 98). Enschede: MSc Thesis.

LIST OF APPENDIX

Appendix-A Meteorological Stations

No	Station name	Longitude	Latitude	Elevation(m)
1	BAHIRDAR	37.380	11.600	1790
2	COMBOLCHA	39.730	11.120	2750
3	DEBREEMARKOS	37.670	10.330	2515
4	GONDER	37.420	12.550	1967
5	ALEMKETEMA	39.300	10.080	2200
6	AMBAMARIAM	39.220	11.020	2980
7	CHAGINI	36.500	10.950	1620
8	CHEFFA	39.450	10.580	2690
9	DANGELA	36.720	11.020	1921
10	DEBREBREHAN	39.300	9.380	2515
11	DEBRETABOR	37.030	12.230	2750
12	ENEWARI	39.150	9.900	2650
13	LALIBELA	39.050	12.030	2500
14	MEHALMEDA	37.260	10.150	3040
15	MEKANESELAM	38.450	10.450	1720
16	MOTA	37.870	11.080	2440
17	METEMA	36.140	12.970	900
18	SIRINKA	39.620	11.550	2000
19	WEREILU	39.620	10.580	2690
20	WOGELTENA	39.220	11.360	3000

Appendix-B Agricultural Statistics of all District in Amhara region from 1999 - 2010

Year	Districts									
	West Gojam		East Gojam		North Gondar		South Gondar		North Shewa	
	Cultivated land(ha)	Production (Quintal)	Cultivated land(ha)	Production (Quintal)	Cultivated land(ha)	Production (Quintal)	Cultivated land(ha)	Production (Quintal)	Cultivated land(ha)	Prod. (Quintal)
1999	568833	9195455	575309	7978174	835903	8097862	821858	6140784	538823	5308730
2000	578029	9437080	573144	8605175	843797	7935839	586505	6487056	531239	4993977
2001	78624	1041232	614257	8856071	716977	7847587	587853	4469455	548506	5608172
2002	408340	5929767	431725	5650957	485009	5263940	370912	3857770	353597	3938673
2003	392763	4481215	397966	3617575	472208	2704661	403552	3122056	375073	2512286
2004	409023	5361453	278735	5065554	523527	4859031	412007	3208232	374207	4655269
2005	491842	5667375	457515	5751625	560435	6888517	465598	3253113	390871	5018611
2006	514988	6970770	484575	5629883	620636	7486564	464254	4566308	454884	6909934
2007	501284	7621152	506910	6646484	597637	8301043	481837	4746418	455736	8086913
2008	511844	9301899	532786	8230919	687567	8359272	496765	5112218	510791	6598498
2009	569386	9961353	570471	10762824	805473	11031874	520013	6683952	502815	6306244

1 Quintal= 100kg= 0.1 ton

Year	North Wello		South Wello		Agew/ Awi		Zikulla		Bati	
	Cultivated land(ha)	Production (Quintal)	Cultivated land(ha)	Production (Quintal)	Cultivated land(ha)	Production (Quintal)	Cultivated land(ha)	Production (Quintal)	Cultivated land(ha)	Production (Quintal)
1999	201891	1497946	406767	3475426	304779	400129	84156	735363	4450253	47056316
2000	228094	1282015	478877	3780384	302547	3907335	106498	395628	84161	595630
2001	229498	1809229	470363	3223848	326881	4373839	117260	322698	83178	705803
2002	204917	2442211	356139	3836259	184740	2554974	67103	489648	44526	500102
2003	193420	1388573	331122	2461770	152166	1665913	74260	402505	59330	390031
2004	217294	2735107	382490	4733845	190986	1972649	79000	572776	55771	553448
2005	232528	2452466	428473	5396082	195225	2060810	95241	515650	56525	619221
2006	232674.	2706403	394130	4761208	254105	2942547	96343	1117813	54221	763283
2007	251456	3056905	411619	5287479	230257	2923134	97986	1184655	5519863	774503
2008	245059	2907577	415187	5407285	237453	3276652	96874	1018001	51818	761643
2009	275637	3971822	436865	7237458	222823	369041	105876	889619	55868	885060

1 Quintal= 100kg= 0.1 ton

Appendix-C Flow Chart of SAF AET Algorithm
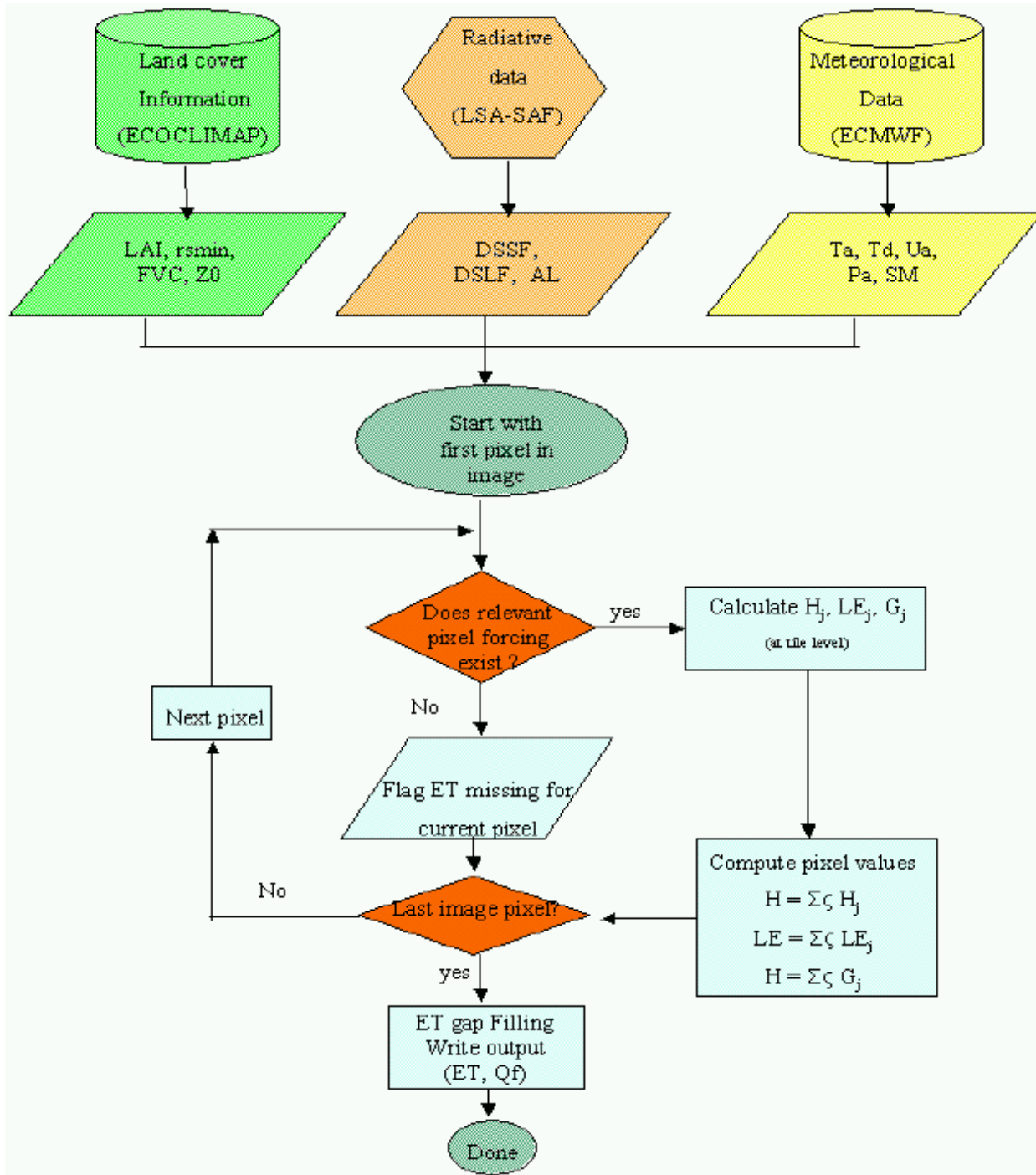
Source: LSA SAF for land surface analysis (LSA SAF), product user manual for SAF AET - http://landsaf.meteo.pt/algorithms.jsp?seltab=7&starttab=7

Appendix-D SEBS Algorithm

I.   **Net Radiation**

Net radiation is the sum of all incoming and outgoing heat fluxes (long wave and short wave). Thus, the surface energy balance expressed in equation (4.1) component of net radiation is written as:

$$R_n = (1 - \alpha) \cdot R_{swd} + \varepsilon_a \cdot R_{lwd} - \varepsilon_s \cdot \delta \cdot T_s^{\,4}$$

Equation D-7-1

Where:- R_n is net radiation, α is the surface reflectance (albedo), R_{swd} is the downward incoming solar short wave radiation, ε_a emissivity of air, R_{lwd} is the downward incoming long wave radiation, ε_s is the emissivity of the surface, σ is the Stefan Boltzmann constant = 5.67x10-8 W/m2k4 and T_s is the surface temperature.

II.   **Soil (Ground) Heat Flux**

Soil heat flux (G) is energy to heat the soil, thus the equation for soil heat flux in SEBS Model is fraction of net radiation in the following expression:

$$G = R_n (f_{veg} \cdot \Gamma_{veg} + (1 - f_{veg} \cdot \Gamma_{soil})$$

Equation D-7-2

Where: f_{veg} =0.05 for full vegetated canopy, and Γ_{soil} = 0.315 for bare soil (Kustas and Daughtry, 1990).

III.   **Sensible Heat Flux**

The most difficult part of the surface energy balance is to quantify the sensible heat flux (H). Therefore, for detailed explanation and reference for the algorithms of the similarity theory and atmospheric stability see Su (2002).

IV.   **Latent Heat Flux**

The latent heat flux (λE) is the amount of energy that is required for evapotranspiration and it is computed as remaining of the surface energy balance by subtracting from equation 7.1. In order to compute evaporative fraction, consideration of limiting cases is important that is under dry limit (when the latent heat or evaporative fraction becomes zero and sensible heat becomes maximum (H_{wet})) and under wet limit (when the sensible heat take its minimum, whereas latent heat takes place at likely rate (λE_{wet})) (Su, 2002). The next step is to compute the λE_{wet} and H_{wet} and a frequent step has been taken for calculation of the final instantaneous evaporative fraction see Su (2002). The evaporative fraction Λ is given by;

$$\Lambda = \frac{\lambda E}{R_n - G} = \frac{\lambda E}{\lambda E + H} = \frac{\Lambda_r \cdot \lambda E_{wet}}{R_n - G}$$

Equation D-7-3

$$\lambda E_{24} = \Lambda_{24} * (R_{n24})$$

Equation D-7-4

Since G_{24}=0 for the time scale of one day, the available energy would be only Rn (Brutsaert, 2005). Daily evapotranspiration in mm/day computed as daily available energy as:-
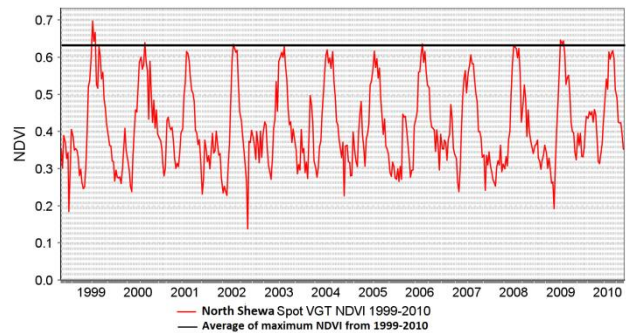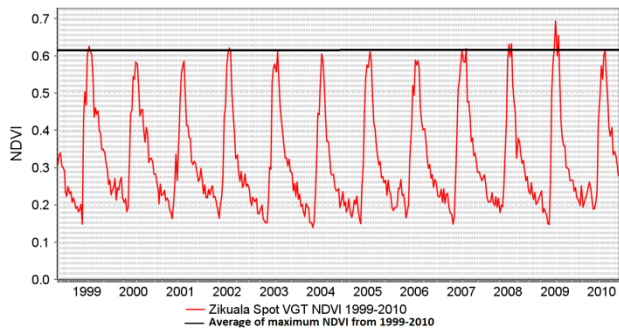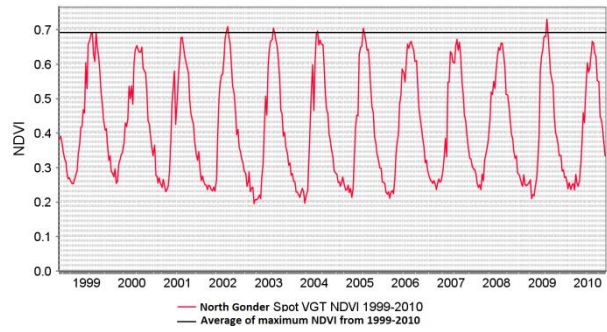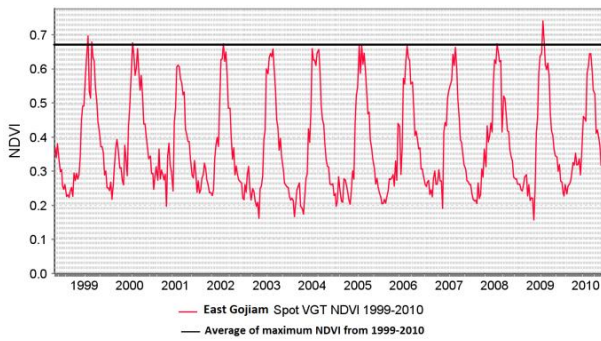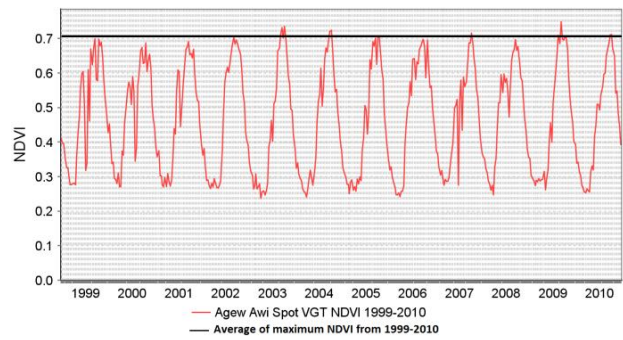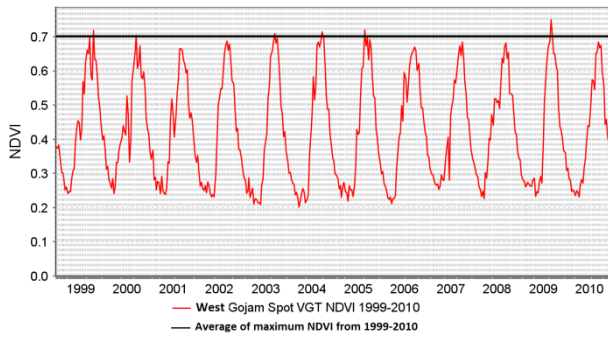
$$ET_{24} = \frac{86400 * 10^3}{\lambda \rho_w} \Lambda \cdot R_{n24}$$

Equation D-7-5

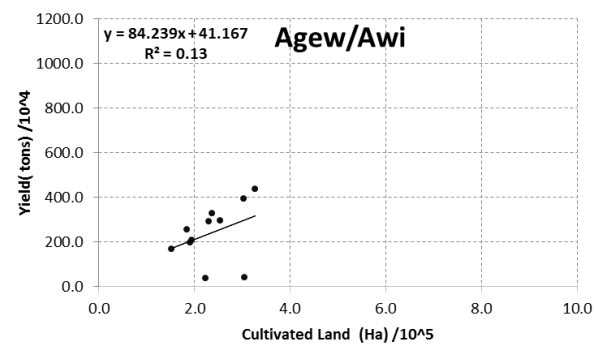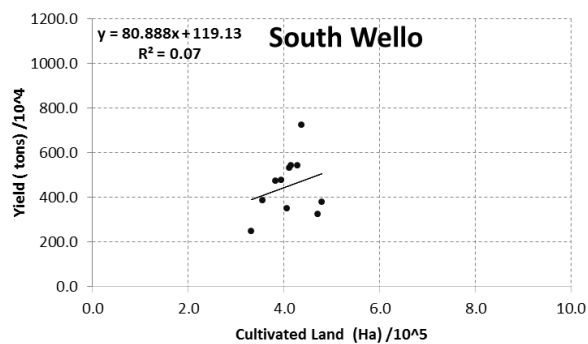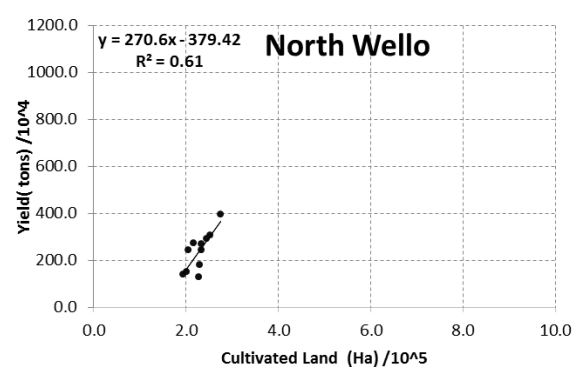Where: R_{n24} (w/m2) is the average 24 hour net radiation, λ (J/kg) is the latent heat of vaporization
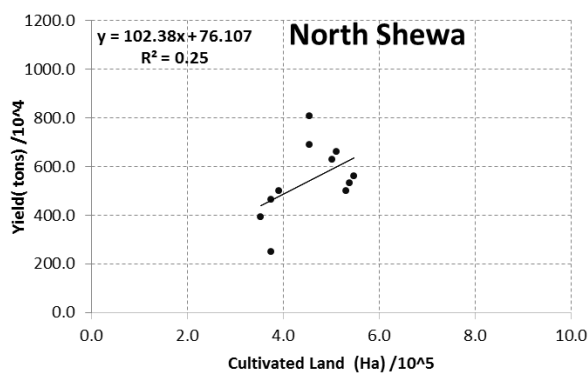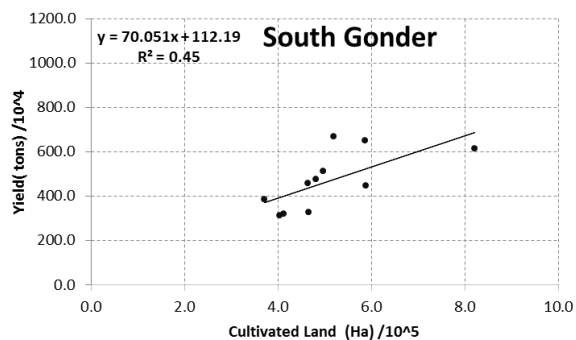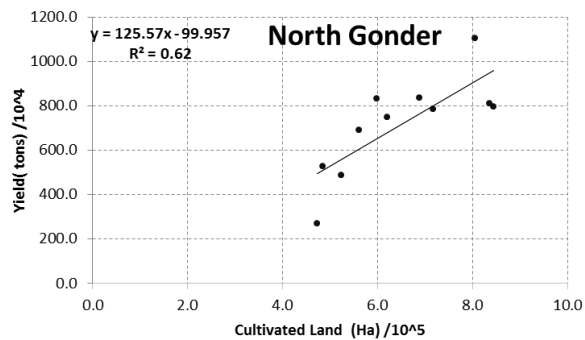
Appendix-E Gaph Showing the Scatter Plots and Correlation coefficient of SAF AET Versus SEBS AET

Agew Awi y = 0.82x + 0.29 R² = 0.72

North Gonder y = 0.82x + 0.20 R² = 0.76

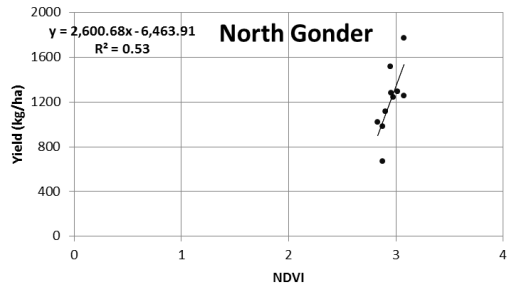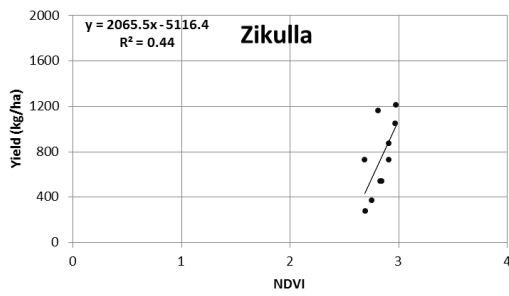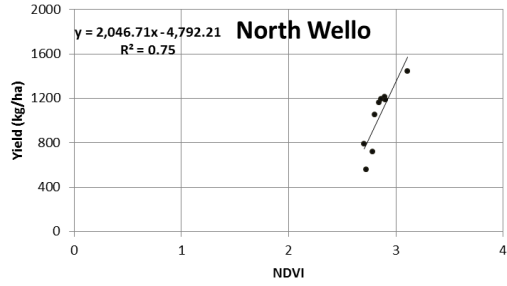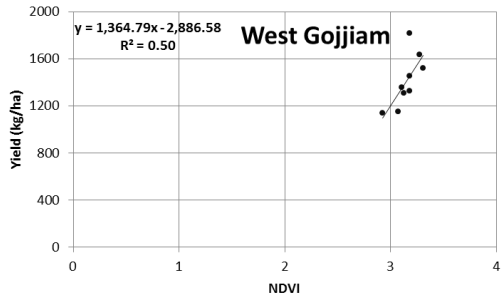Bati y = 0.8216x + 0.1482 R² = 0.50

Zikulla y = 1.0141x - 0.1075 R² = 0.79
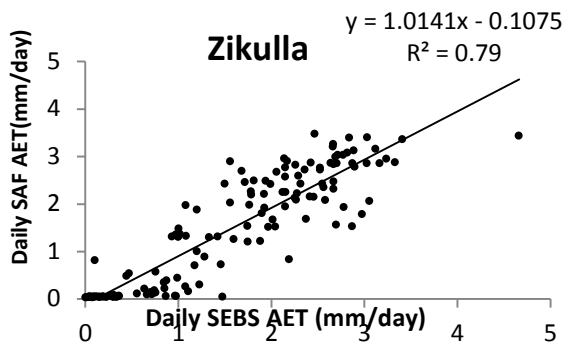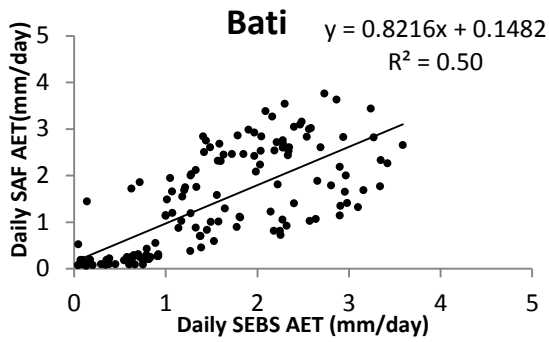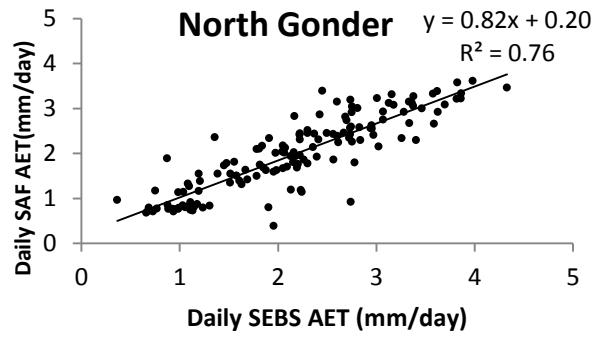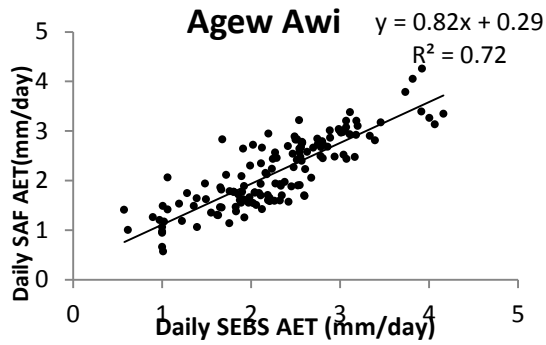
Appendix-F Decadal NDVI Pattern Graphs from 1999 to 2010

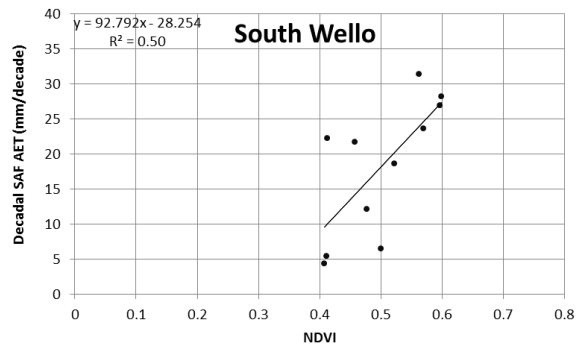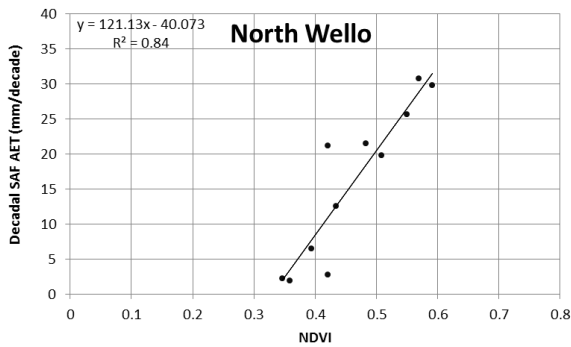West Gojam Spot VGT NDVI 1999-2010
Average of maximum NDVI from 1999-2010

Agew Awi Spot VGT NDVI 1999-2010
Average of maximum NDVI from 1999-2010

East Gojiam Spot VGT NDVI 1999-2010
Average of maximum NDVI from 1999-2010

North Gonder Spot VGT NDVI 1999-2010
Average of maximum NDVI from 1999-2010

Zikuala Spot VGT NDVI 1999-2010
Average of maximum NDVI from 1999-2010

North Shewa Spot VGT NDVI 1999-2010
Average of maximum NDVI from 1999-2010

Appendix-G The Scatter Plot and Correlation Coefficient between Annual Yield and Cultivated Land for each district

North Gonder

$y = 125.57x - 99.957$
$R^2 = 0.62$

South Gonder

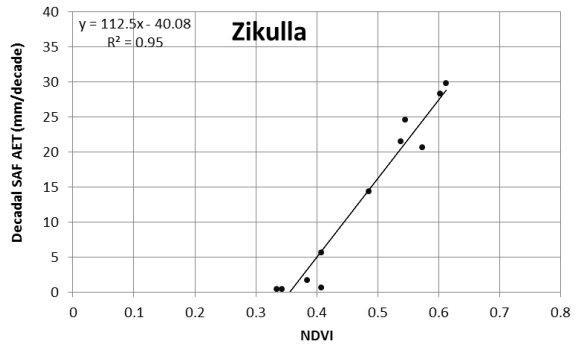$y = 70.051x + 112.19$
$R^2 = 0.45$

North Shewa

$y = 102.38x + 76.107$
$R^2 = 0.25$

North Wello

$y = 270.6x - 379.42$
$R^2 = 0.61$

South Wello

$y = 80.888x + 119.13$
$R^2 = 0.07$

Agew/Awi

$y = 84.239x + 41.167$
$R^2 = 0.13$

West Gojjiam: $y = 1,364.79x - 2,886.58$, $R^2 = 0.50$

North Wello: $y = 2,046.71x - 4,792.21$, $R^2 = 0.75$

Zikulla: $y = 2065.5x - 5116.4$, $R^2 = 0.44$

North Gonder: $y = 2,600.68x - 6,463.91$, $R^2 = 0.53$

East Gojiam: $y = 1,199.37x - 2,122.35$, $R^2 = 0.51$

North Shewa: $y = 1,546.18x - 3,963.75$, $R^2 = 0.69$

Appendix-I The scatter Plot and Correlation Coefficient between NDVI and Actual Evapotranspiration (SAF AET) for each District
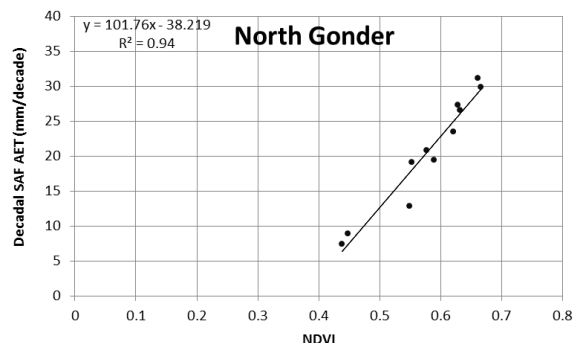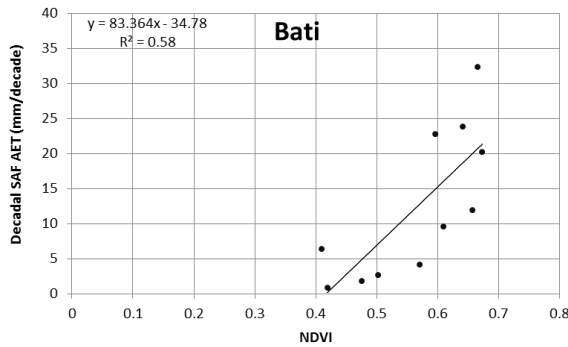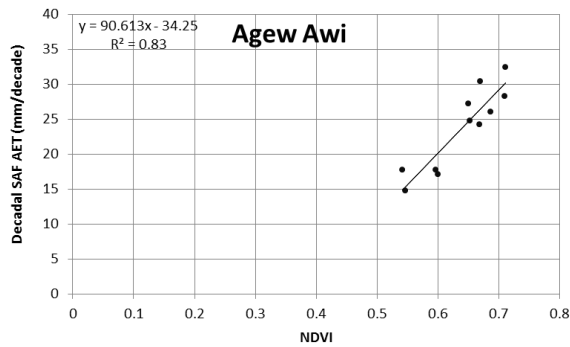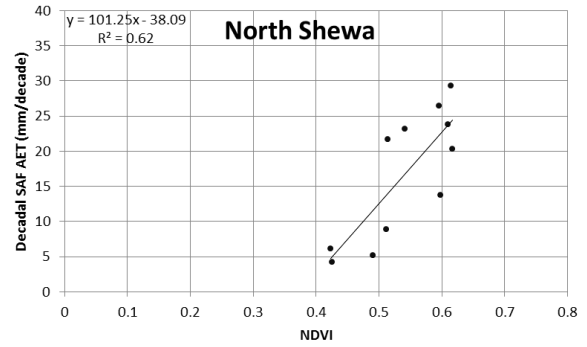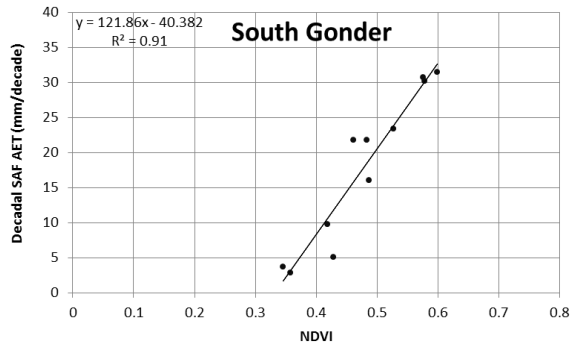
Appendix-J Relationship between NDVI and *In-situ* Rainfall for each District

$y = 450.65x - 180.27$
$R^2 = 0.62$
North Shewa

$y = 303.86x - 102.33$
$R^2 = 0.71$
East Gojiam

$y = 369.86x - 123.85$
$R^2 = 0.48$
South Wello

$y = 343.87x - 122.32$
$R^2 = 0.56$
West Gojiam

$y = 405.96x - 174.58$
$R^2 = 0.684$
Bati

$y = 242.38x - 77.417$
$R^2 = 0.52$
Zikulla

$y = 330.89x - 116.27$
$R^2 = 0.63$
Agew/AWI

$y = 283.51x - 87.983$
$R^2 = 0.54$
North Wello